FIELD MEASUREMENTS AND CORRESPONDING FEA OF CROSS-FRAME FORCES IN SKEWED STEEL I-GIRDER BRIDGES

by

Kelly Ambrose

A thesis submitted to the Faculty of the University of Delaware in partial fulfillment of the requirements for the degree of Master of Civil Engineering

Summer 2012

FIELD MEASUREMENTS AND CORRESPONDING

FEA OF CROSS-FRAME FORCES

IN SKEWED STEEL I-GIRDER BRIDGES

by
Kelly Ambrose

Approved: ____
Jennifer E. Righman McConnell, Ph.D.
Professor in charge of thesis on behalf of the Advisory Committee

Approved: ____
Harry W. Shenton III, Ph.D.
Chair of the Department of Civil and Environmental Engineering

Approved: ____
Babatunde A. Ogunnaike, Ph.D.
Interim Dean of the College of Engineering

Approved: ____
Charles G. Riordan, Ph.D.
Vice Provost for Graduate and Professional Education

ACKNOWLEDGMENTS

I would first like to thank my advisor, Dr. Jennifer Righman McConnell, for giving me this opportunity and helping me along the way. I would also like to thank my family who have supported and motivated me every step of the way. Special thanks also go to Gary Wenczel and Danny Richardson for their invaluable help while conducting my field tests. Also, I would like to thank all the structures graduate students who make coming into the graduate office an enjoyable experience every day. Finally, I would like to thank the Delaware Department of Transportation (DelDOT) for their support of this project.

TABLE OF CONTENTS

LIST OF TABLES vii
LIST OF FIGURES x
ABSTRACT xvi

Chapter

1. INTRODUCTION 1

1.1 Motivation 1
1.2 Objectives and Scope 1
1.3 Thesis Outline 2

2. BACKGROUND 4

2.1 Literature Review 4
2.2 Bridge Descriptions 10

2.2.1 SR 1 Over US 13 10
2.2.2 SR 299 Over SR 1 18

3. FINITE ELEMENT MODELING 26

3.1 Geometry 26
3.2 Elements 27
3.3 Mesh Generation 29
3.4 Boundary Conditions 31
3.5 Loading 32
3.6 Analysis 34
3.7 Future Work Considerations 35

4. FIELD TESTING 37

4.1 Gauge Type and Data Collection 37
4.2 Instrumentation Layout 39

4.2.1 SR 1 Over US 13 41

4.2.2 SR 299 Over US 13 48

4.3 Loading Vehicle 55
4.4 Truck Passes 57

4.4.1 SR 1 Over US 13 58

4.5 Data 65
4.6 Recommendations 76

5. FEA CALIBRATION AND RESULTS 79

5.1 Preliminary Models 79
5.2 Alternative Girder Stress Models 81

5.2.1 SR 1 Over US 13 84
5.2.2 SR 299 Over SR 1 96

5.3 Selected Girder Stress Model Results 107

5.3.1 SR 1 Over US 13 107
5.3.2 SR 299 Over SR 1 108

5.4 Alternative Cross-frame Stress Models 109

5.4.1 SR 1 Over US 13 109
5.4.2 SR 299 Over SR 1 124

5.5 Conclusion 127

6. CONCLUSION 129

6.1 Summary 129
6.2 Results 131
6.3 Future Work 134

REFERENCES 137

Appendices

A. FIELD TEST LABELS 139
B. FIELD TEST DATA 151

C. HAND CALCULATIONS.. 187
D. SR 1 OVER US 13 CROSS-FRAME DATA 194

LIST OF TABLES

Table 4.1 Number of Gauges Per Location, SR 1 Over US 13 46

Table 4.2 Number of Gauges Per Location, SR 299 over SR 1 53

Table 4.3 Triaxle Dump Truck Weights 57

Table 4.4 SR 1 Over US 13 Max Values, Girder Locations 69

Table 4.5 SR 1 Over US 13 Max Values, Cross-frames 12-3, 12-4, & 14-3 Passes 1 & 2 70

Table 4.6 SR 1 Over US 13 Max Values, Cross-frames 12-3, 12-4, & 14-3, Pass 3 71

Table 4.7 SR 1 Over US 13 Max Values, Cross-frames 4-4 & 11-3, Passes 1 & 2 72

Table 4.8 SR 1 Over US 13 Max Values, Cross-frames 4-4 & 11-3, Pass 3........... 73

Table 4.9 SR 299 Over SR 1 Max Values, Girder Locations 74

Table 4.10 SR 299 Over SR 1 Max Values, Cross-frames 14-8, 14-9, & 14-10....... 75

Table 4.11 SR 299 Over SR 1 Max Values, Cross-frames 12-4, 12-5, & 8-4........... 76

Table 5.1 NA Positions for SR 1 Over US 13 89

Table 5.2 NA Positions for FEA Models of SR 1 Over US 13 90

Table 5.3 Bottom Flange Girder Stress Comparisons for SR 1 Over US 13, Pass 1 92

Table 5.4 Bottom Flange Girder Stress Comparisons for SR 1 Over US 13, Pass 2 93

Table 5.5 Bottom Flange Girder Stress Comparisons for SR 1 Over US 13, Pass 3 94

Table 5.6 SR 1 Over US 13 Model Resulting in Lowest Percent Differences for Bottom Flange Girder Stresses 96

Table 5.7 Girder Stress Comparisons for SR 299 Over SR 1................................ 101

Table 5.8 NA Positions for SR 299 Over SR 1 102

Table 5.9 Comparison to Hand Calculations.. 104

Table 5.10 Dead Load Comparison 105

Table 5.11 SR 299 Over SR 1 Distribution Factors 106

Table 5.12 Comparison of Girder Stresses in FEA E1, C1, S5 to Field Test of SR 1 Over US 13 108

Table 5.13 Cross-frame 12-3 Data for SR 1 over US 13 Day 1 Pass 1 112

Table 5.14 Cross-frame 12-4 Data for SR 1 over US 13 Day 1 Pass 1 113

Table 5.15 Cross-frame 14-3 Data for SR 1 over US 13 Day 1 Pass 1 114

Table 5.16 Cross-frame 4-4 Data for SR 1 Over US 13 Day 2 Pass 1 115

Table 5.17 Cross-frame 11-3 Data for SR 1 Over US 13 Day 2 Pass 1 116

Table 5.18 Average Cross-frame Stresses Ranking.. 119

Table 5.19 Bottom Flange Gauge Groupings, SR 1 Over US 13 Pass 1 121

Table 5.20 Bottom Flange Gauge Groupings, SR 1 Over US 13 Pass 2 122

Table 5.21 Bottom Flange Gauge Groupings, SR 1 Over US 13 Pass 3 123

Table 5.22 Cross-frame Data for SR 299 Over SR 1 Day 2 Pass 1......................... 126

Table D-1 Cross-frame 12-3 Data for SR 1 Over US 13 Day 1 Pass 1 195

Table D-2 Cross-frame 12-4 Data for SR 1 Over US 13 Day 1 Pass 1 196

Table D-3 Cross-frame 14-3 Data for SR 1 Over US 13 Day 1 Pass 1 197

Table D-4 Cross-frame 12-3 Data for SR 1 Over US 13 Day 1 Pass 2 198

Table D-5 Cross-frame 12-4 Data for SR 1 Over US 13 Day 1 Pass 2 199

Table D-6 Cross-frame 14-3 Data for SR 1 Over US 13 Day 1 Pass 2 200

Table D-7 Cross-frame 12-3 Data for SR 1 Over US 13 Day 1 Pass 3 201

Table D-8 Cross-frame 12-4 Data for SR 1 Over US 13 Day 1 Pass 3 202

Table D-9 Cross-frame 14-3 Data for SR 1 Over US 13 Day 1 Pass 3 203

Table D-10 Cross-frame 4-4 Data for SR 1 Over US 13 Day 2 Pass 1 204

Table D-11 Cross-frame 11-3 Data for SR 1 Over US 13 Day 2 Pass 1 205

Table D-12 Cross-frame 4-4 Data for SR 1 Over US 13 Day 2 Pass 2 206

Table D-13 Cross-frame 11-3 Data for SR 1 Over US 13 Day 2 Pass 2 207

Table D-14 Cross-frame 4-4 Data for SR 1 Over US 13 Day 2 Pass 3 208

Table D-15 Cross-frame 11-3 Data for SR 1 Over US 13 Day 2 Pass 3 209

LIST OF FIGURES

Figure 2.1 Satellite View of SR 1 Over US 13 (Google Maps, 2012) 11

Figure 2.2 Photograph of SR 1 Over US 13, Elevation View 12

Figure 2.3 SR 1 Over US 13 Elevation View 13

Figure 2.4 SR 1 Over US 13 Plan View 14

Figure 2.5 SR 1 Over US 13 Cross-Section View 15

Figure 2.6 SR 1 Over US 13 Girder Elevation View 16

Figure 2.7 SR 1 Over US 13 Intermediate Cross-frame Detail 17

Figure 2.8 Photograph of SR 1 Over US 13 Cross-frames 18

Figure 2.9 Satellite View of SR 299 Over SR 1 (Google Maps, 2012) 19

Figure 2.10 Photograph of SR 299 Over SR 1, Elevation View 19

Figure 2.11 SR 299 Over SR 1 Elevation View 20

Figure 2.12 SR 299 Over SR 1 Plan View 21

Figure 2.13 SR 299 Over SR 1 Bridge Cross-section 22

Figure 2.14 SR 299 Over SR 1 Girder Elevation 23

Figure 2.15 SR 299 Over SR 1 Intermediate Cross-frame Detail 25

Figure 2.16 Photograph of SR 299 Over SR 1 Cross-frames 25

Figure 3.1 Base Geometry for SR 1 Over US 13 in AutoCAD 27

Figure 3.2 HS-20 Truck Loading (AASHTO 2010) 34

Figure 4.1 Clamped BDI Strain Transducers 38

Figure 4.2 Bonded BDI Strain Transducer 39

Figure 4.3 SR 1 Over US 13 Instrumentation Layout.. 43

Figure 4.4 Girder Strain Gauges Cross-Section Labeling System, SR 1 Over US 13.. 45

Figure 4.5 Cross-frame Strain Gauges Cross-Section Labeling, SR 1 Over US 13.. 45

Figure 4.6 SR 299 Over SR 1 Instrumentation Layout... 50

Figure 4.7 Girder Strain Gauges Cross-Section Labeling System, SR 299 Over SR 1 51

Figure 4.8 Cross-frame Strain Gauges Cross-Section Labeling, SR 299 Over SR 1 52

Figure 4.9 DelDOT Triaxle Dump Truck 56

Figure 4.10 Truck Passes for SR 1 Over US 13: A) Pass 1: Center of Left Lane, B) Pass 2: Straddle Center Line, C) Pass 3: Left Wheels on Center Line 59

Figure 4.11 Photographs of Truck Passes for SR 1 Over US 13: A) Pass 1, B) Pass 2, C) Pass 3.. 61

Figure 4.12 West bound Truck Passes (Pass 1) for SR 299 Over SR 1: A) Day 1 B) Day 2 63

Figure 4.13 Eastbound Truck Passes (Pass 2) for SR 299 Over SR 1: A) Day 1, B) Day 2 64

Figure 4.14 Time vs. Strain, SR 299 over SR 1, Day 1 66

Figure 5.1 FEA vs. Field Test for G3-BF-1 for SR 1 over US 13 83

Figure 5.2 SR 1 Over US 13 Flow Chart 88

Figure A-1 SR 299 Over SR 1 Instrumentation Layout... 140

Figure A-2 SR 299 Over SR 1 Girder Location 1, Day 1 & 2 141

Figure A-3 SR 299 Over SR 1 Girder Location 2, Day 1 & 2 142

Figure A-4 SR 299 Over SR 1 Girder Location 3 142

Figure A-5 SR 299 Over SR 1 Cross-frame 14-8 143

Figure A-6 SR 299 Over SR 1 Cross-frame 14-9 143

Figure A-7 SR 299 Over SR 1 Cross-frame 14-9 144

Figure A-8 SR 299 Over SR 1 Cross-frame 8-4 144

Figure A-9 SR 299 Over SR 1 Cross-frame 12-4 145

Figure A-10 SR 299 Over SR 1 Cross-frame 12-5 145

Figure A-11 SR 1 Over US 13 Instrumentation Layout 146

Figure A-12 SR 1 Over US 13 Girder Location 1 147

Figure A-13 SR 1 Over US 13 Girder Location 2, Day 1 & 2 147

Figure A-14 SR 1 Over US 13 Girder Location 3 148

Figure A-15 SR 1 Over US 13 Cross-frame 12-3 148

Figure A-16 SR 1 Over US 13 Cross-frame 12-4 149

Figure A-17 SR 1 Over US 13 Cross-frame 14-3 149

Figure A-18 SR 1 Over US 13 Cross-frame 4-4 150

Figure A-19 SR 1 Over US 13 Cross-frame 11-3 150

Figure B-1 SR 299 Over SR 1 Day 1 Pass 1 Girder Locations 1 & 2 152

Figure B-2 SR 299 Over SR 1 Day 1 Pass 2 Girder Locations 1 & 2 152

Figure B-3 SR 299 Over SR 1 Day 1 Pass 1 Girder Location 3 153

Figure B-4 SR 299 Over SR 1 Day 1 Pass 2 Girder Location 3 153

Figure B-5 SR 299 Over SR 1 Day 2 Pass 1&2 Girder Location 1 154

Figure B-6 SR 299 Over SR 1 Day 2 Pass 1&2 Girder Location 2 154

Figure B-7 SR 299 Over SR 1 Day 1 Pass 1 Cross-frame 14-8, 1 of 2 155

Figure B-8 SR 299 Over SR 1 Day 1 Pass 1 Cross-frame 14-8, 2 of 2 155

Figure B-9 SR 299 Over SR 1 Day 1 Pass 2 Cross-frame 14-8, 1 of 2 156

Figure B-10 SR 299 Over SR 1 Day 1 Pass 2 Cross-frame 14-8, 2 of 2 156

Figure B-11 SR 299 Over SR 1 Day 1 Pass 1 Cross-frame 14-9, 1 of 2 157

Figure B-12 SR 299 Over SR 1 Day 1 Pass 1 Cross-frame 14-9, 2 of 2 157

Figure B-13 SR 299 Over SR 1 Day 1 Pass 2 Cross-frame 14-9, 1 of 2 158

Figure B-14 SR 299 Over SR 1 Day 1 Pass 2 Cross-frame 14-9, 2 of 2 158

Figure B-15 SR 299 Over SR 1 Day 1 Pass 1 Cross-frame 14-10, 1 of 2 159

Figure B-16 SR 299 Over SR 1 Day 1 Pass 1 Cross-frame 14-10, 2 of 2 159

Figure B-17 SR 299 Over SR 1 Day 1 Pass 2 Cross-frame 14-10, 1 of 2 160

Figure B-18 SR 299 Over SR 1 Day 1 Pass 2 Cross-frame 14-10, 2 of 2 160

Figure B-19 SR 299 Over SR 1 Day 2 Pass 1&2 Cross-frame 8-4, 1 of 2 161

Figure B-20 SR 299 Over SR 1 Day 2 Pass 1&2 Cross-frame 8-4, 2 of 2 161

Figure B-21 SR 299 Over SR 1 Day 2 Pass 1&2 Cross-frame 12-4, 1 of 2 162

Figure B-22 SR 299 Over SR 1 Day 2 Pass 1&2 Cross-frame 12-4, 2 of 2 162

Figure B-23 SR 299 Over SR 1 Day 2 Pass 1&2 Cross-frame 12-5, 1 of 2 163

Figure B-24 SR 299 Over SR 1 Day 2 Pass 1&2 Cross-frame 12-5, 2 of 2 163

Figure B-25 SR 1 Over US 13 Day 1 Pass 1 Girder Location 2 164

Figure B-26 SR 1 Over US 13 Day 1 Pass 2 Girder Location 2 164

Figure B-27 SR 1 Over US 13 Day 1 Pass 3 Girder Location 2 165

Figure B-28 SR 1 Over US 13 Day 1 Pass 1 Girder Location 3 165

Figure B-29 SR 1 Over US 13 Day 1 Pass 2 Girder Location 3 166

Figure B-30 SR 1 Over US 13 Day 1 Pass 3 Girder Location 3 166

Figure B-31 SR 1 Over US 13 Day 2 Pass 1 Girder Location 1 167
Figure B-32 SR 1 Over US 13 Day 2 Pass 2 Girder Location 1 167
Figure B-33 SR 1 Over US 13 Day 2 Pass 3 Girder Location 1 168
Figure B-34 SR 1 Over US 13 Day 2 Pass 1 Girder Location 2 168
Figure B-35 SR 1 Over US 13 Day 2 Pass 2 Girder Location 2 169
Figure B-36 SR 1 Over US 13 Day 2 Pass 3 Girder Location 2 169
Figure B-37 SR 1 Over US 13 Day 1 Pass 1 Cross-frame 12-3, 1 of 2 170
Figure B-38 SR 1 Over US 13 Day 1 Pass 1 Cross-frame 12-3, 2 of 2 170
Figure B-39 SR 1 Over US 13 Day 1 Pass 2 Cross-frame 12-3, 1 of 2 171
Figure B-40 SR 1 Over US 13 Day 1 Pass 2 Cross-frame 12-3, 2 of 2 171
Figure B-41 SR 1 Over US 13 Day 1 Pass 3 Cross-frame 12-3, 1 of 2 172
Figure B-42 SR 1 Over US 13 Day 1 Pass 3 Cross-frame 12-3, 2 of 2 172
Figure B-43 SR 1 Over US 13 Day 1 Pass 1 Cross-frame 12-4, 1 of 2 173
Figure B-44 SR 1 Over US 13 Day 1 Pass 1 Cross-frame 12-4, 2 of 2 173
Figure B-45 SR 1 Over US 13 Day 1 Pass 2 Cross-frame 12-4, 1 of 2 174
Figure B-46 SR 1 Over US 13 Day 1 Pass 2 Cross-frame 12-4, 2 of 2 174
Figure B-47 SR 1 Over US 13 Day 1 Pass 3 Cross-frame 12-4, 1 of 2 175
Figure B-48 SR 1 Over US 13 Day 1 Pass 3 Cross-frame 12-4, 2 of 2 175
Figure B-49 SR 1 Over US 13 Day 1 Pass 1 Cross-frame 14-3, 1 of 2 176
Figure B-50 SR 1 Over US 13 Day 1 Pass 1 Cross-frame 14-3, 2 of 2 176
Figure B-51 SR 1 Over US 13 Day 1 Pass 2 Cross-frame 14-3, 1 of 2 177
Figure B-52 SR 1 Over US 13 Day 1 Pass 2 Cross-frame 14-3, 2 of 2 177
Figure B-53 SR 1 Over US 13 Day 1 Pass 3 Cross-frame 14-3, 1 of 2 178

Figure B-54 SR 1 Over US 13 Day 1 Pass 3 Cross-frame 14-3, 2 of 2 178

Figure B-55 SR 1 Over US 13 Day 2 Pass 1 Cross-frame 4-4, 1 of 3 179

Figure B-56 SR 1 Over US 13 Day 2 Pass 1 Cross-frame 4-4, 2 of 3 179

Figure B-57 SR 1 Over US 13 Day 2 Pass 1 Cross-frame 4-4, 3 of 3 180

Figure B-58 SR 1 Over US 13 Day 2 Pass 2 Cross-frame 4-4, 1 of 3 180

Figure B-59 SR 1 Over US 13 Day 2 Pass 2 Cross-frame 4-4, 2 of 3 181

Figure B-60 SR 1 Over US 13 Day 2 Pass 2 Cross-frame 4-4, 3 of 3 181

Figure B-61 SR 1 Over US 13 Day 2 Pass 3 Cross-frame 4-4, 1 of 3 182

Figure B-62 SR 1 Over US 13 Day 2 Pass 3 Cross-frame 4-4, 2 of 3 182

Figure B-63 SR 1 Over US 13 Day 2 Pass 3 Cross-frame 4-4, 3 of 3 183

Figure B-64 SR 1 Over US 13 Day 2 Pass 1 Cross-frame 11-3, 1 of 2 183

Figure B-65 SR 1 Over US 13 Day 2 Pass 1 Cross-frame 11-3, 2 of 2 184

Figure B-66 SR 1 Over US 13 Day 2 Pass 2 Cross-frame 11-3, 1 of 2 184

Figure B-67 SR 1 Over US 13 Day 2 Pass 2 Cross-frame 11-3, 2 of 2 185

Figure B-68 SR 1 Over US 13 Day 2 Pass 3 Cross-frame 11-3, 1 of 2 185

Figure B-69 SR 1 Over US 13 Day 2 Pass 3 Cross-frame 11-3, 2 of 2 186

ABSTRACT

While it is known that bridges have the capacity to easily sustain loads greater than their design loads, a codified method for quantifying this reserve capacity that accounts for the three-dimensional structural behavior does not exist. This state of practice is the overall motivation for this research. Cross-frames have been shown to significantly influence the load distribution behavior that leads to significant reserve capacity. Furthermore, it is also known that the role of cross-frames becomes more significant in skewed and curved bridges and also that the skew angle influences the reserve capacity. Thus, this research aims to quantify the forces in cross-frames of two in-service skewed, steel I-girder bridges and calibrate corresponding finite element models that accurately capture these forces.

Two bridges of varying skews, SR 1 over US 13 and SR 299 over SR 1, both located in New Castle County, Delaware, were selected for field testing. Cross-frames and girder locations were instrumented and the bridges were load tested with a weighed truck. Overall between the two bridges, the field tests captured data for 11 cross-frames and 6 girder locations. For the bridge with less skew, SR 299 over SR 1, the maximum bottom flange stress was 1.7 ksi while the maximum cross-frame stress is of similar magnitude, 1.5 ksi. For the more-heavily skewed bridge, SR 1 over US 13, the maximum bottom flange stress was 1.5 ksi while the maximum cross frame stress is more than double this value, 3.6 ksi. This suggests that the potential for cross-frame yielding is an important consideration in determining the reserve capacity of steel bridges.

Finite element models of each bridge were created and calibrated based on results from the field tests in order to accurately capture the forces in the structure. The finite element model for SR 1 over US 13 predicted stresses at bottom flange girder locations within 20% of the field test results. Cross-frames with a pinned connection to the stiffener were shown to result in the best representation of the cross-frame stresses, but future work is needed to further explore this connection. Hand calculations of the expected stress in the bottom flange according to American Association of State Highway and Transportation Officials specifications matched the finite element model for SR 299 over SR 1 well, but the bridge behavior captured during the field testing differs from conventional expectations. Further work is needed to identify the source of this unexplained behavior and more accurately calibrate this model. The knowledge gained from these efforts can be used in future work to more broadly study the three-dimensional behavior of steel I-girder bridges. Specifically, through calibrating a FEA technique in this work, additional finite element analysis exploring additional variables can be carried out in future work.

Chapter 1

INTRODUCTION

1.1 Motivation

Steel I-girder bridges are one of the most common bridge configurations in use today. Cross-frames are an important secondary member in this type of bridge, providing lateral-load resistance, improving live-load distribution, and reducing the buckling length of the compression flanges of the steel girders. They also provide redundant load paths, contribute significantly to a bridge's inelastic response, and contribute to its response to vehicular impacts. While it is known that bridges have the capacity to easily sustain loads greater than their design loads, a codified method for quantifying this reserve capacity that accounts for the three-dimensional structural behavior does not exist. In order to better understand and quantify the effect of lateral bracing on a bridge's response, additional research is necessary. Furthermore, it is also known that the role of cross-frames becomes more significant in skewed and curved bridges and also that skew influences reserve capacity. Therefore, two skewed bridges, one highly skewed and one moderately skewed, will be studied to investigate the cross-frame forces.

1.2 Objectives and Scope

The objective of this project is to quantify the forces in cross-frames via field testing of two in-service, skewed steel I-girder bridges and calibrate corresponding finite element models that accurately capture these forces in order to gain knowledge of the three-dimensional behavior of steel I-girder bridges. Specifically, one bridge is heavily skewed with a skew angle of 65 degrees and the other is moderately skewed with a skew angle of 32 degrees. Because skew has been shown to have a significant impact on a bridge's reserve capacity, these two levels of skew were chosen for study.

The work done to quantify these effects was completed in a number of tasks. First, the bridges were selected for field testing based upon key parameters such as skew, length, cross-frame type, and location. A finite element model for each bridge was then built and analyzed. The results of the finite element models were used to develop instrumentation plans for the bridges. Field testing under weighed truck passes was done in cooperation with the Delaware Department of Transportation (DelDOT). From the results of field testing and finite element validation, preliminary finite element models were refined in order calibrate the models to most accurately reflect these forces. Both the field testing and FEA results were used to assess the cross-frame forces in these two skewed steel I-girder bridges.

1.3 Thesis Outline

In the pages that follow is an investigation of cross-frame forces in skewed steel I-girder bridges. The highlights are the development of the finite element models as well as field tests of the two bridges. The material has been divided into the following chapters.

Chapter 2 presents the background of the project including a literature review of related research and a detailed description of the two bridges chosen for field testing.

Chapter 3 describes the steps taken in the development of the preliminary finite element models of the two bridges chosen for field testing.

Chapter 4 presents the field testing aspect of the project. It explains the instrumentation plan created for both bridges and the testing procedure. This chapter also includes results from the field tests.

Chapter 5 compares and calibrates the finite element bridge models with the field test data. A comparison of girder stresses for both bridges is included here. Because the SR 1 over US 13 model was deemed to be successfully calibrated for girder stresses, cross-frame data from the SR 1 over US 13 finite element model is also presented and evaluated.

Chapter 6 presents the conclusion of the research. This chapter also provides recommendations for future work for a larger parametric study on the cross-frames' effects on the reserve capacity of bridges.

Chapter 2

BACKGROUND

2.1 Literature Review

Cross-frames are an important secondary member in steel I-girder bridges. The American Association of State Highway and Transportation Officials (AASHTO 2010) LRFD Bridge Design Specifications define a cross-frame as a transverse truss framework connecting adjacent longitudinal flexural components. It defines skew angle as the angle between the centerline of a support and a line normal to the roadway centerline (AASHTO 2010). There are two main types of cross-frames: X-type or K-type. According to Bishara and Elmir (1990), intermediate cross-frames are primarily used in multibeam steel bridges as a means for lateral-load resistance, live-load distribution, and reduction of the buckling length of the compression flanges of the steel girders. Skew, cross-frame type, and cross-frame spacing, among other variables, are important considerations when investigating cross-frame forces as detailed in this section.

Researched have used finite element analysis to investigate the interaction between cross-frames and girders. Bishara and Elmir (1990) studied cross-frame forces in skewed steel bridges, looking specifically at X-type cross-frames in simply supported welded steel plate girder bridges with composite reinforced concrete decks with variable skew angles. This research determined that the effect of skew on the forces induced in cross-frame members may be neglected for skew angles less than twenty degrees. It was also found that the higher the skew angle, the higher the maximum forces that are induced in the cross-frame members. The investigation also concluded that increasing the cross-sections of the cross-frame members increases the internal forces in the cross-frames. It showed that the maximum compressive forces occurred in members attached to the ends of exterior girders situated at the obtuse angles of the bridge and maximum tensile forces occurred in the chord members at midspan. Bishara and Elmir (1990) used three-dimensional finite element analysis that using the computer program ADINA. They used triangular plate elements to discretize the concrete deck and beam elements to discretize the cross-frame members. Stringers were divided into two top and bottom halves. Each half is discretized as beam elements joined to the other half by steel link elements. The top halves of the stringers were connected to the slab plate elements by rigid link elements.

Wang and Helwig (2008) studied the influence of cross-frame orientation on cross-frame requirements in bridges with skewed supports, which they explain are more susceptible to large live load in cross-frames than bridges with normal supports. They performed computational studies on the torsional bracing behavior of steel girders with skewed supports using the three-dimensional finite element program ANSYS. They focused on two-, three-, and four-girder systems with lines of bracing oriented either parallel to the skew angle or perpendicular to the longitudinal axis of the girders. In most cases, transverse stiffeners were created using shell elements, while cross-frames were modeled using truss elements. The skew angles considered ranged from 0 to 45 degrees. Elastic material properties were used in analysis and three different types of loading were considered: uniform moment loading, a uniformly distributed load applied along the girder length, and a single point load applied at midspan. They found that for cases when the bracing is oriented perpendicular to the girder lines, the effects of the skew angle had little effect on the stiffness and strength requirements of the bracing. When the bracing was oriented parallel to the skew angle, the skew angle had a more significant impact on the stiffness and strength requirements of the bracing (Wang and Helwig 2008). Additional work by Wang et al (2011) showed that cross-frame forces can be less in bridges with staggered cross-frames.

Full scale bridge models have also been tested in a structural laboratory to determine the influence of cross-frames on load resisting capacity of steel girder bridges. Azizinamini et al. (1995) carried out full scale tests on a bridge built in the laboratory. The bridge was a 70 ft long simple span with a total width of 26 ft consisting of 3 welded plate girders 54 in. deep, built compositely with a 7 ½ in-thick reinforced concrete deck. By doing 12 different tests using this model, the researchers were able to vary the type of cross-frame (K or X), cross-frame spacing, and loading using the same girders. It was found that when both lanes of the bridge were loaded, when the truck load was applied straddling the bridge centerline, and when only one lane was loaded, the maximum strain in the girders was not significantly affected by the cross-frame type. Ultimately it was concluded that cross-frames had little influence on steel bridges with skews smaller than 20 degrees after construction. The influence of cross-frames on bridges with skews greater than 20 degrees was not investigated. Also, they concluded that simpler and cheaper forms of cross-frames such as the X-type provide the same good behavior as the more expensive K-type of cross-frame in bridges less than 20 degrees skew.

Research has also been done using the finite element method to analyze girder-diaphragm interaction. Tedesco et al. (1995) modeled an actual simply supported steel highway bridge with no skew located in Birmingham, Alabama. The deck slab was modeled with four-node shell elements to accurately represent membrane stresses, while the diaphragms were modeled with two-node beam elements. The objective was to determine whether or not diaphragms can be removed from an existing bridge. The finite element analysis was compared with actual field testing of the bridge in order to validate the model. It was discovered that the removal of diaphragms had a modest effect on bridge response, increasing flexural stress and vertical deflection for the most highly stressed girders by 8% and 9%, respectively.

Although this thesis focuses mainly on cross-frame forces in skewed bridges, there has also been research dealing with the influence of skew on ultimate capacity, which informs the selection of bridges to fit the motivation of this work. While investigating the ultimate capacity of skewed simple-span bridges, Bechtel (2001) evaluated six bridge models using the finite element analysis software ABAQUS with skews ranging from zero to seventy five degrees. The cross braces were placed at a maximum spacing of 25 feet and the length of the girder was held constant in order to keep the width to length ratio constant at approximately 1:5 which kept factors that affect longitudinal stiffness constant. Bechtel (2001) discovered that the magnitude of load causing yielding in each girder increases as the skew angle increases, but there is no significant contribution until the skew is greater than sixty degrees when the bridge begins to behave differently and load redistribution is different. From this research, it was ultimately discovered that large skews have a significant beneficial effect on the reserve capacity of a bridge. Other researchers, such as Fell and Kanvinde (2010), who conducted several large scale tests on bracing members undergoing seismic loading, have explored how cross-frame bracing aides seismic design along with other considerations.

Other researchers have looked at more specific cross-frame detailing. Quadrato et al. (2010) looked specifically at cross-frame connection details and discovered that many states use a bent plate for this connection since code provisions require end cross-frames to be aligned parallel to the skew angle. The research explains that although cross-frames can often represent an expensive component per unit weight on a bridge due to fabrication complexities and construction fit-up issues, they are essential to the stability of steel girder bridges during construction. Finite element analysis was then used to investigate how the cross-frame connection affected the bracing behavior of the bridge and how it could be possibly altered to reduce cost.

The influence of cross-frame placement and skew angle in steel bridges subject to distortion-induced fatigue has also been investigated. Hartman et al. (2010) conducted forty high-resolution, three-dimensional finite element analyses of a bridge with multiple cross-frame and skew arrangements in order to study the relationships between skew angle, cross-frame placement, and distortion-induced fatigue stresses. In the models, skew angles of 0, 20, and 40 degrees were used with cross-frames spaced at 15 ft and 30 ft. Each model was composed of a deck, girder top flanges and concrete haunch, girder webs, girder bottom flanges, and cross-frames with element types, mesh sizes, and boundary conditions remaining constant among all the models. The loading consisted of one AASHTO fatigue truck placed to induce maximum positive moment on the east span of the two-span continuous bridge. Ultimately, they found that in bridges with cross-frames placed parallel to the skew angle, increased cross-frame spacing slightly increased the maximum principle web-gap stress. They found that in bridges with staggered cross-frames, the web-gap stresses were not found to increase proportionally with skew angle.

Numerical models of continuous, skewed, steel bridges have also been created to study the effect of lateral-torsional buckling during deck placement and the role of cross-frames in deck placement. Liu and Chajes (2008) studied a 63 degree four-span continuous plate girder bridge made with high performance steel (HPS) with three spans of 199.25 ft and one span of 175 ft. It had K-shaped cross-frames designed parallel to the skewed supports. They created two three-dimensional finite element models using ANSYS with the girders and wet concrete represented as shell elements and the cross-frames as frame elements. When investigating the deck pour sequence, the hardening concrete was assumed to have 10% of its fully cured modulus of elasticity. From their research, they discovered that the deck pour sequence on skewed bridges could be adjusted to avoid complications with lateral-torsional buckling. Fasl et al. (2009) commented on how buckling capacity is improved for lateral torsional buckling of steel plate girder bridges during deck placement by providing bracing in the form of intermediate cross-frames and made recommendations to be implemented in the design of three bridges in Texas.

Investigation of cross-frame forces will help to provide a better understanding of bridge service and reserve capacity. Research has shown that skew angle is an important factor in a bridge’s response, but more research to understand the behavior at inelastic load levels is needed. Therefore, two skewed bridges will be investigated for this research. Other variables such as cross-frame spacing and cross-frame type were also considered as a result of this study. K versus X shaped cross-frames were not found to be significant; therefore we can include both in this study. Cross-frame spacing has a larger influence than cross-frame type; therefore an attempt was made to keep this variable as constant as possible between the two bridges considered. The work from this project will help to quantify cross-frame forces under truck loadings as well as enhance the knowledge of the influence of cross-frames on the reserve capacity of steel I-girder bridges.

2.2 Bridge Descriptions

The two bridges presented in this thesis were chosen by considering the ideas presented in the literature review and bridges available for testing in Delaware. Many of Delaware's bridges that were good candidates for this study intersected Interstate 95, a main highway on the East Coast. The traffic control to field test these bridges was considered too difficult; therefore any bridges that crossed or contained I95 were not considered for this study. After these bridges were removed from consideration, the number of steel I-girder bridges left was limited. It was decided to pick a moderately and a heavily skewed bridge in order to assess a range of skews. Because the difference between cross-frame shapes was not found to be significant, both K shaped cross-frames and X-shaped cross-frames were considered in this study. Two bridges of relatively the same length and span configuration were also desired. When taking all these restrictions into considerations, SR 1 over US 13 and SR 299 over SR 1 were chosen for study and are described in the following subsections.

2.2.1 SR 1 Over US 13

SR 1 over US 13 is a 65 degree skew steel I-girder bridge on Delaware State Route 1. Twin spans carry the north- and southbound lanes. The tested bridge carries the southbound lanes of State Route 1 over U.S. 13 approximately 5 miles south of the Chesapeake and Delaware Canal in Delaware, immediately south of Road 423 and just north of Boyd’s Corner, Delaware. Figure 2.1 indicates the location of this bridge. It consists of two continuous spans of equal (165 feet) lengths as seen in photograph in Figure 2.2 and in plan in Figure 2.3. Figure 2.4 demonstrates a plan view of the bridge. There are five girders spaced 9’- 6” on center with exterior girders spaced 2’-10” and 3’- 10” away from the outer edge of the bridge parapets on the west and east sides, respectively, as seen in Figure 2.5. Therefore, the total width of the bridge is 44’-8”, carrying two 12’ lanes, a 12’ shoulder on the west side, and a 6’ shoulder on the east side, while also having parapets 1’-4” in width on each side of the bridge. A girder elevation view is included in Figure 2.6.

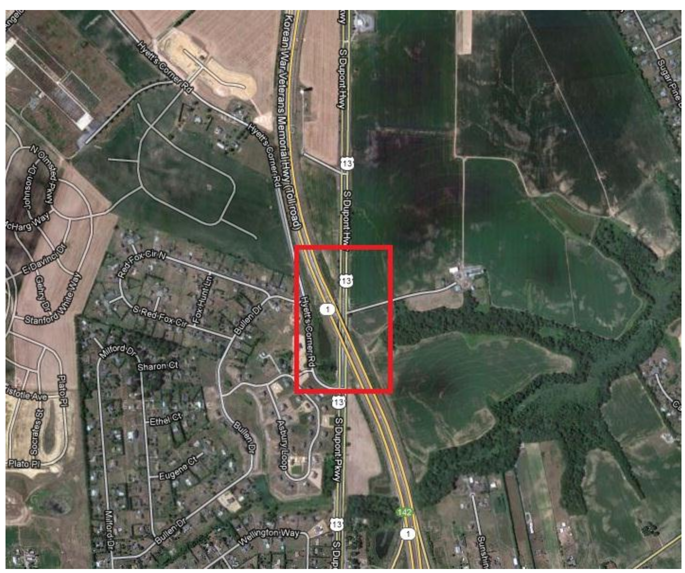

Figure 2.1 Satellite View of SR 1 Over US 13 (Google Maps, 2012)

Figure 2.2 Photograph of SR 1 Over US 13, Elevation View

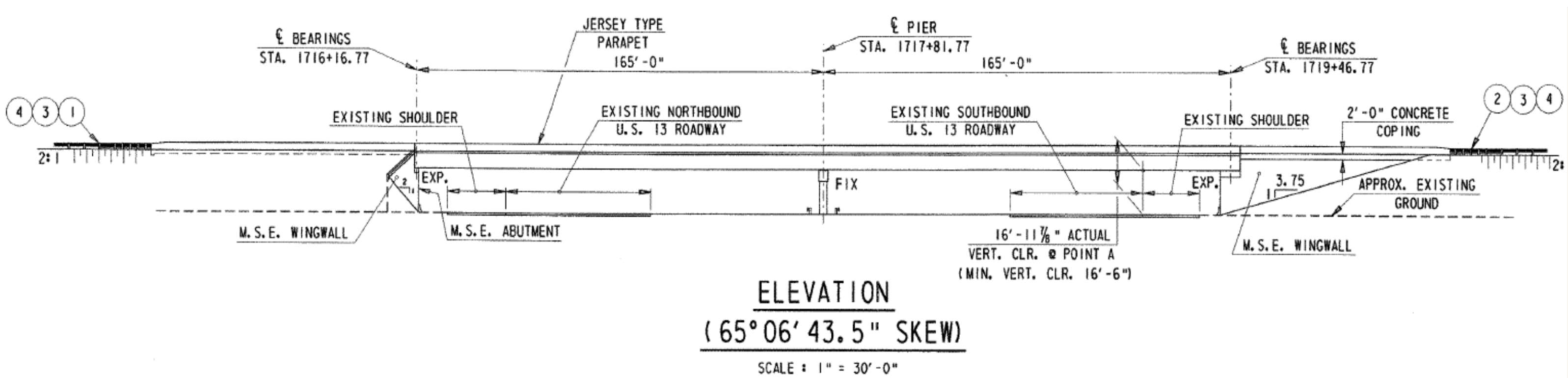

Figure 2.3 SR 1 Over US 13 Elevation View

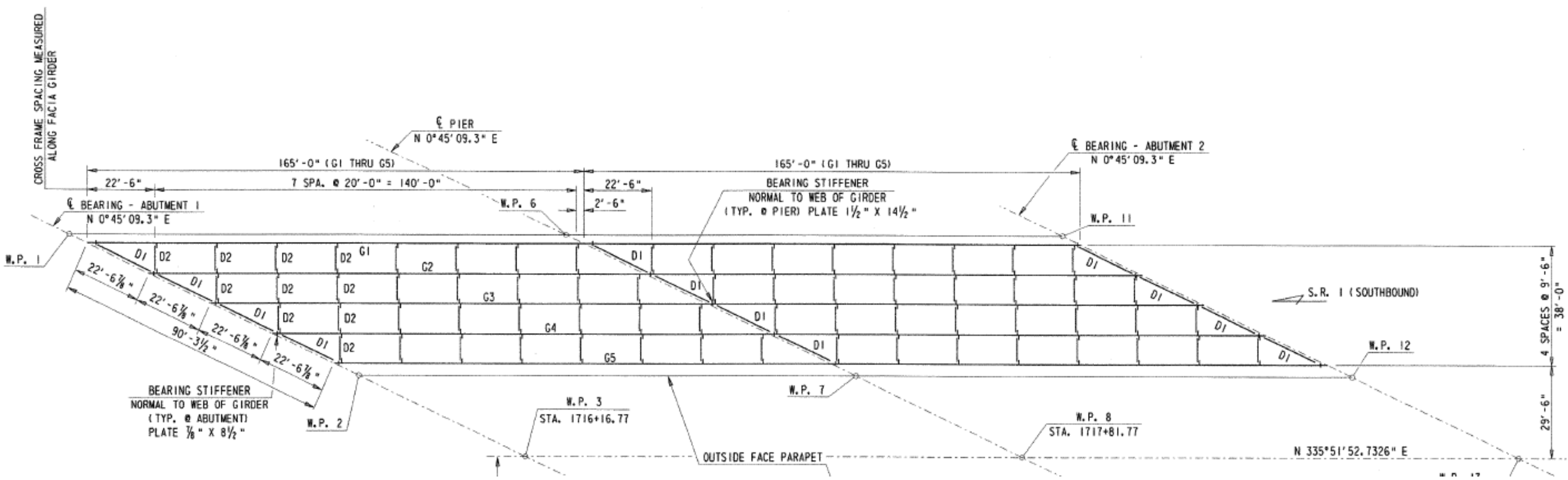

Figure 2.4 SR 1 Over US 13 Plan View

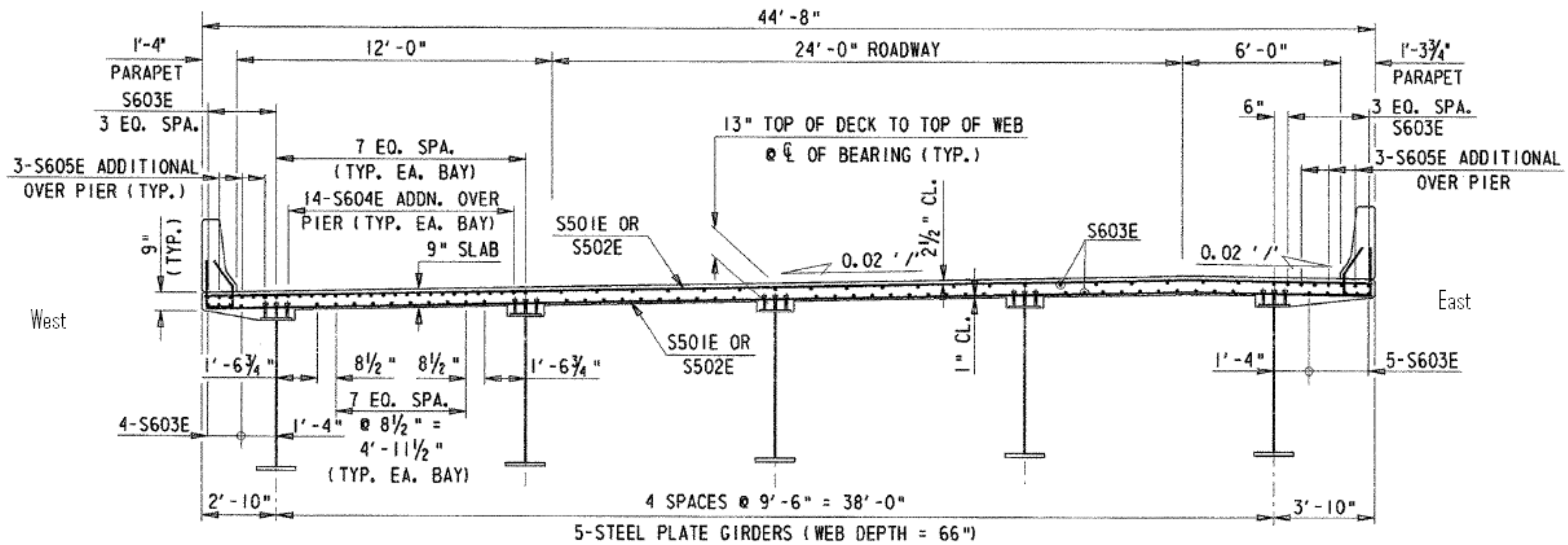

Figure 2.5 SR 1 Over US 13 Cross-Section View

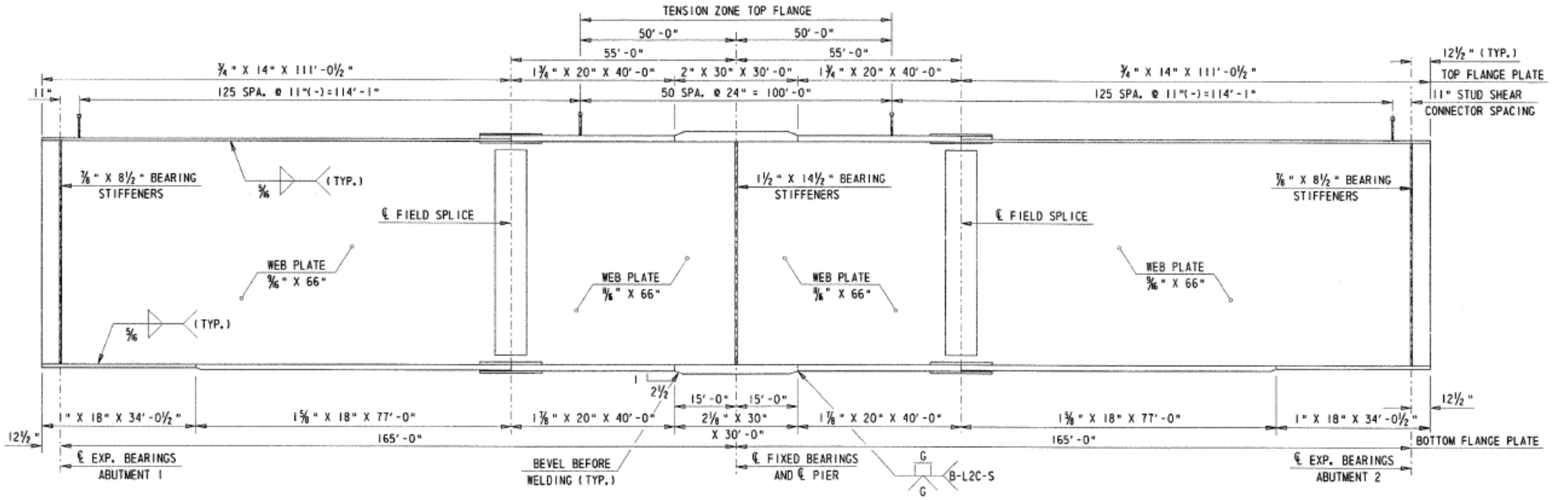

Figure 2.6 SR 1 Over US 13 Girder Elevation View

As represented in Figure 2.7, X-type cross-frames are used to laterally brace girders of the bridge and are spaced 20 feet on center with the exception of the first cross-frame from the end and the first cross-frame from the support which are spaced at 22'- 6" on center. As seen in Figure 2.7, the cross-frames consist of two 3 ½ x 3 ½ x 3/8 inch steel angles that comprise the inclined members of the cross-frame and a 4 x 4 x ½ inch steel angle serves as the bottom chord. The two inclined members are bolted at their intersection by a ½" x 6" x 1'- 1" fill plate. All of the angles are bolted to the girders with Type 1, 7/8" diameter A325 high strength mechanically galvanized friction bolts via a ½" x 10" connection plate fillet welded along the full height of the web. The cross-frames are seen in photograph in Figure 2.8.

All structural steel is AASHTO M270 Grade 50 (F_y = 50,000 psi) painted with a urethane paint. The steel girder is composite with the bridge deck.

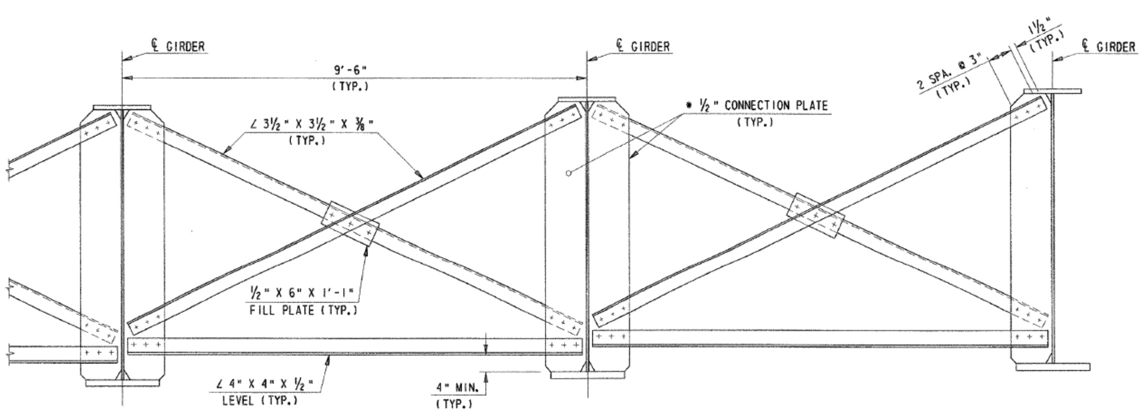

Figure 2.7 SR 1 Over US 13 Intermediate Cross-frame Detail

Figure 2.8 Photograph of SR 1 Over US 13 Cross-frames

2.2.2 SR 299 Over SR 1

SR 299 over SR 1 is a 32 degree skew steel I-girder bridge on Delaware State Route 299 over Delaware State Route 1. It is located in the Middletown-Odessa area of Delaware, approximately 9 miles south of the Chesapeake and Delaware Canal in Delaware. Location is shown in Figure 2.9. It consists of two spans, of 128 feet and 134 feet, as seen in photograph in Figure 2.10 and in plan in Figure 2.11. Figure 2.12 demonstrates a plan view of the bridge. There are eleven girders in the cross-section, spaced 9'- 1" with exterior girders spaced 2'-11" away from the outer edge of the bridge parapets, as shown in Figure 2.13. Therefore, the total width of the bridge is 95'-11", carrying four 12' lanes of traffic, two 12' outside shoulders, a 22' median and turning lane which varies position along the length of the bridge, and two 1'-4" parapets. A girder elevation is included in Figure 2.14.

Figure 2.9 Satellite View of SR 299 Over SR 1 (Google Maps, 2012)

Figure 2.10 Photograph of SR 299 Over SR 1, Elevation View

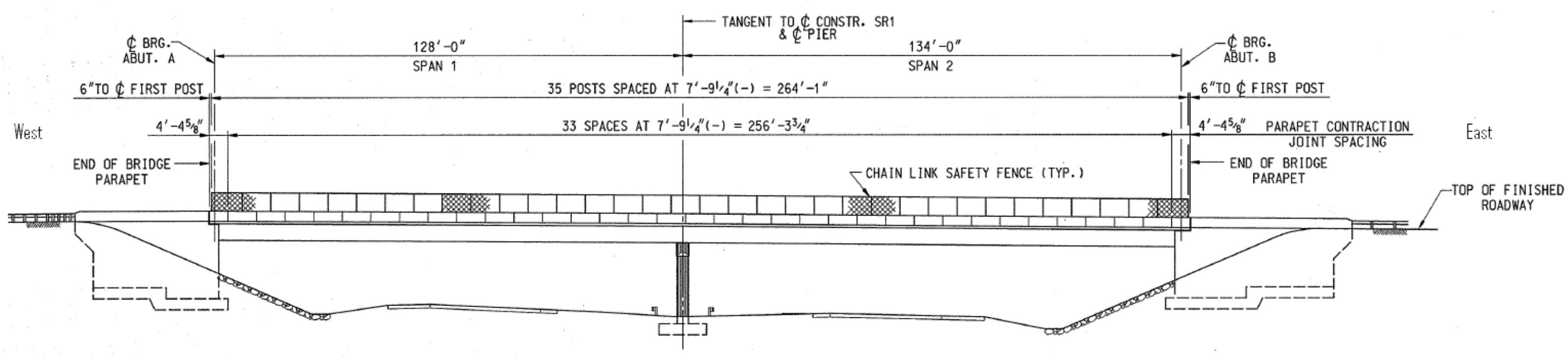

Figure 2.11 SR 299 Over SR 1 Elevation View

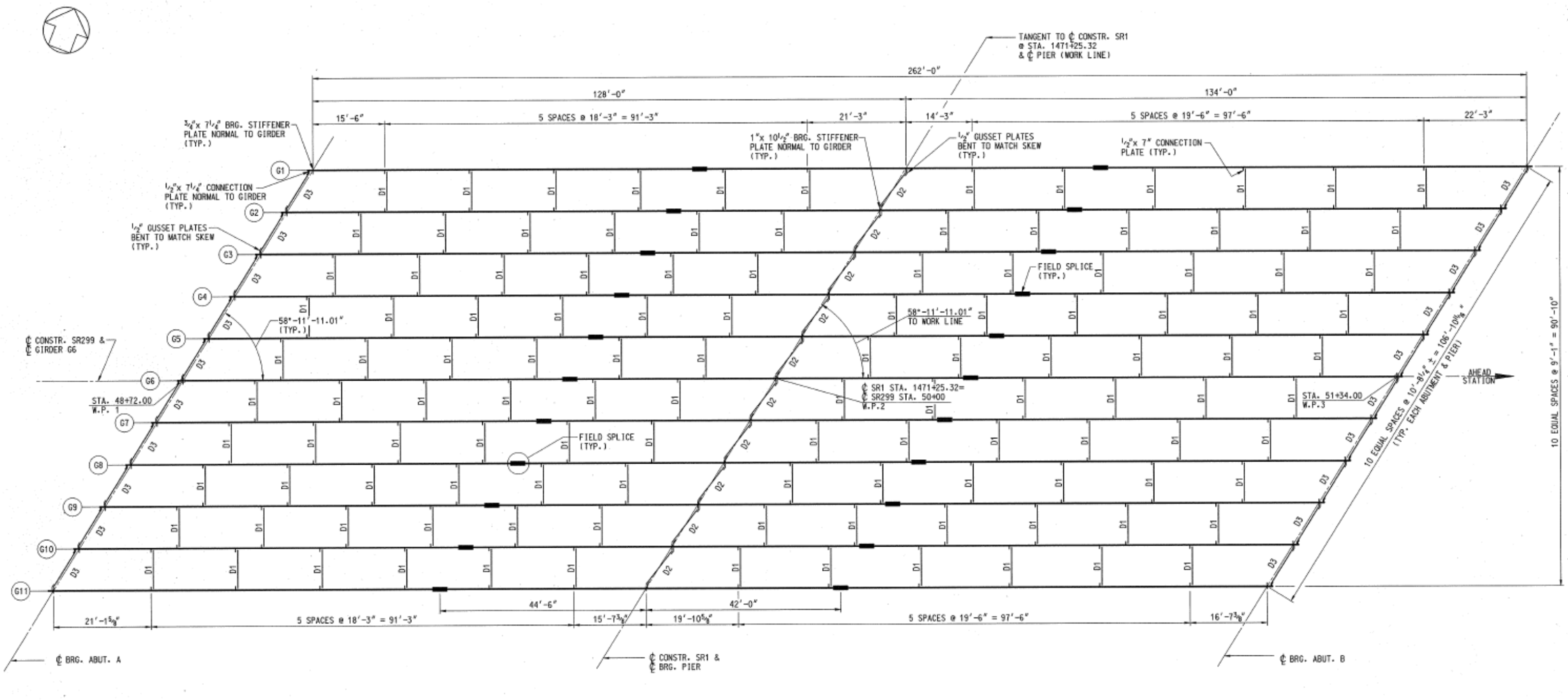

Figure 2.12   SR 299 Over SR 1 Plan View

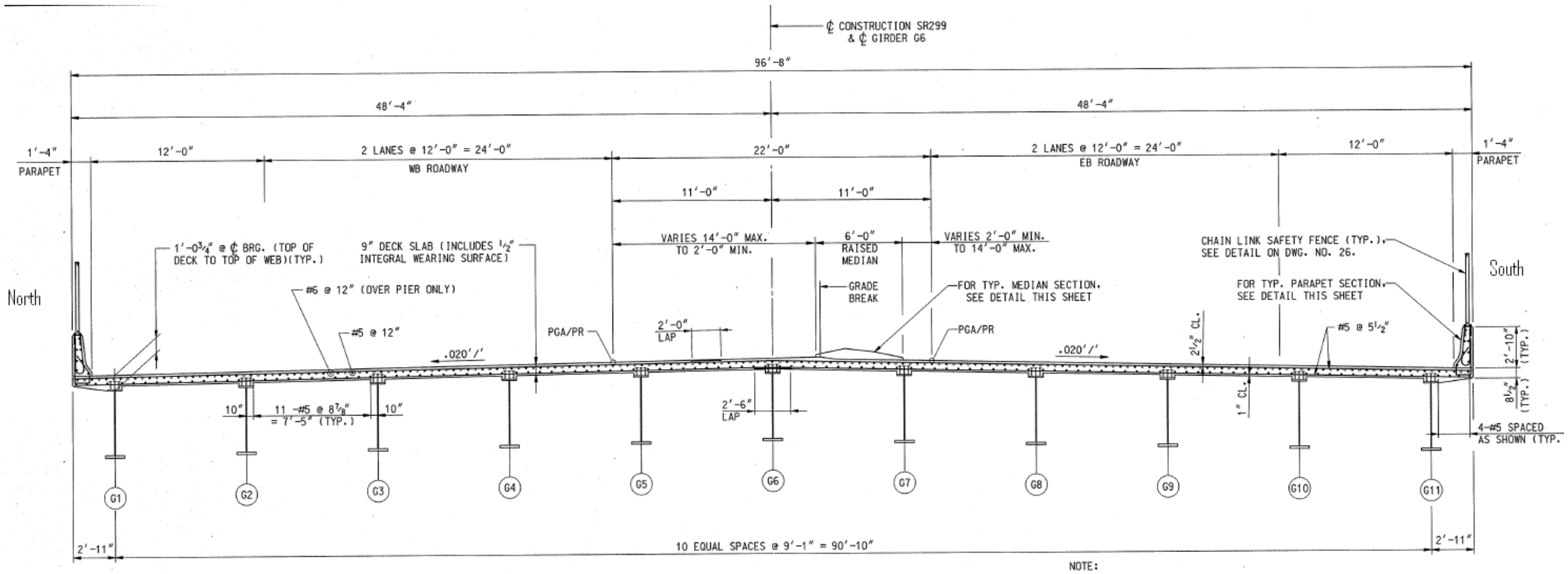

Figure 2.13 SR 299 Over SR 1 Bridge Cross-section

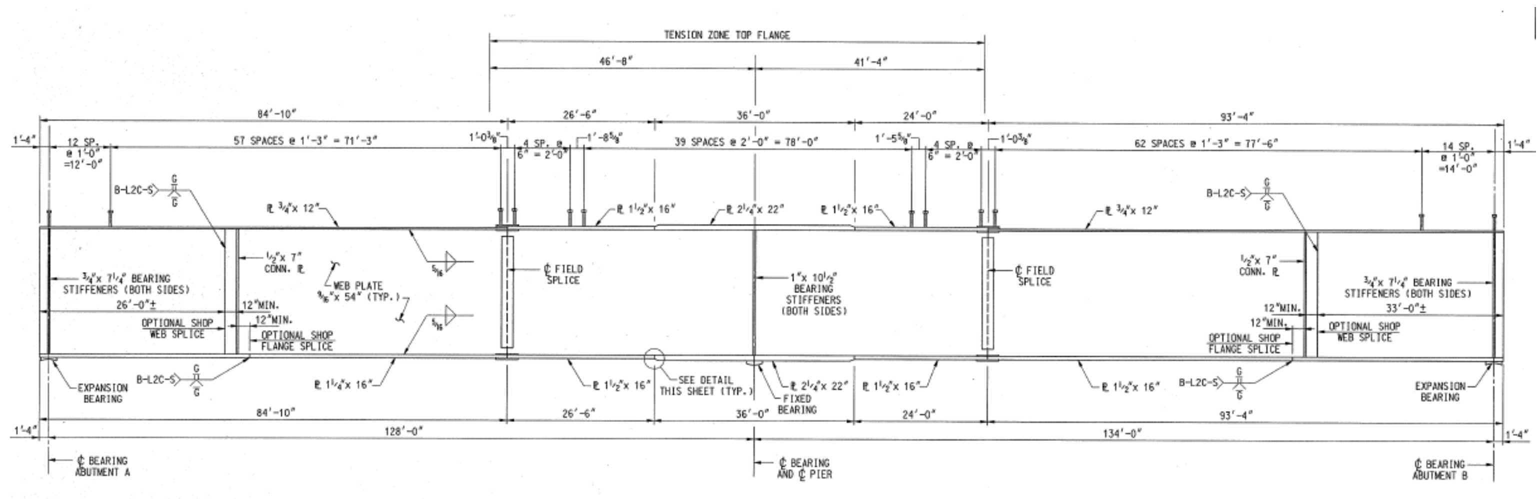

Figure 2.14 SR 299 Over SR 1 Girder Elevation

As represented in Figure 2.15, K-type cross-frames are used to laterally brace the girders of the bridge and are spaced 18’- 3” on center on the west span and 19’ – 6” on the east span with the exception of the first cross-frame from each support, where the spacing varies (see Fig. 2.12). As seen in Figure 2.15, the typical cross-frames consist of two 3 ½” x 3 ½” x 3/8” steel angles that comprise the inclined members of the cross-frame and one 4” x 4” x ½” steel angle that serves as the bottom chord. The two steel angles of the inclined members are welded with a 5/16” fillet weld on both sides to a 1/2” gusset plate, which is also connected by a 5/16” fillet weld on both sides to the midspan of the bottom chord. All fillet welds are at least 4” in length. All of the angles connected with 5/16” fillet welds to ½” gusset plates that are connected to the ½” x 7” connection plate fillet welded to the girders along the full height of the web.

All structural steel is AASHTO M270 Grade 50 (F_y = 50,000 psi) and is painted. The cross-frames are seen in photograph in Figure 2.16.

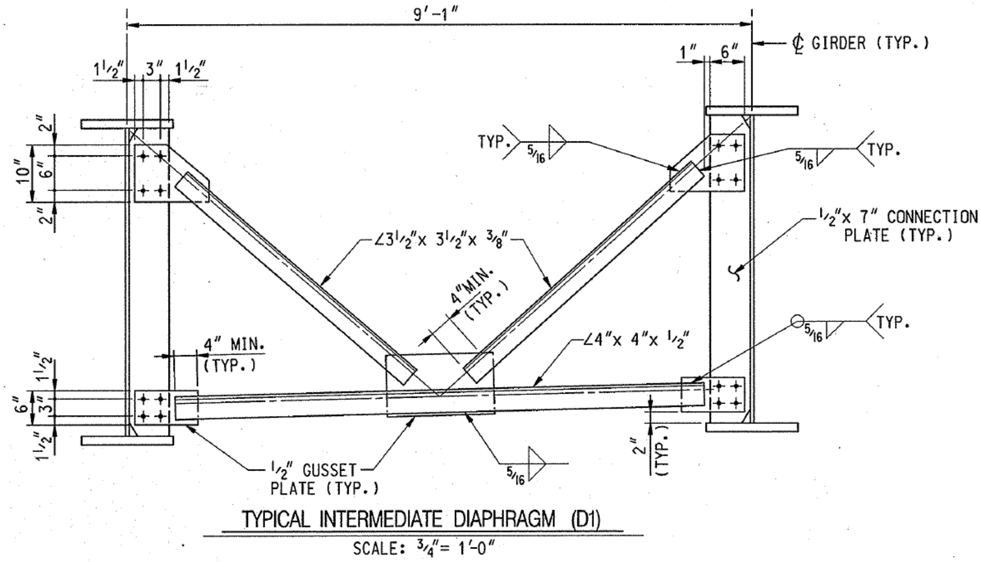

Figure 2.15 SR 299 Over SR 1 Intermediate Cross-frame Detail

Figure 2.16 Photograph of SR 299 Over SR 1 Cross-frames

Chapter 3

FINITE ELEMENT MODELING

Finite element analysis (FEA) is a numerical technique for finding approximate solutions of partial differential equations, often done as a computer simulation in engineering analysis. For this project, computer-aided modeling was employed to create and analyze finite element models for each of the bridges studied. This section describes the development of the finite element models for the two skewed bridges described in Section 2.2. For this work, AutoCAD was used to create the basic geometry, the commercial software Femap 10.1.1 was used for pre-processing, and ABAQUS 6.9-2 was used for analysis and post-processing.

3.1 Geometry

The geometry of each bridge was first created based on structural plans provided by DelDOT. It was initially drawn using the software program AutoCAD. Here the coordinate system was oriented with the structural components of the bridge so that the z-axis aligned with the length of the bridge, x-axis was aligned with the transverse direction, and the y-axis was aligned with the vertical direction. Main structural components of the bridge used to make the superstructure model included girders, concrete haunches, a reinforced concrete deck, and parapets. These components were connected together with cross-frames and stiffeners serving as connection plates. Figure 3.1, below, demonstrates an example of the base geometry drawn in AutoCAD.

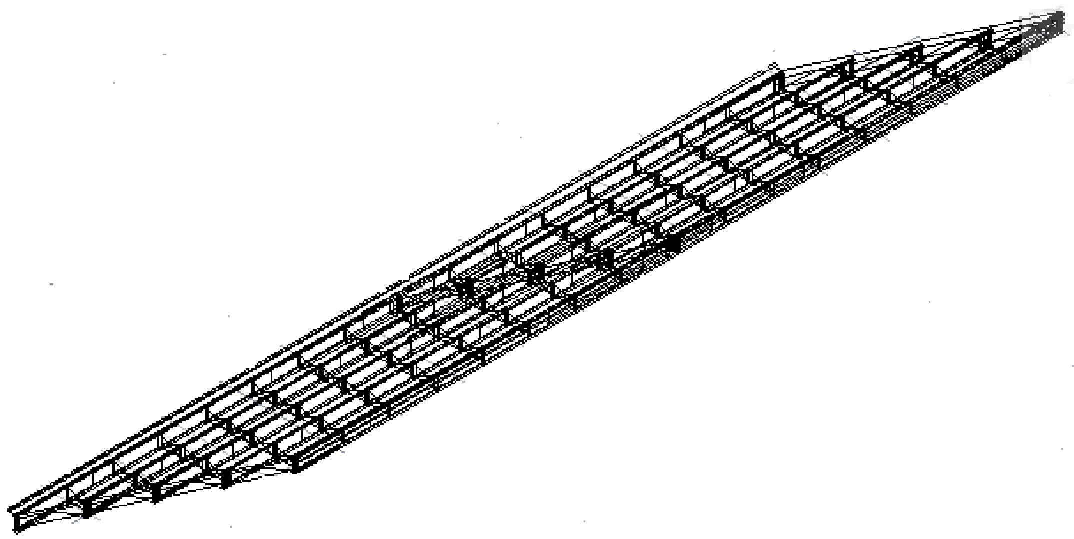

Figure 3.1 Base Geometry for SR 1 Over US 13 in AutoCAD

Once the basic geometry was completed in AutoCAD, it was then imported into Femap to begin the next stage of the model construction. As will be discussed in Section 3.2, material properties were assigned to the different components drawn in AutoCAD and surfaces were created to make up each component. The surfaces were then meshed to form elements.

3.2 Elements

The girder flanges and webs, stiffeners, haunch, and parapet were modeled using 4-node, reduced integration shell elements, labeled as type S4R in ABAQUS. The deck was modeled with both 4-node (S4R) and 3-node (S3R) reduced integration shell elements; 4-node elements were generally used but 3-node elements were needed at the ends of the bridge to accommodate the skew angle. Shell elements have displacement and rotational degrees of freedom. Reduced integration elements contain one integration point for three- and four-node elements, thus they can greatly reduce computing time, and have been shown to better correlate to actual performance of steel bridge girders.

Cross-frame members were modeled using beam elements. A beam element is a one-dimensional line element in three-dimensional space. These two-noded elements contain 3 translational and 3 rotational degrees of freedom at each node. Beam type B31 in ABAQUS, which is a beam element in space that uses linear interpolation, was used. The material and cross-sectional properties corresponding to each of the beam elements were created by defining specific dimensions on a standard section, such as an angle provided by Femap, and were based on the structural plans provided by DelDOT. The beam elements are defined by an orientation vector perpendicular to the element in the upward direction based on how the angle was defined. This orientation vector can be complicated by the angle of the angled portions of the cross-frames where the orientation vector contains definitions in three directions.

The girder, haunch, and deck were connected using rigid links. Multiple point constraint (MPC) beams were used to link the elements of the top flange and the haunch as well as the haunch and the deck. In order for this connection to be made, the mesh was carefully created so that deck nodes were transversely aligned along the centerline of the girder and haunch and the longitudinal coordinates of all nodes to be connected were identical. The MPC elements then equate the displacement and rotation at the slave node to the displacement and rotation at the master node. The rigid links conceptually model the composite action between the slab and girders in the bridges.

Linear elastic material properties were defined for the models. Elastic properties were input for both the concrete and the steel. Concrete in the preliminary models was defined with a modulus of elasticity of 4,286,830 psi (5 ksi strength) and a Poisson's ratio of 0.2. Steel was defined with a modulus of elasticity of 29,000 ksi and a Poisson's ratio of 0.32.

3.3 Mesh Generation

A critical part of the finite element model is the size and number of elements used to discretize the different components of the bridge. This can have a large effect on the accuracy of the model as well as the time and amount of memory it takes to process the analysis. Larger element sizes reduce the number of degrees of freedom in the system, and thus the computation time. On the other hand, a finer mesh is required in order to provide higher accuracy up to the point where convergence is achieved. The size of the elements was selected in order to evenly divide the girders and was consistent with element sizes that have been validated in previous research. Therefore, the mesh size was carefully considered while developing the finite element models for each of the bridges.

In order to utilize the rigid links to connect the girder, haunch, and deck, it was critical that the nodes along the centerline of each of these elements lined up vertically along the entire length of the structure. When initially planning the mesh, it became clear that this was going to be a difficult task. Non-uniform spacing in some locations of the bridge of the transverse stiffeners on the webs of the girders and changes in girder geometry along the length of the bridge caused a need for the element size along the length of the girder to vary so that the node in the flanges and web align with the nodes in the transverse stiffeners. In order to solve the problem, the beam was broken down into sections (or surfaces, to use Femap terminology) based on the locations of the web stiffeners; then each section was independently meshed in order to assure alignment between the flanges, web, and transverse stiffeners. Subsequently, the deck was also broken down into similar sections in order to assure alignment. Finally, the parapet was meshed to match the size of the deck elements so that it too could be connected with rigid links. Large skews cause elements to be misaligned with each other, especially in the deck which is not square where elements end up being aligned with the skew. In order to solve this problem, portions of the deck above the girders were aligned in sections with the top flange in order to assure vertical alignment of nodes. The portion of the deck between the girders was then meshed to align with the skew of the bridge. Efforts to find a way to keep all deck elements square and not aligned with the skew were unsuccessful. This process required several iterations in order to find a mesh size that would not only allow for these elements to be connected, but produce a mesh that was not too fine that it required a large amount of computer memory to process and was consistent with element sizes validated in previous research. In several cases, mesh sizes had to be reconsidered when the density of the mesh caused the computer to slow to the point where it would not function.

In general, two elements were used along the width of the flanges except at the sections with the largest flange width for each bridge where four elements were used along the width of the flanges to keep element sizes consistent and aspect ratios close to 1. For the SR 1 over US 13 model, 8 elements were used along the height of the web. For the SR 299 over SR 1 model, 10 elements were used along the height of the web. These element spacings were chosen to be consistent with element sizes validated in previous research (Ross 2008 and Michaud 2011) and to keep aspect ratios close to unity. All elements used in the girders were rectangular in shape, but element sizes were chosen in an effort to keep the aspect ratio of the elements as close to unity as possible, which generally yields the best results. The spacing produced elements with aspect ratios ranging between 0.85 and 1.2, changing in the various sections that were created in order for the mesh to align with the transverse stiffeners.

10 elements were used along each of the inclined members of the X-shape cross-frames in the SR 1 over US 13 model, while 8 elements were used along each of the inclined members of the K-shape cross-frames in the SR 299 over SR 1 model. In both models, 10 elements were used along the bottom chord of the cross-frame. These spacings were chosen to conform to previously validated research and to capture locations of where gauges may be placed in field testing. The transverse stiffeners were meshed to align with the mesh of the web and where the cross-frames were bolted to the stiffeners. The elements were more rectangular in shape than the elements used in the flanges and web with aspect ratios closer to 0.4 for the SR 1 over US 13 model and closer to 0.8 for the SR 299 over SR 1 model due to differences between the two bridges in sizes of stiffeners and how the cross-frames framed into them. The beam elements that represent the cross-frames were connected to the transverse stiffeners by merging the node from the beam element with the node located on the mesh of the transverse stiffener where the cross-frame is bolted.

3.4 Boundary Conditions

After the mesh was generated and material properties were added, appropriate boundary conditions had to be specified for each of the models. These were specified along the line of nodes along the width of the bottom flange of each girder at each of the bridge supports. For the initial models, translation in the transverse and vertical directions were constrained at the two supports at either end of the bridge representing a roller bearing and translation in the transverse, longitudinal, and vertical directions were constrained at the support located at the longitudinal center of the bridge between the two spans, representing a translation-fixed bearing. These were representations of the actual support conditions of both bridges which had expansion bearings at both ends of the bridge and a translation-fixed bearing at the center support, between the two spans. At the center node of the line of nodes along the bottom flange of the middle girder at the support located at the longitudinal center of the bridge, translation was constrained in all three directions and rotation was constrained in the longitudinal and vertical directions.

3.5 Loading

The final step before analyzing the model in ABAQUS is to apply the loading. For the preliminary models, the loading was based on a standard truck loading (AASHTO HS-20), shown in Figure 3.2, consisting of a front axle of 8 kips spaced fourteen feet from the two rear axles, each 32 kips, spaced fourteen apart. When calibrating the models, the truck loading present during field testing was used. In both cases, the truck was modeled using six point loads (one to represent each wheel) with a pair of equal magnitude point loads spaced six feet apart transversely to comprise each axle. These point loads were applied to the deck nodes.

For the preliminary analysis used to construct the instrumentation plans for field testing, four different load cases for SR 1 over US 13 were investigated for dead load plus live load: the first three with the truck loading centered over the center support 2 feet from the left parapet, 2 feet from the right parapet, and with the right line of truck wheels centered on the lane boundary and the last with the centroid of the truck loading positioned at 40 % of the span length from the abutment and 2 feet from the left parapet. The latter case is intended to produce the maximum moment in Girder 4, while the former provide additional information about the cross-frame response. The first three were determined by finding the maximum negative and positive moment positions using the HS-20 truck loading for girders 1, 3, and 5. The fourth case is based on the theoretical position for maximum positive moment. For the preliminary analysis of the SR 299 over SR 1 model, three different load positions were investigated under dead load plus live load and live load only. The three positions were the truck loading in the obtuse corner of the bridge between girders 9 and 10 approximately 10’ from the end of the bridge, the centroid of the truck loading positioned at 40 % of the length of the 134’ span between girders 5 and 6, and the truck loading centered over the center support of the bridge. These load cases were investigated to represent three known severe loading types: load in the obtuse corner of the bridge, loading causing maximum positive moment, and loading over the location experiencing maximum negative moment. Because forces have been shown to be higher in the obtuse corner of skewed bridges, the obtuse corner load case was added. Dead load was applied in the negative vertical direction as a gravity load by adding material densities to the models. The results from the live load only case are more relevant to determining instrumentation plans since only these results will be captured by the field instrumentation.

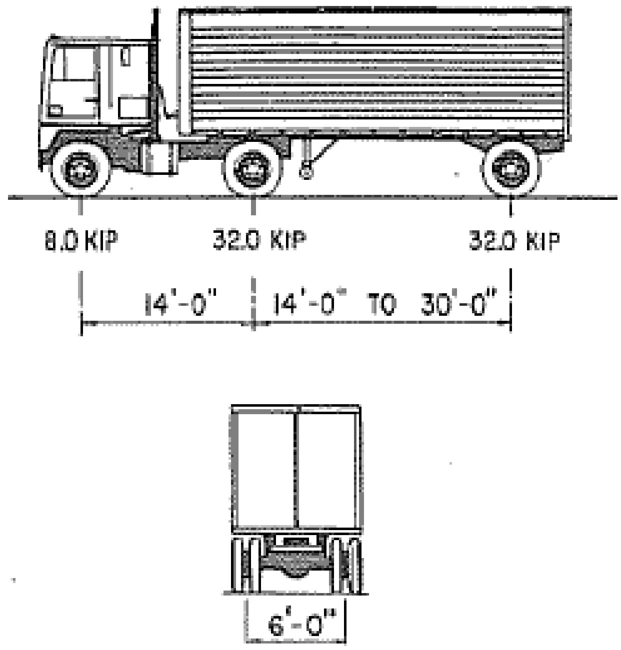

Figure 3.2 HS-20 Truck Loading (AASHTO 2010)

3.6 Analysis

After all of the modeling was completed, Femap was used to create an ABAQUS input file. This converts all the information that was inputted through Femap into ABAQUS language. This input file can then be processed using the analysis program ABAQUS. Visual inspections were performed on the output to ensure everything was connected, that stresses were in the correct range of magnitude, and that the relative magnitudes of stress displayed in various elements were logical. The analysis was an implicit analysis which means the dependent variables were defined by coupled sets of equations and solved through an iterative technique. It was also a linear-elastic, static analysis which means elastic material properties were defined, geometric non-linearity was ignored, and non-moving point loads were used.

3.7 Future Work Considerations

There are several things to be considered for any future work done on this project. First, the amount of available memory and computing power of the computers being used for modeling and analysis should be considered. Remeshing, if possible, can be a solution to this problem. In several instances in both bridges during the modeling of these two bridges a finer mesh was considered for the transverse stiffeners in order for the aspect ratio to become closer to 1 while keeping nodes at the desired locations for connection with the cross-frame elements, but was unable to be used due to limitations with available RAM and memory on the hard drive of the computers being used.

Other considerations arise when looking at the stiffeners and the manner in which they were modeled. First, the mesh of the stiffeners and the influence of this refinement should be investigated to determine a refined manner in which to model them. This can be done in a number of ways, one of which will be discussed. First, the aspect ratio of the elements that comprise the stiffeners is approximately 0.4 in both bridges, as discussed in Section 3.3. This result occurred in order to have a node exist at the actual location at the center of the bolt group where the cross-frames were bolted to the stiffeners and maintain a mesh size within the limitations of the available computing power; thus, the elements became more rectangular and less square in shape. If RAM and computer hard drive memory was increased, the mesh on the stiffeners could be made finer and the aspect ratio could be made closer to one, making the elements more square in shape. The influence this may have on the accuracy of the cross-frame forces is unknown. This change is not expected to have a significant influence on the results for other member types.

Separation between the nodes on the stiffener and the web should also be investigated. Currently, the number of elements along the height of the stiffener is twice as many as the number of elements along the height of the web. Therefore, every other node along the height of the stiffeners is not connected to the web which can cause separation between the web and the stiffeners in some cases. This was investigated and not found to be a problem with the models completed in this project, but it is an important consideration to note for any future work.

Chapter 4

FIELD TESTING

Two bridges of varying skews, SR 1 over US 13 and SR 299 over SR 1, both located in New Castle County, Delaware, were selected for field testing. SR 1 over US 13 is a 65 degree skew bridge with X-type cross-frames, while SR 299 over US 13 is a 32 degree skew bridge with K-type cross-frames. Between both bridges, 11 different cross-frames and 6 different girder locations were instrumented using BDI ST-350 strain transducers. Gauges were clamped at cross-frame and bottom flange locations and bonded at web locations. The bridges were loaded with multiple passes of a weighed test vehicle provided by the Delaware Department of Transportation (DelDOT). A bucket truck was also provided by DelDOT to facilitate gauge installation. They also facilitated lane closures in order to ensure safe access to all testing locations. This chapter explains the choice to use the BDI strain transducers, the instrumentation layouts for both bridges, and the loading of the bridges used for testing. It also highlights how the data from the tests was processed, presents the data, and includes recommendations for future similar field tests.

4.1 Gauge Type and Data Collection

BDI ST-350 strain transducers and their associated structural testing system were used in field testing. BDI strain transducers are bigger and easier to handle and install than traditional foil type gauges. The ease in installation stems from their ability to be clamped in place on cross-frame angles and flanges, eliminating the need from fastening through welds or adhesives. This ease in installation was the primary criteria leading to the selection of this testing system since both bridges that were tested serve as highway overpasses. Thus, installation time was critical because lane closures were necessary to install much of the instrumentation and minimizing lane closure time was of importance.

Figure 4.1 demonstrates two BDI strain transducers clamped onto respective legs of a cross-frame angle. When clamping was not possible, which was the case at web locations, steel tabs were connected to the gauges using small bolts and bonded to the steel surface using an adhesive. Surfaces were grinded to remove paint prior to installation of the gauge to ensure proper adherence when gauges were bonded. Figure 4.2 demonstrates a BDI strain transducer bonded to a girder web.

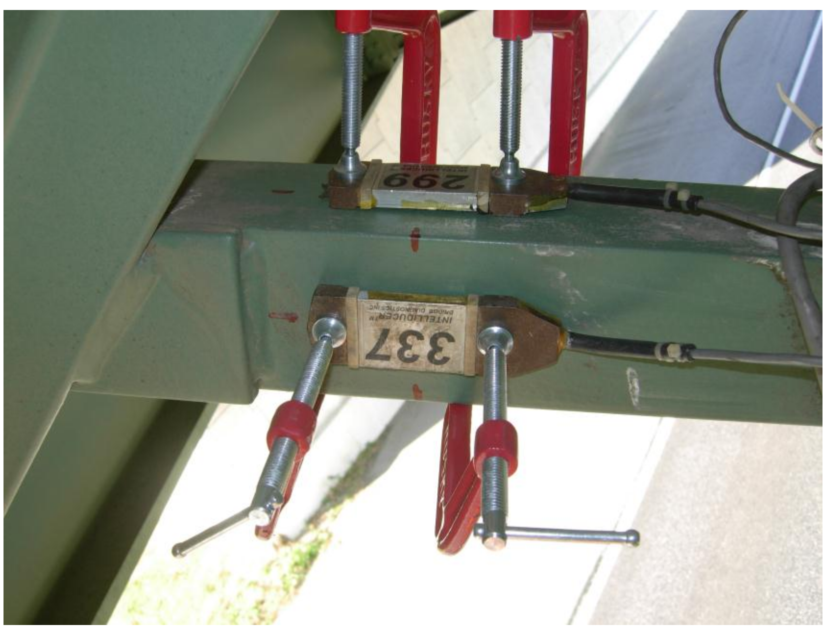

Figure 4.1 Clamped BDI Strain Transducers

Figure 4.2 Bonded BDI Strain Transducer

The BDI strain transducers have a strain range of ± 4000με and are individually calibrated to ± 2 % per NIST standards (Bridge Diagnostics, 2006). A calibration certificate is provided by the company with each transducer. Each strain transducer is a full Wheatstone bridge with four active 350W foil gauges and a four wire hookup (Bridge Diagnostics, 2006). Bridge Diagnostics, Inc. supplies each transducer with an identification number and a calibration factor that are incorporated into the data acquisition system in order to ensure accuracy of results.

4.2 Instrumentation Layout

The field testing equipment at the University of Delaware has the capability to record 36 strain transducers at one time; therefore it was decided to conduct each bridge test in two phases utilizing all or most of the strain transducers in each test in order to maximize the amount of data that could be recorded at each bridge. Two days were allotted for testing at each bridge and the gauges were broken down into groups to be tested on each day. There was overlap of the testing locations between the two days in order to be able to assess uniformity between tests completed over the course of multiple days.

Between both bridges, 11 different cross-frame locations and 6 different girder locations were instrumented in order to record data at cross-frames and their adjacent girders. Through instrumenting the adjacent girders, the global response of the structure in the vicinity of the cross-frames will be known, which will provide insight into the cross-frame behavior and assist in future FEA calibration efforts. Preliminary finite element models created for each bridge were used to determine locations of interest and produce an instrumentation layout. While the instrumentation plan for each bridge was unique, there were similarities between the two. Three girder locations were instrumented on each bridge, with a gauge on each side of the bottom flange and a gauge on each side of the web at mid height. The same labeling system was used at the girder location on each bridge. Girder locations are labeled as G followed by a number that corresponds to the locations (for example G1). BF-1 and BF-2 represent the two bottom flange gauges respectively, while W-1 and W-2 represent the two web gauges respectively. For SR 1 over US 13, BF-1 and BF-2 are always on the west and east sides of the girder respectively, while for SR 299 over SR 1, BF-1 and BF-2 are always on the north and south sides of the girder respectively. Since the cross-frame type differed between the two bridges, the cross-frame labeling system differed slightly between the two bridges. Cross-frames themselves are labeled with two numbers. The first number corresponds to the longitudinal position of the cross-frame on the bridge, while the second number refers to its transverse position. In both cases, gauges were labeled by the cross-frame number followed by a letter that corresponded to a location on the cross-frame. For example, Cross-frame 12-4-A corresponds to the twelfth longitudinal line of cross-frames at the fourth transverse positioning with Location A instrumented. This position can be seen in Figure 4.3. The letter designation represented the same location (e.g., west end of bottom chord) on each cross-frame shape.

4.2.1 SR 1 Over US 13

The instrumentation layout for the first bridge to be discussed, SR 1 over US 13, consisted of fifty-eight strain gauges. Multiple points on five cross-frames and three girder cross-sections were instrumented. Specifically, the cross-frames instrumented were Cross-frame numbers 4-4, 11-3, 12-3, 12-4, and 14-3 and Girder locations G1, G2, and G3 as identified in Figure 4.3. The instrumentation plan was developed using the finite element analysis of the bridge under several loading conditions as previously discussed in Section 3.5 to determine areas of interest. Peak cross-frame forces and adjacent girder locations were investigated under dead load plus live load of an HS-20 truck (AASHTO 2010) in four different load positions: the first three with the truck loading centered over the center support 2 feet from the left parapet, 2 feet from the right parapet, and with the right line of truck wheels centered on the lane boundary and last with the truck loading positioned at 40 % of the span length from the abutment 2 feet from the left parapet. The latter case is intended to produce the maximum moment in Girder 4, while the former provide additional information about the cross-frame response. Each of the cross-frames instrumented exhibited peak stresses under the four loading scenarios investigated, therefore they and their adjacent girder locations were chosen for testing. All cross-frames that were selected for instrumentation frame into a common girder (Girder 4, labeled as “G4”, the fourth girder from the top of in Fig. 4.3) to enable recording the range of responses occurring as the longitudinal position of the cross-frame varies while attempting to minimize the number of girder locations that would need to be instrumented in order to have a basis for comparison to the cross-frame data and keep the overall number of gauges to a minimum. All members of the cross-frames were investigated and instrumentation was placed on members that exhibited highest stresses.

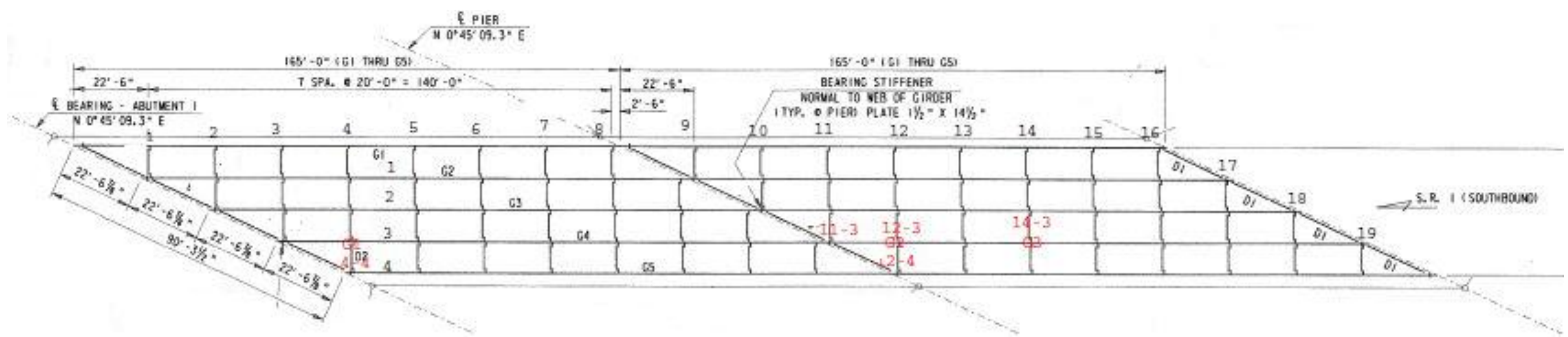

Figure 4.3 SR 1 Over US 13 Instrumentation Layout

Each of the three girder locations, which were selected because of their position adjacent to instrumented cross-frames, has four strain gauges, one on each side of the web (W-1 and W-2) and two on the bottom of the bottom flange (BF-1 and BF-2) as seen in Figure 4.4 below. These girder locations allow for the stresses at these sites to be correlated to the stresses in the adjacent cross-frame. The position of the gauges within these cross-sections was chosen in order to assess the variation of stresses throughout the girder cross-section and to locate the neutral axis of the girder location. Specifically, by installing two gauges at each height, lateral bending effects can be captured and redundancy in the data is obtained in the event of a malfunctioning gauge. Because of limitations imposed by the number of data channels that could be connected to the data acquisition system, gauges were not placed on the top flange because composite action with the deck would cause these strains to be very small and thus difficult to accurately capture. Girder locations 2 and 3 were fully instrumented (W-1, W-2, BF-1, and BF-2) on the first day of testing. On the second day of testing, Girder locations 1 and 2 were fully instrumented (W-1, W-2, BF-1, and BF-2). Therefore, there was an overlap between the gauges (W-1, W-2, BF-1, and BF-2) at Girder location 2 between the two days of testing. Figure 4.4 shows the labeling system that was used for the girder strain gauges.

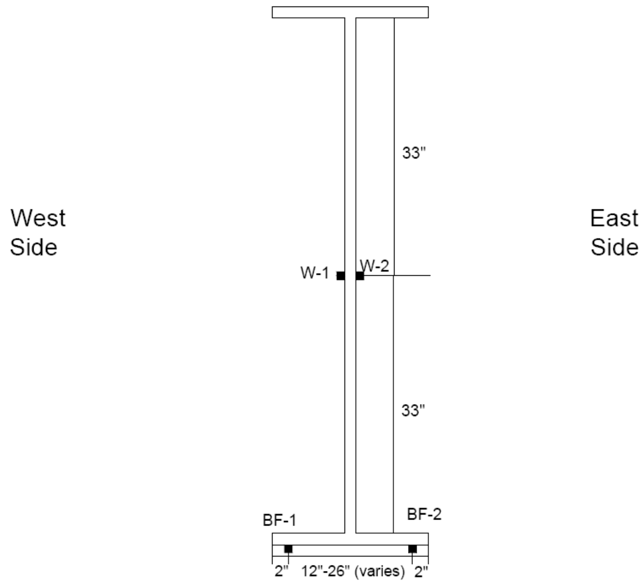

Figure 4.4 Girder Strain Gauges Cross-Section Labeling System, SR 1 Over US 13

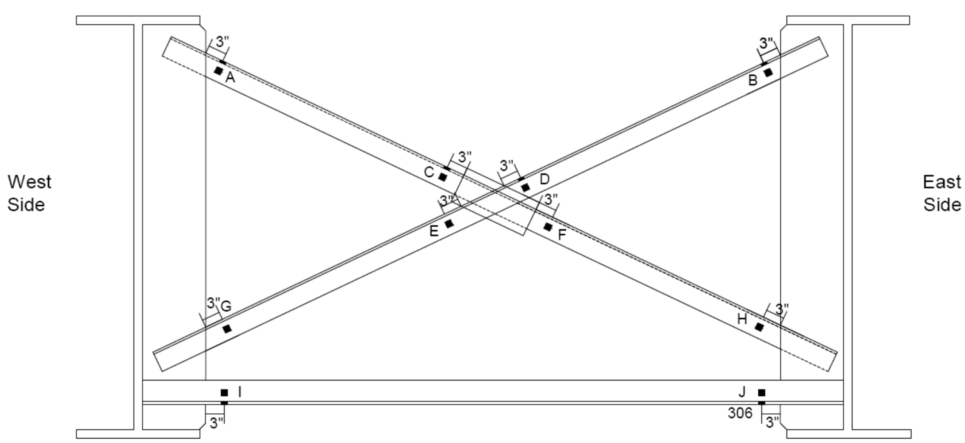

Figure 4.5 Cross-frame Strain Gauges Cross-Section Labeling, SR 1 Over US 13

Each of the five cross-frames chosen was instrumented with slight differences to reflect where peak stresses occurred in the preliminary finite element analysis. Five cross-frames were chosen, reflecting the areas of highest stress shown by the results of the finite element model (as described above) and capture the transfer of force from the girders through the cross-frames. Each of the cross-sections that were instrumented was labeled A thru J (see Fig. 4.5) such that the same label applied for the same location on each cross-frame. For example, as shown in Fig. 4.5, the bottom east side of the inclined member, three inches from the connection plate, is always referenced as location H. Note all gauges are placed three inches from the connection plate. Each cross-section typically had two gauges, one on each leg of the angle, but in some cases only the concentric leg of the angle is instrumented. This occurs in less critical locations when instrumentation is limited. The complete labeling system used in testing can be found in Appendix A. Table 4.1 specifies which positions were instrumented on each cross-fame by indicating the number of legs instrumented at that location.

Table 4.1 Number of Gauges Per Location, SR 1 Over US 13

	Number of Gauges at Location										
Cross-frame	A	B	C	D	E	F	G	H	I	J	Total
4-4	2		2		2		1		2	2	11
11-3		1				1		2	2	2	8
12-3		2		2				2	2	2	10
12-4	2		2				1		2	2	9
14-3		1				2		2	2	2	9

The finite element analysis tended to show one of the inclined members of the cross-frame as containing significantly higher stresses than the other inclined member. In each loading scenario, this was the inclined member that framed into the top of Girder 4. Two cross-sections were instrumented on whichever of the two inclined members demonstrated highest stresses, one three inches from the connection plate to the girder (Location A, B, G, or H) and one three inches off the plate that connects the two angles, on the side closest to the gauge already placed (Location C, D, E, or F) to evaluate bending throughout the member. The gauges were placed on the end of the angle that demonstrated the highest stresses. At each of these cross-sections, two gauges were placed, one on each leg of the angle. Two cross-sections were instrumented on the bottom chord of the cross-frame, three inches off the connection plate on each side (Locations I and J). This chord experienced lower, but still significant, stresses than the inclined member already instrumented; therefore two gauges were placed at each cross-section. For four of the cross-frames (12-3, 12-4, 11-3, and 14-3), only one cross-section was instrumented on the second inclined member. Here the finite element analysis reported relatively low stresses so a gauge was placed on the same side (i.e. east or west) of the angle that gauges on the higher stress angle were oriented. For example, in Cross-frame 12-4, Locations B and D correspond to the anticipated locations of highest stress, so Location H is also instrumented since it is also on the east side of the cross-frame. Due to limitations with equipment and relatively low predicted stresses, only one gauge was placed at these cross-sections. For the fifth cross-frame (4-4), both of the inclined members experienced significant stresses in the finite element analysis; therefore two cross-sections were also selected for the remaining angle with these gauges also oriented on the west side of the members, as was done for the other inclined angle of the cross-frame. Schematics for the gauge locations on each cross-frame and girder location can be found in Appendix A.

The field tests for SR1 over US13 were conducted on Friday, December 2nd, 2011 and Monday, December 5th, 2011. On Day 1 of the field tests (Dec. 2nd), Cross-frames 12-3, 12-4, and 14-3, along with Girder locations 2 and 3 were instrumented and tested. At the end of the day, all of the equipment was removed. On Day 2 of the field tests (Dec. 5th), Cross-frames 4-4 and 11-3, as well as Girder locations 1 and 2 were instrumented and tested. Because of time limitations and difficulty of set-up due to testing at two locations in the bridge requiring a time-consuming process to connect the two segments of instrumentation over traffic lanes, fewer locations were tested on Day 2 than originally planned. This was not a significant detriment to the testing plans as the cross-sections that were not tested as planned were a repetition of cross-sections on Cross-frame 12-4 that were tested the previous day. On both days, the data acquisition system was set up in the median of the underpass roadway, approximately beneath Girder four. Overall, 56 gauges were instrumented on five different cross-frames and 12 gauges were instrumented on three different girder cross-sections over the two days of testing.

4.2.2 SR 299 Over US 13

The instrumentation layout for the second bridge to be discussed, SR 299 over SR 1, consisted of sixty strain gauges. Multiple points on six cross-frames and three girder cross-sections were instrumented. Specifically, the cross-frames instrumented were Cross-frame numbers 8-4, 12-4, 12-5, 14-8, 14-9, and 14-10 and Girder locations G1, G2, and G3 as identified in Figure 4.6. G1 is position halfway between the stagger between Cross-frames 12-4 and 12-5, while G2 is at Cross-frame 12-4. The instrumentation plan was developed using the finite element analysis of the bridge under the loading conditions described in Section 3.5 to determine areas of interest. Peak cross-frame forces and adjacent girder locations were investigated under dead load plus live load and live load only. Both load cases were considered, but the live load only case is a better representation of the loading during field testing. The three different load positions investigated for these load combinations were loading in the obtuse corner of the bridge, the truck load positioned at 40 % of the length of one of the spans to approximate the maximum positive bending location for Girder 5, and the truck load centered over the center support of the bridge. Each of the cross-frames instrumented exhibited peak stresses under the loading scenarios considered, therefore they and their adjacent girder locations were chosen for testing. The general positions of the cross-frames selected for testing include three cross-frames in line with one another in the obtuse corner of the bridge, a cross-frame at the pier, and cross-frames at the maximum positive moment location for Girder 5.

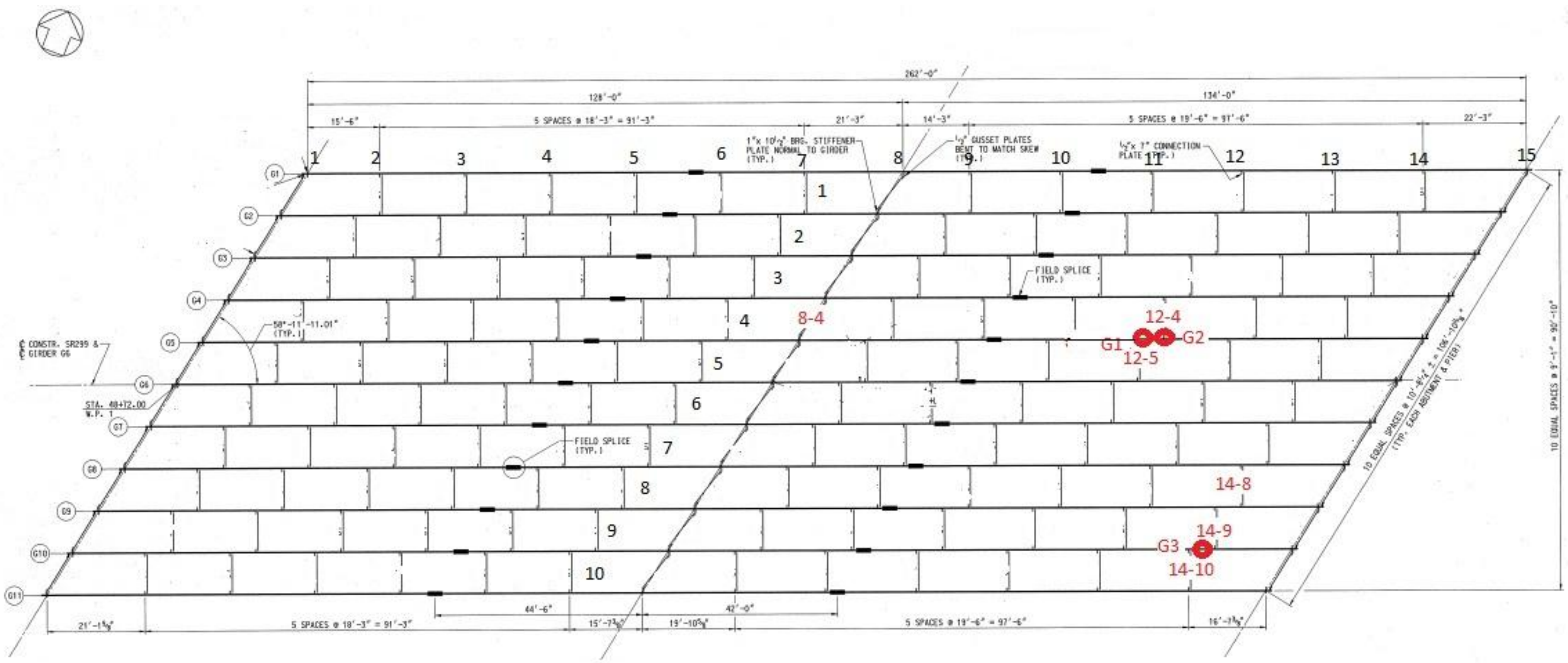

Figure 4.6 SR 299 Over SR 1 Instrumentation Layout

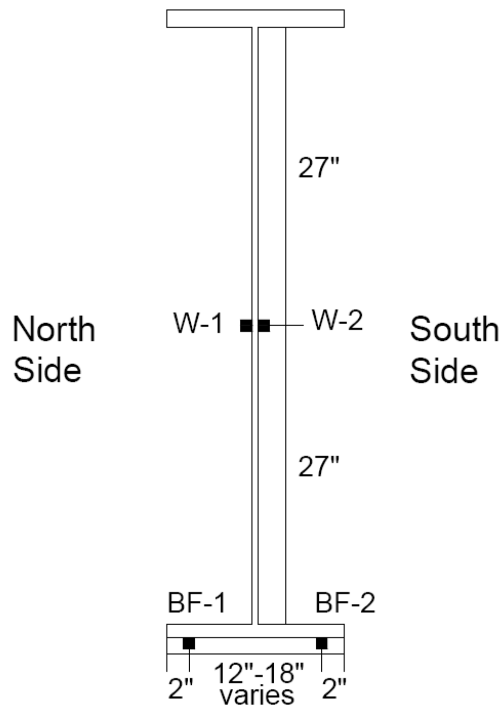

Figure 4.7 Girder Strain Gauges Cross-Section Labeling System, SR 299 Over SR 1

As with the other bridge, SR 1 over US 13, discussed in the previous section, each of the three girder locations, which were selected because of their position adjacent to instrumented cross-frames (in the obtuse corner of the bridge and at the maximum positive moment location for Girder 5), has four strain gauges, one on each side of the web (W-1 and W-2) and two on the bottom of the bottom flange (BF-1 and BF-2) as seen in Figure 4.7 above. This was selected in order to assess the variation of stresses throughout the girder cross-section and to locate the neutral axis of the girder location. Because of limitations imposed by the amount of data channels that could be connected to the data acquisition system, gauges were not placed on the top flange because composite action with the deck would cause these strains to be very small and thus difficult to accurately capture. The same labeling system used for SR 1 over US 13 for girder locations was used as demonstrated by Figure 4.7 above. Girder location 3 was fully instrumented (W-1, W-2, BF-1, and BF-2) on the first day of testing, while only the bottom flange locations (BF-1 and BF-2) were instrumented at Girder locations 1 and 2 on that day. On the second day of testing, Girder locations 1 and 2 were fully instrumented (W-1, W-2, BF-1, and BF-2). Therefore, there was an overlap between the bottom flange gauges (BF-1 and BF-2) at Girder locations 1 and 2 between the two days of testing.

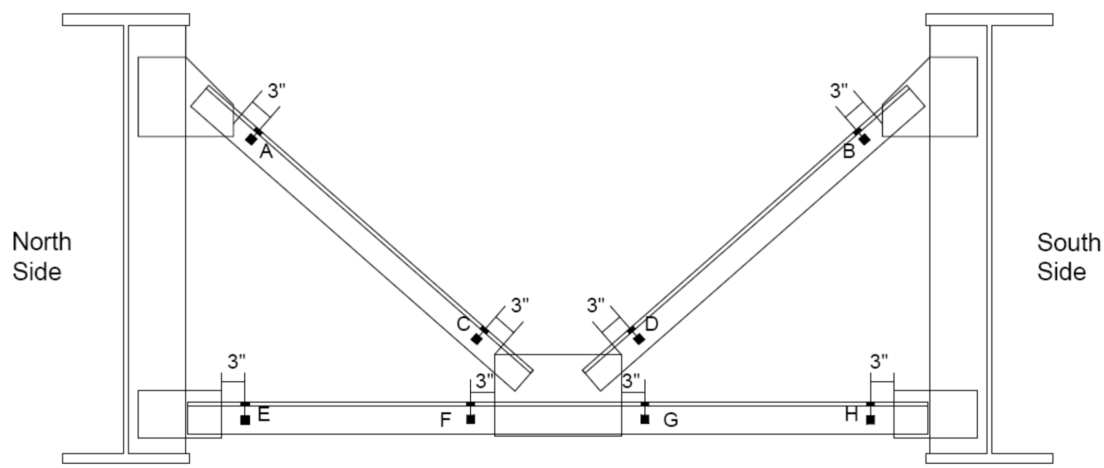

Figure 4.8 Cross-frame Strain Gauges Cross-Section Labeling, SR 299 Over SR 1

Each of the six cross-frames chosen was instrumented with slight differences to reflect where peak stresses occurred in the preliminary finite element analysis and capture the transfer of the force from the girders through the cross-frames. Six cross-frames were chosen, reflecting the areas of highest stress shown by the results of the finite element model. Each of the cross-sections that were instrumented was labeled A thru H (see Fig. 4.8) so that the same label applied for the same location on each cross-frame. For example, as shown in Figure 4.8 the top south side of the inclined member, three inches from the connection plate, is always referenced as Location B. Note all gauges are placed 3" from the connection plates. Each location had two gauges, one on each leg of the angle. The complete labeling system used in testing can be found in Appendix A. Table 4.2 below specifies which positions were instrumented on each cross-frame by indicating the number of legs instrumented at that location (two for all cases for this bridge).

Table 4.2 Number of Gauges Per Location, SR 299 over SR 1

	Number of Gauges at Location								
Cross-frame	A	B	C	D	E	F	G	H	Total
8-4		2		2			2	2	8
12-4		2		2			2	2	8
12-5	2		2		2	2			8
14-8		2		2			2	2	8
14-9		2		2	2		2	2	10
14-10	2		2		2	2			8

The gauge locations on the different members of the cross-frames also represented areas of highest stress as seen in the finite element analysis which tended to show one of the inclined members of the cross-frame as containing significantly higher stresses. Two cross-sections were instrumented for the inclined member that demonstrated highest stresses, Locations A and C or Locations B and D depending on whether the north or south side member demonstrated highest stresses. For cross-frames 12-4, 12-5, 14-9, and 14-10, the side with the highest stresses that was chosen for instrumentation also coincided with the side where the adjacent instrumented girder was located. Girder locations were not instrumented at Cross-frames 8-4 and 14-8 due to limitations with the amount of gauges available. At each of these locations, two gauges were placed, one on each leg of the angle. Two cross-sections were instrumented on the bottom chord of the cross-frame, at Locations E and F if the north side inclined member was instrumented or Locations G and H if the south side inclined member was instrumented. For Cross-frame 14-9, Location E (not on the same side as the inclined member that was instrumented) on the bottom chord, was also instrumented to compare the forces in the cross-frames at this location on both sides of Girder 8 (see Fig. 4.6). Specifically, since there were three adjacent cross-frames (14-8, 14-9, and 14-10) instrumented and Cross-frame 14-9 was the middle cross-frame of the grouping, this location was selected in order to collect data throughout the bottom chord in an effort to relate the data to Cross-frames 14-8 and 14-10, the cross-frames on either side of Cross-frame 14-9. Thus, each cross-frame was instrumented with 8 or 10 strain gauges. Schematics for the gauge locations on each cross-frame and girder location can be found in Appendix A.

The field tests for SR 299 over SR 1 were conducted on Wednesday, November 30th, 2011 and Thursday, December 1st, 2011. On Day 1 of the field tests (Nov. 30th), Cross-frames 14-8, 14-9, and 14-10, along with Girder location 3 and the bottom flange locations on Girder locations 1 and 2 were instrumented and tested. At the end of the day, all of the equipment was removed. On Day 2 of the field tests (Dec. 1^{st}), Cross-frames 8-4, 12-4, and 12-5 as well as Girder locations 1 and 2 were instrumented and tested. Thus, the data at bottom flange gauge locations on Girder locations 1 and 2 were recorded on both days of testing to capture any differences in the data between the two days. On both days, the data acquisition system was set up underneath the bridge on the outside shoulder of the underpass, northbound SR 1. Overall, 50 gauges were instrumented on six different cross-frames and 12 gauges were instrumented on three different girder cross-sections over the two days of testing.

4.3 Loading Vehicle

On each testing day, DelDOT provided a loaded triaxle dump truck (Fig. 4.9) to use as the test vehicle. The vehicle was outfitted with a large plow on the right side which, at least in part, caused the weights on the right side of the vehicle to be higher. The same dump truck was provided each day and remained loaded throughout the week during which the testing was conducted.

Figure 4.9 DelDOT Triaxle Dump Truck

On the first two days of testing each wheel was weighed using Intercomp Model PT 300 Wheel Load Weigher scales. Individual wheel weights were recorded by using two scales to weigh one axle at a time. Two other scales were placed under the wheels of the nearest adjacent axle during measurement in an effort to keep the truck level and account for the variation in weight distribution that may occur due to the truck's suspension system. On the second day, DelDOT also took the truck to their scale house and provided a report of the recorded weights of each axle. There is a maximum of 3 % difference for the front axle, 2.9 % difference for the middle axle, and 0.5 % difference for the rear axle between the total axle weights of the three different measurements for each of the axles. In order to determine an averaged weight to use in the finite element analysis, the percentage of the total axle weight measured in each individual wheel load was calculated for Measurements 1 and 2 in order to determine the distribution of weight between the two wheels of the axle (the large plow on the right side caused heavier weights on the right side). The weight distribution of the two wheels within each axle between the two measurements was within 1 %. The percentages of the total axle weight for each wheel were averaged for each axle and the averaged percentages were used to distribute the axle weight recorded at the scale house. The individual wheel weights were then averaged to calculate values to use in the finite element analysis. These measured weights as well as the averaged weight that was used in the finite element analysis can be found in Table 4.3 below.

Table 4.3 Triaxle Dump Truck Weights

	Front Axle		Middle Axle		Rear Axle	
	Left Side	Right Side	Left Side	Right Side	Left Side	Right Side
Wheel Measurement 1	6690 lb	7850 lb	8330 lb	12140 lb	8250 lb	12070 lb
Wheel Measurement 2	6490 lb	7840 lb	8440 lb	12430 lb	8060 lb	12280 lb
Scale House	14780 lb		20260 lb		20240 lb	
FEA	6693 lb	7857 lb	8419 lb	12155 lb	8120 lb	12180 lb

4.4 Truck Passes

The load tests for each of the bridges were conducted by driving the triaxle dump truck provided by DelDOT and mentioned in Section 4.3 in a series of passes across the bridge. Before each truck pass, traffic on the bridge was stopped and the strain gauges were balanced with no live load on the bridge. The truck then drove across various predetermined transverse positions at approximately 10 to 15 mph while other traffic was stopped. The transverse positions were selected by determining positions of the truck that would either maximize stress in different instrumented sections of the bridge or induce differential displacements at opposite ends of instrumentation while following markings on the roadway that would be easy for the driver to follow. The specific transverse positions for each bridge are discussed in the following subsections.

4.4.1 SR 1 Over US 13

Three different truck passes were conducted for the load test of SR 1 over US 13. The same three passes were used on both days of testing and are depicted in Figure 4.10. These passes were selected based on their proximity to instrumentation and based on roadway markings that could be easily followed. Pass 1 had the dump truck travel down the center of the left lane. This position was intended to maximize the stress in the instrumented girder, G4, and induce differential displacements in the instrumented cross-frames. Pass 2 had the dump truck travel straddling the center line of the two lanes. This pass is intended to produce a high level of stress in each of the girders (G3 and G4) to which the majority of the cross-frames are connected. Pass 3 had the dump truck travel with the left side wheels straddling the center line of the two lanes, intending to maximize the stress in the girder at the other end of the majority of the instrumented cross-frames, G3, and produce differential displacements between the two ends of the cross-frame. Thus, the passes were generally shifted to the side of the bridge closest to where the instrumentation was installed. Data was recorded for each of these three passes on both days of testing.   Figure 4.11 shows each of the passes in photograph, where it can be seen that the actual position of the truck is closer to the lane boundary than intended for Pass 1, but the actual position of Pass 2 and Pass 3 is in accordance with the testing plan. However, the difference between the point loadings depicted in the figures and the actual centroid of the wheel width is a slight difference that may affect future FEA calibration efforts.

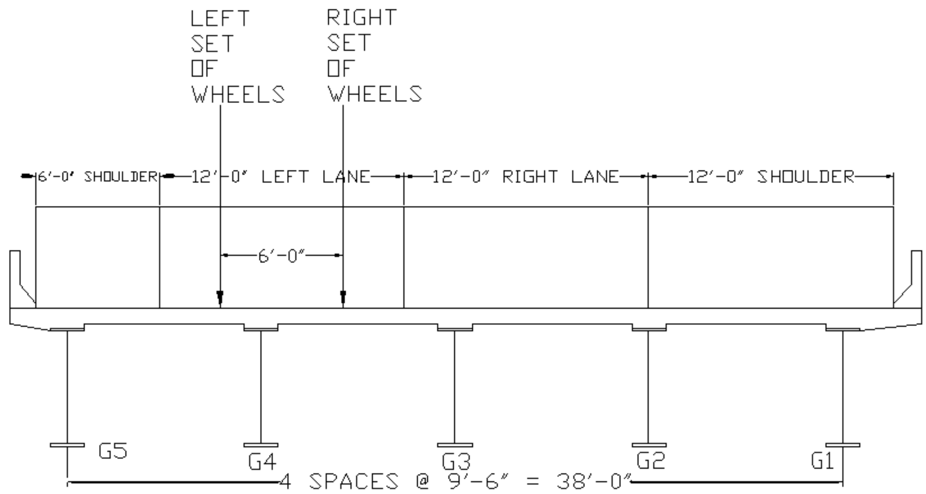

A)

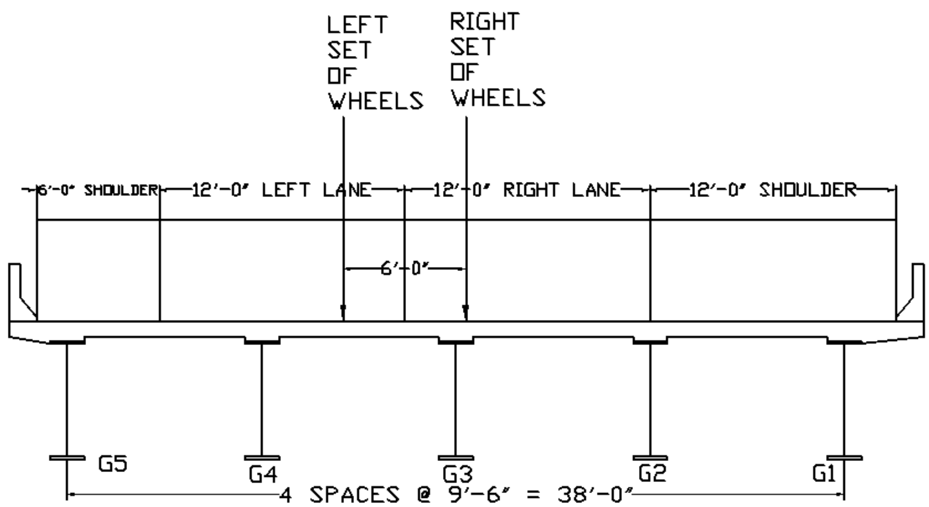

B)

Figure 4.10 Truck Passes for SR 1 Over US 13: A) Pass 1: Center of Left Lane, B) Pass 2: Straddle Center Line, C) Pass 3: Left Wheels on Center Line

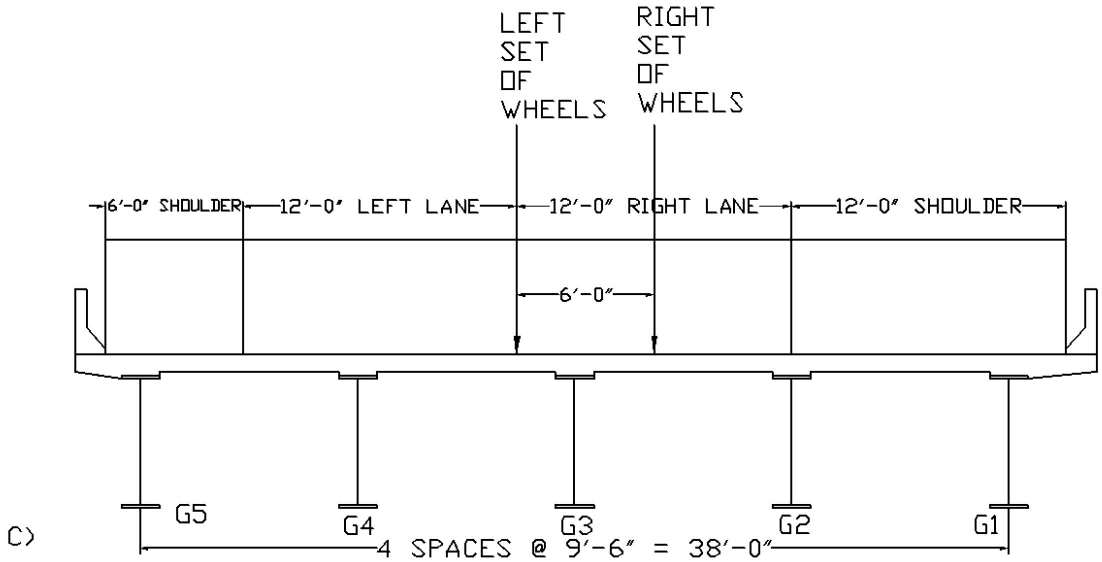

Figure 4.10 Continued

A) 

B) 

Figure 4.11 Photographs of Truck Passes for SR 1 Over US 13: A) Pass 1, B) Pass 2, C) Pass 3

C) 

Figure 4.11 Continued

Two different truck passes were conducted for the load test of SR 299 over SR 1. The location of the two passes was intended to be the same for both days of testing, but differed slightly between the two days due to a miscommunication with the driver of the dump truck. On the first day of testing, Pass 1 had the dump truck travel westbound across the bridge with the outside of its left set of wheels on the edge of the left lane boundary as marked on the roadway (excluding the turning lane) and shown in Fig. 4.12. On the second day of testing, for pass 1 the dump truck traveled westbound across the bridge approximately 1 foot to the right of the left lane boundary and the Day 1 position as shown in Fig. 4.12. Fig. 4.13 shows that Pass 2 for the first day of testing the dump truck traveled eastbound across the bridge about 1 foot to the inside of the right side yellow line. Fig. 4.13 also shows that Pass 2 for the second day of testing the dump truck traveled eastbound with the outside of its left set of wheels on the edge of the right lane boundary.

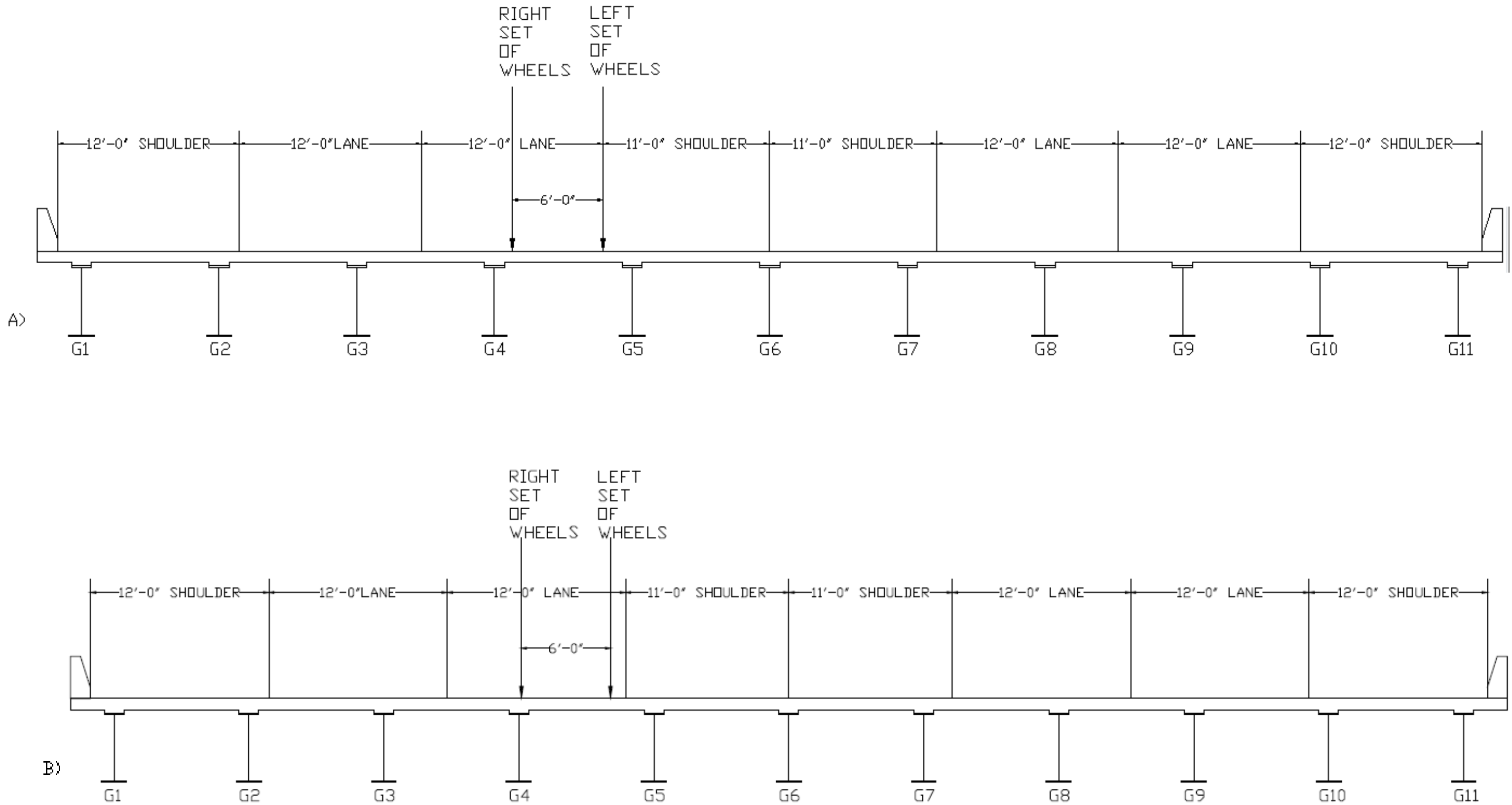

Figure 4.12 West bound Truck Passes (Pass 1) for SR 299 Over SR 1: A) Day 1 B) Day 2

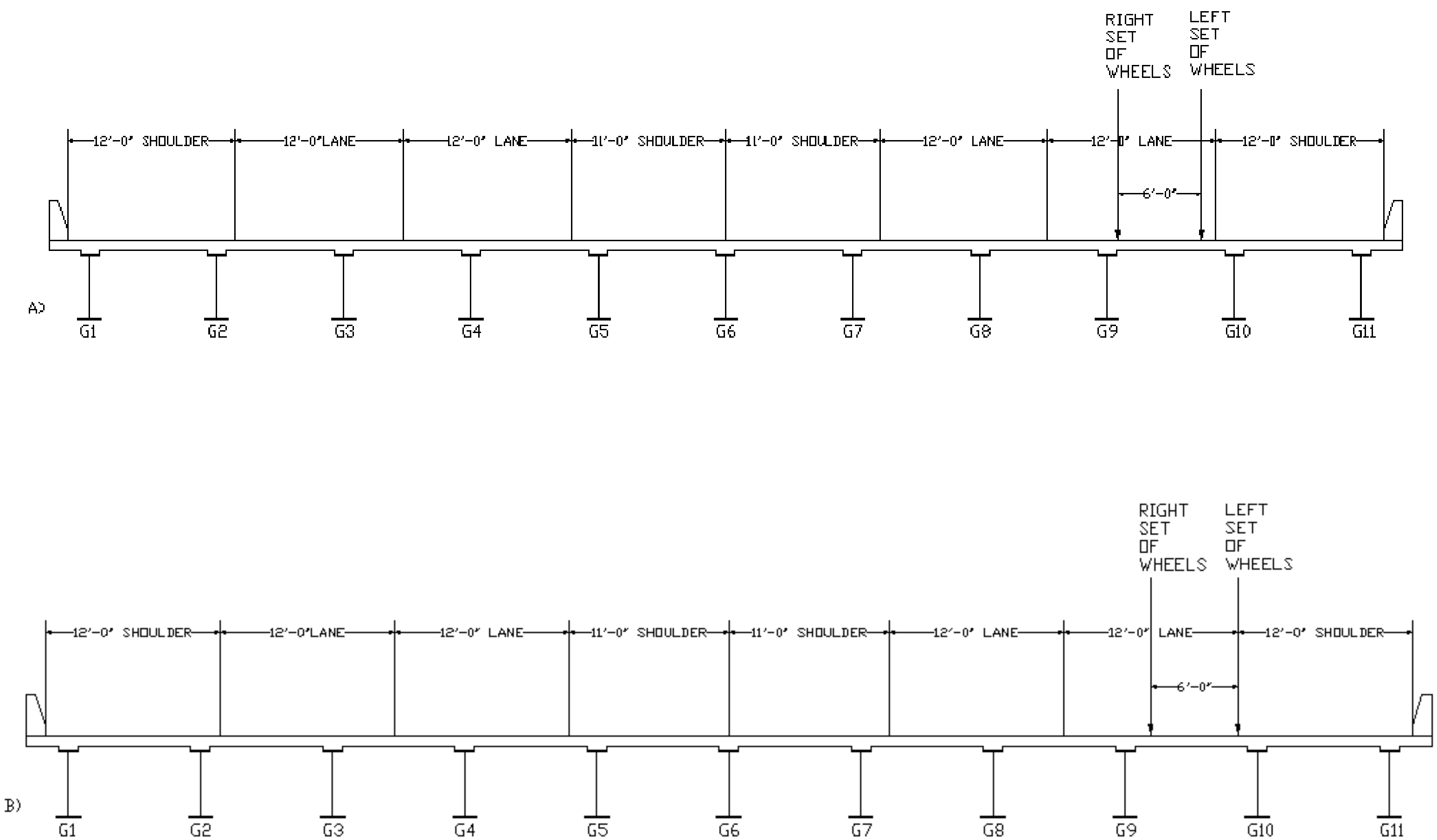

Figure 4.13 Eastbound Truck Passes (Pass 2) for SR 299 Over SR 1: A) Day 1, B) Day 2

4.5 Data

After four days of field testing, during which data was collected for 11 different cross-frames and 6 different girder cross-sections, a large amount of data had been collected and needed to be processed. All of the gauges were balanced using the data acquisition system after traffic was stopped on the bridge prior to the truck passes, but once transferred from the data acquisition system the data still had to be "zeroed", or processed so that the starting value of the data when no live load was on the bridge was zero. This was done by averaging the first 20 data points collected at each gauge and subtracting that average from every data point of that gauge. Data on the first day of field testing (Nov. 30th, SR 299 over SR 1) was collected at a sample rate of 5 Hz, meaning 5 data points were collected each second. On the remaining days of testing, the sample rate was increased to 20 Hz, or 20 data points per second. The increase in sample rate was decided after a quick analysis of the data from Day 1 suggested a higher sample rate would yield more data points and better capture trends in the data.

All of the data was processed in MATLAB by using the "smooth" function to take a 5-point moving average of the data. This eliminated a large amount of noise in the data. In order to graphically represent this data, a short MATLAB script was written that smoothed the original data as mentioned previously and down sampled (only graphed every 20th data point) the data in order to create uniform plots with the same formatting for each gauge. An example of the time versus strain plot created for Girder locations 1 and 2 for SR 299 over SR 1 on Day 1 of testing is shown in Figure 4.14. The x-axis represents time in seconds and the y-axis represents microstrain. The legend includes both the identification number of the gauge and the designation of its location (for example, B1477, G1-BF-1). The complete set of time versus strain plots for every location tested can be found in Appendix B.

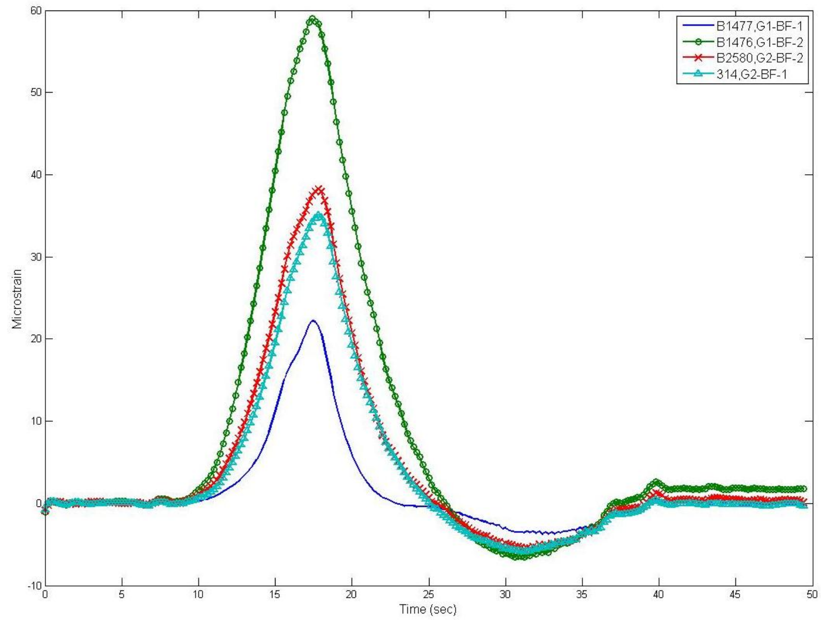

Figure 4.14   Time vs. Strain, SR 299 over SR 1, Day 1

Using the data that was balanced and smoothed out by taking a moving average, the maximum strain values (ε_{MAX}) for each gauge for each pass were tabulated. These maximum strain values were converted to stresses (σ_{MAX}) by multiplying by the modulus of elasticity of steel (29,000 ksi). At cross-sections where there were two gauges, the maximum stress values were averaged ($\sigma_{MAX\text{-}AVG}$). The maximum values for the girder locations (when a gauge was tested on two days the maximum of the two days was considered) of SR 1 over US 13 are presented in Table 4.4, while the maximum values for the cross-frames of SR 1 over US 13 are presented in Tables 4.5, 4.6, 4.7, and 4.8. The maximum values for the girder locations of SR 299 over SR 1 are presented in Table 4.9, while the maximum values for the cross-frames of SR 299 over SR 1 are presented in Tables 4.10 and 4.11. Maximum values for bottom flange and web gauges are not concurrent; therefore averages that are reported may not entirely represent actual stress state, particularly for webs. When a gauge did not balance, it is denoted by the letters “NB”, but the data is not treated differently. Other possible errors in gauges functioning are noted as footnotes to the tables as needed. Trends in the bottom flange test data are generally as expected, which is the best measure available of global response. For SR 1 over US 13, the bottom flange gauges at Girder Location 3 exhibit the highest tensile stresses as expected and the bottom flange gauges at Girder Location 2, the location where the highest negative moments is expected, exhibit the highest compressive stresses. Also for SR 1 over US 13, in general the bottom flange stresses for Pass 1 are greater than for Pass 2 which are greater than Pass 3, which is expected as the truck load moves further from the instrumented girder as the passes progress. For SR 299 over SR 1, the bottom flange stresses for Girder Locations 1 and 2 are similar as is expected since the two locations are in close proximity to one another. Furthermore the peak stresses at these locations are greater than the peak stresses at G3, which is closer to the abutment and thus should experience less moment. It is also logical that the stresses in G1 and G2 are maximized by Pass 1, since this loading is closest to these gauge locations, while the peak stresses in G3 occur under Pass 2, which travels closest to this gauge location.

As mentioned in the literature review in Chapter 2, Bishara and Elmir (1990) found that the higher the skew angle, the higher the maximum forces that are induced in the cross-frame members. The maximum cross-frame force recorded for SR 1 over US 13, the 65 degree skew bridge, is 3.6 ksi which is higher than the maximum cross-frame force recorded for SR 299 over SR 1 of 1.5 ksi. In comparison with Tedesco et al's (1995) discovery that the removal of diaphragms had only a modest effect on bridge response, the removal of cross-frames was considered also for the SR 299 over SR1 model. It was found that the removal of cross-frames in the model created on average a 5 % difference in maximum stresses at girder locations than the model with the cross-frames included.

Table 4.4 SR 1 Over US 13 Max Values, Girder Locations

			Pass 1			Pass 2			Pass 3		
Gauge Location	Gauge Number	Day	ε_{MAX}	σ_{MAX} (psi)	$\sigma_{MAX\text{-}AVG}$ (psi)	ε_{MAX}	σ_{MAX} (psi)	$\sigma_{MAX\text{-}AVG}$ (psi)	ε_{MAX}	σ_{MAX} (psi)	$\sigma_{MAX\text{-}AVG}$ (psi)
G1-W-1	337	2	-18.40	-533	314	11.79	342	500	11.25	326	403
G1-W-2	299	2	40.05	1161		22.67	658		16.56	480	
G1-BF-1	2171	2	37.02	1073	1267	34.35	996	999	31.27	907	835
G1-BF-2	317	2	50.37	1461		34.52	1001		26.30	763	
G2-W-1	2171	1	12.48	362	322	10.8	313	313	-4.76	-138	-138
G2-W-2	B1477	2	-7.69	-223	-223	-3.87	-112	-112	-4.60	-133	-133
G2-BF-1	293	1	-22.33	-567	7	-15.48	-449	-385	-11.37	-330	-296
G2-BF-2	348	1	17.29	581		-11.07	-321		-9.02	-262	
G3-W-1	355	1	15.82	459	27	9.51	276	217	6.08	176	161
G3-W-2	339	1	-13.96	-405		5.44	158		5.01	145	
G3-BF-1	292	1	50.29	1458	1307	42.88	1244	1095	34.68	1006	906
G3-BF-2	3317	1	39.83	1155		35.59	945		27.8	806	

*Note: G2-W-2 only recorded on Day 2

Table 4.5 SR 1 Over US 13 Max Values, Cross-frames 12-3, 12-4, & 14-3 Passes 1 & 2

		Pass 1			Pass 2		
Gauge Location	Gauge Number	ε_{MAX}	σ_{MAX} (psi)	$\sigma_{MAX-AVG}$ (psi)	ε_{MAX}	σ_{MAX} (psi)	$\sigma_{MAX-AVG}$ (psi)
12-3-B	2581	36.62	1062	621	71.8	2082	1199
12-3-B	2172	6.20	180		10.88	316	
12-3-D	1475	15.81	458	504	42.26	1226	1018
12-3-D	1478	18.92	549		27.9	809	
12-3-H	2579	22.69	658	658	-23.39	-678	-678
12-3-I	3318	47.98	1392	747	41.08	1191	718
12-3-I	3315	3.48	101		8.46	245	
12-3-J	294	45.36	1315	688	38.64	1121	348
12-3-J	318	2.1	61		-14.69	-426	
12-4-A	314	-85.08	-2467	-1489	-90.59	-2627	-1570
12-4-A	2580	-17.58	-510		-17.69	-513	
12-4-C	1476	-100.55	-2916	-1597	-91.4	-2651	-1646
12-4-C	1477	-9.69	-281		-22.11	-641	
12-4-G	3319	98.28	2850	2850	66.51	1929	1929
12-4-I	2173	7.82	227	319	-26.85	-779	-212
12-4-I	356	14.13	410		12.25	355	
12-4-J	2578	8.44	245	-357	-21.44	-622	-752
12-4-J	306	-33.05	-958		-30.40	-882	
14-3-B	3314	44.79	1299	1356	108.99	3161	3161
14-3-F	337	31.65	918	973	-27.96	-811	108
14-3-F	299	35.4	1027		35.43	1027	
14-3-H	344	49.04	1422	1123	6.63	192	484
14-3-H	317	28.38	823		26.73	775	
14-3-I	295	84.57	2453	1302	99.87	2896	1629
14-3-I	338	5.20	151		12.48	362	
14-3-J	346	85.88	2491	1426	103.86	3012	1453
14-3-J	3316	12.42	360		-3.64	-106	

Table 4.6 SR 1 Over US 13 Max Values, Cross-frames 12-3, 12-4, & 14-3, Pass 3

		Pass 3		
Gauge Location	Gauge Number	ε_{MAX}	σ_{MAX} (psi)	$\sigma_{MAX-AVG}$ (psi)
12-3-B	2581	79.22	2297	1335
12-3-B	2172	12.86	373	
12-3-D	1475	52.34	1518	1143
12-3-D	1478	26.48	768	
12-3-H	2579	-45.02	-1305	-1246
12-3-I	3318	26.93	781	549
12-3-I	3315	10.92	317	
12-3-J	294	25.03	726	65
12-3-J	318	-20.58	-597	
12-4-A	314	-89.36	-2591	-1562
12-4-A	2580	-18.34	-532	
12-4-C	1476	-80.24	-2327	-1538
12-4-C	1477	-25.8	-748	
12-4-G	3319	39.21	1137	1137
12-4-I	2173	-38.54	-1118	-413
12-4-I	356	10.08	292	
12-4-J	2578	-33.5	-972	-880
12-4-J	306	-27.13	-787	
14-3-B	3314	123.73	3588	3588
14-3-F	337	-56.46	-1637	-398
14-3-F	299	29.04	842	
14-3-H	344	-27.26	-790	-107
14-3-H	317	19.87	576	
14-3-I	295	90.84	2634	1527
14-3-I	338	14.47	420	
14-3-J	346	95.21	2761	1229
14-3-J	3316	-10.46	-303	

Table 4.7 SR 1 Over US 13 Max Values, Cross-frames 4-4 & 11-3, Passes 1 & 2

		Pass 1			Pass 2		
Gauge Location	Gauge Number	ε_{MAX}	σ_{MAX} (psi)	$\sigma_{MAX-AVG}$ (psi)	ε_{MAX}	σ_{MAX} (psi)	$\sigma_{MAX-AVG}$ (psi)
4-4-A	3318	-102.72	-2979	-1656	-86.38	-2505	-1397
4-4-A	3315	-11.44	-332		-9.93	-288	
4-4-C	1475	-108.02	-3133	-1662	-80.21	-2326	-1340
4-4-C	294	-6.56	-190		-12.16	-353	
4-4-E	2579	113.80	3300	2287	76.66	2223	1487
4-4-E	2581	43.95	1275		25.88	751	
4-4-G	2172	145.45	4218	1972	85.83	2489	1184
4-4-G	1478	-9.46	-274		-4.17	-121	
4-4-I	355	40.07	1162	938	8.15	236	339
4-4-I	3317	24.63	714		15.20	441	
4-4-J	339	36.28	1052	43	9.07	263	-284
4-4-J	3316	-33.32	-966		-28.63	-830	
11-3-B	3319	46.74	1409	1409	55.95	1623	1710
11-3-F	292	-53.10	-1540	-1540	-50.86	-1475	-1408
11-3-H	2173	-47.73	-1384	-784	-46.04	-1335	-551
11-3-H	2170	-6.36	-184		8.05	233	
11-3-I	2578	14.44	419	311	13.12	380	286
11-3-I	306	7.01	203		6.62	192	
11-3-J	356	16.48	478	19	15.44	448	14
11-3-J	533	-15.18	-440		-14.48	-420	

Table 4.8 SR 1 Over US 13 Max Values, Cross-frames 4-4 & 11-3, Pass 3

		Pass 3		
Gauge Location	Gauge Number	ε_{MAX}	σ_{MAX} (psi)	$\sigma_{MAX\text{-}AVG}$ (psi)
4-4-A	3318	-71.64	-2077	-1174
4-4-A	3315	-9.36	-271	
4-4-C	1475	-63.08	-1829	-1153
4-4-C	294	-13.22	-383	
4-4-E	2579	59.08	1713	1126
4-4-E	2581	18.55	538	
4-4-G	2172	60.25	1747	894
4-4-G	1478	1.42	41	
4-4-I	355	-12.23	-355	-18
4-4-I	3317	11.00	319	
4-4-J	339	-9.07	-263	-509
4-4-J	3316	-26.03	-755	
11-3-B	3319	67.14	1947	1947
11-3-F	292	-85.49	-2479	-2479
11-3-H	2173	-80.75	-2342	-1368
11-3-H	2170	-13.57	-394	
11-3-I	2578	16.18	469	395
11-3-I	306	11.04	320	
11-3-J	356	16.18	469	-87
11-3-J	533	-22.18	-643	

Table 4.9 SR 299 Over SR 1 Max Values, Girder Locations

			Pass 1			Pass 2		
Gauge Location	Gauge Number	Day	ε_{MAX}	σ_{MAX} (psi)	$\sigma_{MAX\text{-}AVG}$ (psi)	ε_{MAX}	σ_{MAX} (psi)	$\sigma_{MAX\text{-}AVG}$ (psi)
G1-W-1	294	2	28.53	828	505	4.34	126	79
G1-W-2	317	2	6.25	181		1.14	33	
G1-BF-1	3318	2	37.68	1093	1133	7.09	205	180
G1-BF-2	3314	2	40.41	1172		5.33	155	
G1-BF-1	1477	1	23.34	677	1213	8.92	259	185
G1-BF-2	1476	1	60.29	1748		3.80	110	
G2-BF-1	314	1	35.31	1024	1073	4.18	121	164
G2-BF-2	2580	1	38.66	1121		7.11	206	
G2-W-1	348	2	34.84	1010	297	5.79	168	52
G2-W-2	299	2	-14.38	-417		-2.18	-63	
G2-BF-1	3319	2	60.27	1748	1233	-5.80	-168	59
G2-BF-2	337	2	24.76	718		9.89	287	
G3-W-1	292	1	-4.76	-138	-153	12.72	369	453
G3-W-2	344	1	-5.81	-168		18.54	538	
G3-BF-1	3317	1	2.75	80	-73	25.68	745	810
G3-BF-2	3316	1	-7.78	-225		30.20	876	

Table 4.10 SR 299 Over SR 1 Max Values, Cross-frames 14-8, 14-9, & 14-10

		Pass 1			Pass 2		
Gauge Location	Gauge Number	ε_{MAX}	σ_{MAX} (psi)	$\sigma_{MAX\text{-}AVG}$ (psi)	ε_{MAX}	σ_{MAX} (psi)	$\sigma_{MAX\text{-}AVG}$ (psi)
14-8-B	2170	-8.38	-243	-134	-31.51	-914	-475
14-8-B	2578	-0.86	-25		-1.19	-35	
14-8-D	2171	-7.44	-216	-148	-24.26	-703	-368
14-8-D	2173	-2.72	-79		-7.61	-32	
14-8-G	318	-13.40	-388	-222	42.31	1227	701
14-8-G	339	-1.89	-55		6.05	175	
14-8-H	293	-14.14	-410	-175	49.61	1439	572
14-8-H	355	2.08	60		-10.19	-296	
14-9-B	3318	-7.49	-217	-102	24.05	697	320
14-9-B	3314	0.49	14		-1.95	-57	
14-9-D	3319	-6.72	-195	-134	21.94	636	470
14-9-D	3315	-2.52	-73		10.48	304	
14-9-E	346	-16.63	-482	-246	63.41	1839	NA
14-9-E (NB)	535	-0.32	-9		NA	NA	
14-9-G	2581	-7.29	-212	-133	32.63	946	587
14-9-G	2579	-1.86	-54		7.81	227	
14-9-H	1478	-5.97	-173	-79	29.18	846	357
14-9-H	2172	0.55	16		-4.55	-132	
14-10-A	348	5.58	162	92	-32.07	-930	-507
14-10-A	337	0.75	22		-2.86	-83	
14-10-C	317	5.01	145	100	-26.68	-774	-576
14-10-C	298	1.86	54		-13.03	-378	
14-10-E	306	-9.82	-285	-111	41.32	1198	463
14-10-E	533	2.20	64		-9.41	-273	
14-10-F	294	-8.20	-238	-142	36.60	1061	598
14-10-F	299	-1.71	-50		4.65	135	

Table 4.11 SR 299 Over SR 1 Max Values, Cross-frames 12-4, 12-5, & 8-4

		Pass 1			Pass 2		
Gauge Location	Gauge Number	ε_{MAX}	σ_{MAX} (psi)	$\sigma_{MAX-AVG}$ (psi)	ε_{MAX}	σ_{MAX} (psi)	$\sigma_{MAX-AVG}$ (psi)
12-4-B	2170	53.78	1560	801	1.76	51	797
12-4-B	2578	1.46	42		-0.98	-28	
12-4-D	2171	49.98	1450	994	1.33	39	981
12-4-D	2173	18.56	538		-1.01	-29	
12-4-G	314	45.50	1320	783	-9.67	-280	793
12-4-G	2580	8.46	246		-2.28	-66	
12-4-H	1476	47.73	1384	654	-10.78	-313	649
12-4-H	1477	-2.66	-77		1.19	35	
12-5-A	295	-47.09	-1366	-656	-3.95	-115	-664
12-5-A	338	1.89	55		0.63	18	
12-5-C	346	-38.75	-1124	-761	-3.74	-109	-743
12-5-C	344	-13.70	-397		-1.14	-33	
12-5-E	292	52.02	1509	560	-13.87	-402	560
12-5-E	3315	-13.43	-389		1.99	58	
12-5-F	3317	42.45	1231	691	-13.62	-395	691
12-5-F	3316	5.21	151		1.04	30	
8-4-B	1478	-10.47	-304	-186	-11.89	-345	-113
8-4-B	2172	-2.32	-67		-0.78	-23	
8-4-D	2579	-7.32	-212	24	-7.81	-227	24
8-4-D	2581	9.00	261		9.00	261	
8-4-G	318	5.30	154	110	7.06	205	110
8-4-G	293	2.29	66		2.86	83	
8-4-H	339	7.26	210	154	9.68	281	154
8-4-H	355	3.40	98		2.04	59	

4.6 Recommendations

The field testing of the two bridges used in this research was a task that required a large amount of preparation and planning in order for the tests to be successfully conducted. This section explains several things that were learned during the field testing process that may help things run more smoothly when conducting future field tests. First it is recommended to carefully consider the amount of time that is allowed for set-up, testing, and take-down of all the gauges. Depending on the structure, there can be many restrictions on the amount of time lanes can be closed to allow for field testing. It is important to have a field testing plan with a reasonable amount of set-up for the time given so that researchers are not rushing and mistakes are not made. With the exception of the final day of testing for SR 1 over US 13, which called for testing two groupings that were more than 100 feet apart, requiring significant time to move equipment and alter traffic control, the two days allotted for testing on each bridge was a reasonable but not generous amount of time. The majority of the time needed is for set-up. Although the gauges are relatively easy to install, it takes time and careful maneuvering of a bucket truck to get into position for installation. It is recommended that for the amount of gauges used in this study at least 4 hours is allotted for this, assuming the personnel doing the installation are familiar with both the gauges and the operation of the lift vehicle. Only approximately half an hour is needed for the truck passes and collection of data. The take-down of the gauges moves much faster than the set-up as much less care is needed in placement, an hour is a good approximation of the time needed for this task. The location and number of traffic lanes that will need to be closed down to allow for installation should also be considered. A testing plan that closes both lanes of traffic in one direction is not recommended unless an elaborate traffic control plan is utilized or a detour for traffic is provided. It results in a rushed set-up and a line of angry motorists.

Second, when installing the strain transducers care should be taken not to clamp them too tightly. They should be clamped firmly in place, but not excessively tight. This can result in an unbalanced gauge. It wastes time and energy to move equipment to access and loosen them when checking that the gauges are balanced before testing.

Finally, it is recommended that the truck passes be closely monitored and carefully documented before the final testing process is completed. This eliminates estimating and questioning when using the positioning to calibrate future finite element models.

Chapter 5

FEA CALIBRATION AND RESULTS

After the field testing was complete, the next step was to compare the results from the field tests to the preliminary finite element models in order to calibrate the models to accurately capture the girder and cross-frame forces. Section 5.1 provides a brief description of the assumptions made in the preliminary models, on which the field testing plans were based. Section 5.2 explains the process of how the preliminary finite element models were calibrated and discusses the different variations of the model that were investigated to calibrate the girder stresses as well as the rationale used to select the final input parameters. Section 5.3 highlights results from the selected girder stress models that were determined from the process described in the previous section. These models were then used in Section 5.4 to calibrate the cross-frame stresses; this section also summarizes the results of the alternative cross-frame stress models. Section 5.5 presents a conclusion on the research presented in this chapter.

5.1 Preliminary Models

Results from the preliminary finite element models were used to create the field testing plans for both bridges, presented in Section 4.2. As discussed in Chapter 3, the girder, haunch, deck, and parapet were modeled with shell elements, while the cross-frame members were modeled using beam elements. The beam elements were connected to the shell elements through merged nodes. The girder, haunch, and deck were connected to one another using rigid links. These simulate composite action between the steel girder and the concrete slab. Both the preliminary models for SR 1 over US 13 and SR 299 over SR 1 were developed from the plans provided by DelDOT and a few initial assumptions.

In both bridges, the assumption for the strength of the concrete in the deck was 5 ksi. This assumption was confirmed by DelDOT officials who verified this as a commonly used strength concrete in bridge decks. In both preliminary models, rigid links were used to connect the girder to the deck along every node along the center line of the girder to simulate full composite action. The original support conditions had the longitudinal and transverse directions constrained at the line of nodes along the width of the bottom flange of the girder at the two ends of the bridge with translation in the transverse, longitudinal, and vertical directions constrained along this line of nodes at the center support. It was these three initial assumptions that were later altered in different variations of the models in order to attempt to achieve a better correlation between the FEA and the field testing results.

Another parameter that was varied between the preliminary models and the final calibrated models was the loading. The original finite element analysis was completed with the HS-20 truck loading which was shown in Figure 3.2 in Section 3.5. The averaged loading magnitudes and actual positioning of the triaxle dump truck, as shown in Figures 4.10, 4.12, and 4.13, was used in the calibration of the models by stepping the truck loading across the bridge in small increments of 10’ or less (sometimes in smaller increments of approximately 2.5’ or 5’ to validate a maximum value had been obtained) to determine the position that induced the highest stresses in each location as will be described in Section 5.2. These loading magnitudes were provided previously in Table 4.3 in Section 4.3. In both cases, the loads were applied to the deck using a grouping of six nodal loads representing the wheel loads.

5.2 Alternative Girder Stress Models

The calibration process began with comparing the FEA and field test strains in the girders since these are the primary structural members and thus provide general information about the load distribution behavior of the bridge. Specifically, the bottom flange strains at the gauge locations were used as one metric for comparison because these readings are the largest in magnitude and are thus the least sensitive to noise in the field instrumentation. A second metric that was evaluated was the neutral axis position at each of the instrumented sections. An estimated location of the neutral axis was determined by using the data associated with the strain transducers attached to the bottom flange and web locations at each of the tested girder locations. The strains at the two bottom flange locations were averaged and the strains at the two web locations were averaged. This data was extrapolated between the two points to determine where a zero strain value would occur. The output of the FEA was also used to determine the neutral axis position via extrapolation of data. It was also visually located in the colored contours of the output of the FEA in order to assure extrapolation calculations were in the correct range of magnitude. An additional comparison was that theoretical values for the neutral axis position for each of the locations were calculated based on the girder geometry.

After the field tests were completed, the actual truck loading recorded during the tests was placed in the preliminary finite element models. The loading from the DelDOT triaxle dump truck, summarized in Table 4.3 in Section 4.3 was used in the model as six nodal loads comprising the wheel loads applied to the deck. The transverse positioning of the truck during each of the truck passes, found in Figures 4.10, 4.11, and 4.12 above, was used to position the known loading in the models. The truck loading was then moved longitudinally in separate analyses for each pass along the bridge in increments of approximately 10 feet or less (sometimes in smaller increments of approximately 2.5’ or 5’ to validate a maximum value had been obtained) in order to find the longitudinal truck position causing maximum strain for each of the girder locations for each pass, focusing on positions that were anticipated to produce maximum stresses. A sequential numbering system was used to label the different load cases as the truck was stepped across the bridge. It is slightly different for each unique truck pass.

The maximum strains recorded for the bottom flange girder locations were converted to stresses by multiplying by the modulus of elasticity of steel and compared to maximum values found from the different truck positions in the finite element models. Figure 5.1 below illustrates this process for the BF-1 gauge at Girder location 3 for Pass 1 on Day 1 of the field testing for SR 1 over US 13. Here the data from the field test was superimposed on the same plot as the data from the FEA where the truck loading was stepped gradually across the model simulating the truck passes. The y-axis represents stress in psi, while the x-axis represents the arbitrary step of the truck loading from when the loading was stepped across the model in small increments to determine the maximum. The shape of the data for this pass matched well with the shape of the data that was observed during field testing as shown below in Figure 5.1. This trend was consistently observed when comparing data at each of the girder locations, but it can be seen by comparing the two series in Figure 5.1 that the stress magnitudes were initially appreciably different.

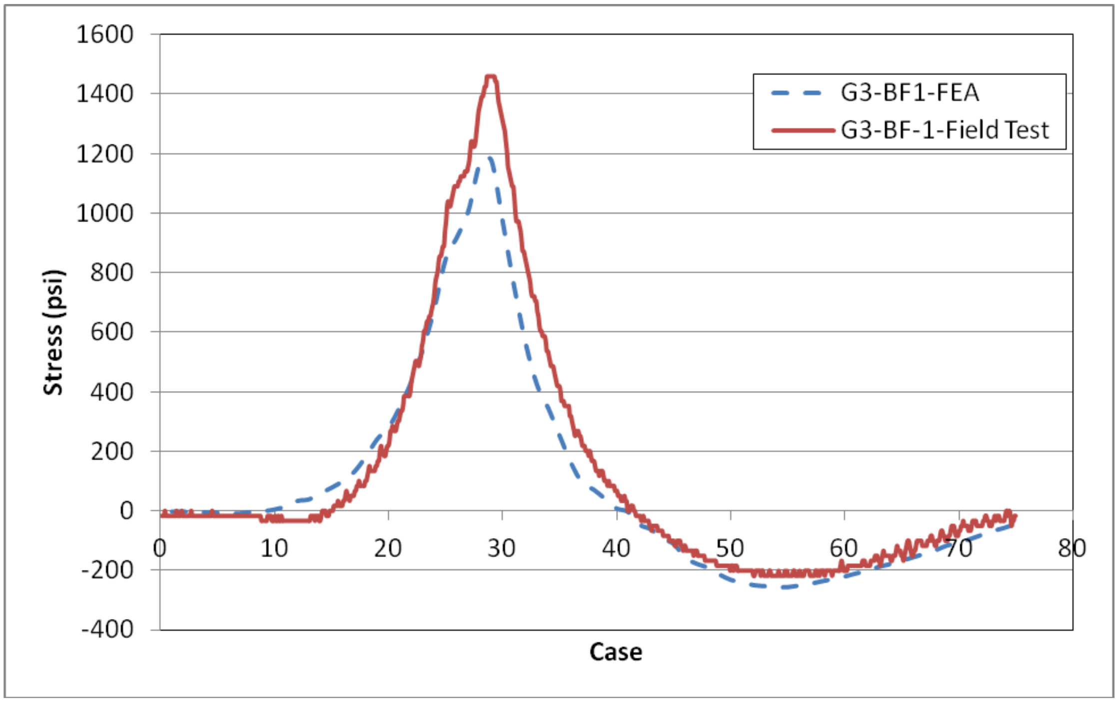

Figure 5.1 FEA vs. Field Test for G3-BF-1 for SR 1 over US 13

In order to achieve improved correlation between the FEA and field test, different variations of the models were considered by changing three different parameters. The first was the elastic modulus (E) of the concrete in the deck, parapets, and haunch; this would vary in reality if the strength of the concrete is different from the 5 ksi that was originally assumed. The second was the spacing of the rigid links connecting the girder, haunch, and deck that were used to simulate composite action. The reason for this was that previous research by Ross (2007) determined that by increasing the spacing of the rigid links along the girder, it will at some point lose its ability to replicate full composite action forcing the steel and concrete to act more independently. He studied the spacing of rigid links at 8”, 16”, 40”, 80”, and 272” intervals. As the spacing increased, the deck slab and plate girder began to act more independently. Since shear studs are not completely rigid, increasing the spacing of the rigid links is an indirect way of mimicking the flexibility. The third was the support conditions that were assumed. The constraint for translation in the transverse direction was removed from the nodes on the outside edge of the line of nodes on the bottom flange at the center support of the bridge.   Because the preliminary finite element models predicted different stresses than what was observed during the field test, it was investigated how changing these three parameters would best help calibrate the models.

5.2.1 SR 1 Over US 13

Once the field tests results for SR 1 over US 13 were compared to its preliminary finite element model, changes in each of the three parameters identified in Section 5.2 (elastic modulus, rigid link spacing, and support constraints) were made to determine the variation of the model that most accurately captured the girder forces before moving on to calibrate the cross-frame forces. The way in which the parameters were changed was first guided by the knowledge that the field test neutral axis positions were generally lower than predicted by theory or the FEA. The first parameter that was changed was the elastic modulus (E) of the concrete. The strength of the concrete was changed from an original assumption of 5 ksi concrete to a new assumption of 4 ksi concrete. Model variations with 4 ksi strength concrete are represented as E1, while models with initial assumed strength of 5 ksi are represented as E0. Altering the modulus of elasticity of the concrete affects the overall stiffness of the structure; lowering the modulus of elasticity of the concrete also lowers the neutral axis position.

The second parameter that was changed was the number and spacing of the rigid links that connect the haunch to the deck. The Multiple Point Constraint (MPC) beams, or rigid links, are used to produce a rigid connection to represent the composite action in the girder. In a real structure this connection is not completely rigid; therefore the amount of rigid links was varied in an effort to mimic the flexibility found in the actual structure. Based on the research by Ross (2007), discussed in Section 5.2, which showed that increasing the spacing of rigid links forces the steel and concrete to act more independently, and the spacing of elements in the preliminary model, the spacing of the rigid links was first changed to approximately 160 inches, based on the spacing of the elements along the top flange of the girders and Ross's finding that a link spacing of 80" would produce a 13% difference with the theoretical. The variations of the model with rigid links spaced at approximately 160 inches are represented as C1. The second variation of the spacing that was considered was spacing the rigid links at approximately 320 inches, or double the previous spacing of 160 inches. The variations of the model with rigid links spaced at approximately 320 inches are represented as C2. The preliminary model included a rigid link at every node on the centerline of the top flange of the girders (C0), i.e. approximately spaced at 10 inches.

The third parameter that was changed was the support conditions. The original support conditions (S0) had translation in the transverse and vertical directions constrained at the two supports at either end of the bridge with translation in the transverse, longitudinal, and vertical directions constrained at the support located at the center of the bridge between the two spans. For every support condition variation, the center node of the line of nodes along the bottom flange of the middle girder at the support located at the longitudinal center of the bridge, translation was constrained in all three directions and rotation was constrained in the longitudinal and vertical directions. New support conditions had translation in the transverse and vertical directions constrained at the two nodes on either edge of the bottom flange where the support is located and had translation in the transverse direction constrained at the node in the center of the line of nodes on the bottom flange at the location of the support. The longitudinal constraint at the center was thus removed in this variation. These changes allow for greater lateral bending. The variations of the model with these assumed support conditions are represented as S1. After further thought, it was decided that constraining the vertical direction at the two nodes on either edge of the bottom flange where the support is located instead of constraining the nodes in the transverse direction would be a more accurate representation of the actual conditions of the bridge. The variations of the model with these assumed support conditions (vertical constraint at all support nodes, transverse constraint at the nodes in the middle of the cross-section at the support, and rotation about the longitudinal and vertical axes constrained at the center bottom flange node of the middle girder at the center support) are represented as S5.

Several different combinations of these three parameters were considered while investigating the calibration of this model with each of these parameters altered in series, meaning first an optimum E value, then optimum rigid link spacing, then optimum support conditions were determined as illustrated in the flow chart in Figure 5.2. The first variation considered changing the strength of the concrete in the deck to 4 ksi (FEA E1, C0, S0). In general, this caused only a slight increase in stresses at the girder locations as was generally desired from those found with the preliminary model

(FEA E0, C0, S0) as seen in Tables 5.3, 5.4, and 5.5. The second variation (FEA E1, C1, S0) considered changing the spacing of the rigid links to indirectly increase the flexibility of the connection between the steel and concrete components of the bridge while the strength of the concrete remained at 4 ksi as in FEA E1, C0, S0. In general, FEA E1, C1, S0 produced a smaller percent difference with the field test than the FEA E1, C0, S0 model as seen in Tables 5.3, 5.4, and 5.5. The third variation (FEA E1, C2, S0) investigated doubling the spacing of the rigid links from the previous variation, FEA E1, C1, S0, to further capture the effects of increased flexibility and the steel-concrete interface in the girder. In general, FEA E1, C2, S0 produced a larger percent difference with the field test than FEA E1, C1, S0 as seen in Tables 5.3, 5.4, and 5.5; therefore it was determined that spacing of rigid links at approximately 160 inches was the best representation of the level of composite action in the actual structure. The final variation (FEA E1, C1, S5) considered changing the support conditions of the model. In general, this model variation resulted in the smallest percent differences between the FEA and field test results with an average % difference of bottom flange average tension stresses of 15.55%.

Figure 5.2 SR 1 Over US 13 Flow Chart

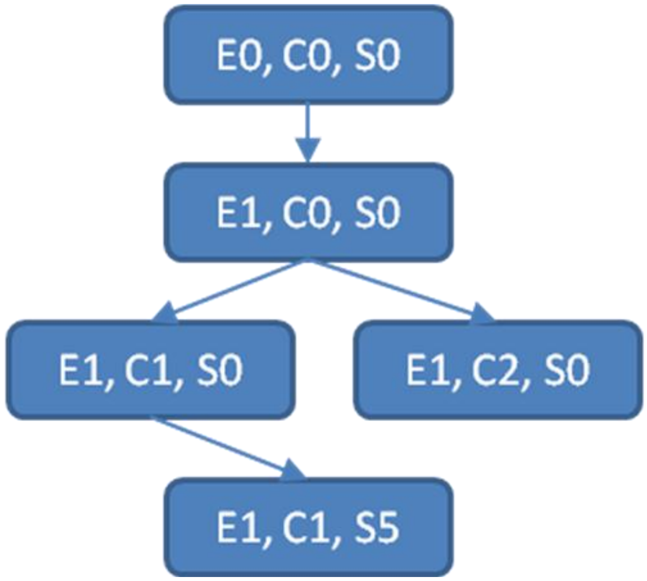

The neutral axis position was used to guide how to change each of these parameters as described in Section 5.2. The resulting neutral axis (NA) positions from the field test are included in Table 5.1 below, where the locations are measured from the bottom of the bottom flange. Both tension and compression are considered. The depth of the web in this girder is 66 inches and the total depth of the section (including the deck) is 79 inches. NA positions are generally between 59 and 63 inches for G1, between 40 and 44 inches for G2, and 37 and 39 inches for G3 based on the field test results for the different truck passes. These values were based on the maximum magnitude stresses (tension or compression) in the bottom flange and the concurrent web stresses. Theoretical values for the neutral axis position for each of the locations were also calculated based on the girder geometry ultimately assuming both 4 ksi and 5 ksi strength concrete and are also included in Table 5.1 below. However, as shown in the table, the results are not particularly sensitive to this variation. The differences between the theoretical values and the field test estimates suggested that the actual position of the neutral axis was lower than expected by theory, assuming that averaging the gauge pairs accurately reflects the flexural stresses and filters the lateral bending effects. Thus it is also expected from this that the bottom flange stresses will be larger than theoretically permitted. The missing value for G2 on Day 1 for Pass 2 for the field test NA estimates is due to a malfunctioning gauge which in turn produced incorrect results. The value for G1 for Pass 1 for the field tests is greater than the total depth of the section and therefore may also be due to a malfunctioning gauge.

Table 5.1 NA Positions for SR 1 Over US 13

	Field Test NA Estimates (inches)			Theoretical NA Values (inches)	
Location	Pass 1	Pass 2	Pass 3	4ksi	5 ksi
G1	82.92	63.08	59.08	57.01	58.19
G2 (Day 1)	---	---	---	54.19	55.47
G2 (Day 2)	39.99	42.42	42.02	54.19	55.47
G3	38.13	37.72	37.35	54.49	55.87

The neutral axis positions from the different finite element models for the longitudinal load position that caused the maximum absolute value of stresses in the bottom flange of each of the girder locations were also evaluated and compared to the field test estimates and calculated theoretical values. NA positions were calculated as described in Section 5.2. Table 5.2 summarizes the neutral axis positions that were estimated for each of the different model variations. It is difficult to obtain the desired NA position at all three locations simultaneously; therefore, a perfect match cannot be achieved. In general, the position estimated from the FEA was higher than the position calculated from the field test; therefore it was decided to decrease the assumed modulus of elasticity in order to lower the neutral axis as well as increase the spacing of the rigid links in order to better correlate the FEA with the field test. The resulting NA values are generally reduced as a result of these changes, but there is a slight increase of the NA position between E1, C1, S0 and E1, C2, S0 for Pass 2 and 3 for G2 which is unexpected as the NA positions at the other locations decrease between the two models. After the neutral axis positions were lowered via these changes, the support conditions were altered to attempt to achieve better correlation with the bottom flange stresses.

Table 5.2 NA Positions for FEA Models of SR 1 Over US 13

		Neutral Axis Position (inches)				
Location	Pass	E0,C0,S0	E1,C0,S0	E1,C1,S0	E1,C2,S0	E1,C1,S5
G1	1	48.18	---	---	---	37.08
	2	46.12	---	---	---	36.62
	3	46.21	---	---	---	36.85
G2	1	51.59	50.11	45.52	44.02	49.14
	2	46.95	44.67	45.36	47.21	45.871
	3	47.73	45.40	45.75	47.20	45.58
G3	1	62.59	60.73	54.06	56.61	52.13
	2	66.84	64.00	57.39	48.24	57.38
	3	37.35	63.08	57.02	48.08	56.1

The bottom flange stress results comparing the different model versions are summarized in Tables 5.3, 5.4, and 5.5 in the following pages. The maximum stress values at the girder locations for each of the three passes for each of the different model variations, in psi, are presented along with the maximum stress values from the field tests. The gauge location and whether the stress is tension or compression is indicated. G2 and G3 were instrumented on Day 1, while G1 and G2 were instrumented on Day 2. An entry of “---“ in the tables means the maximum stress for the version of the model was not investigated at that location. The absolute value of the percent difference between each of the values for the different variations and the field test is also presented. Both the individual gauge readings and the average of the two bottom flange gauges at each location are considered. For general calibration purposes, more emphasis is placed on the average values, but the individual readings indicate the amount of bending in the flanges, which is also important to consider.

Table 5.3 Bottom Flange Girder Stress Comparisons for SR 1 Over US 13, Pass 1

		Pass 1											
Gauge Location	Tension or Compression	Field Test (psi)	E0,C0, S0 (psi)	E1,C0, S0 (psi)	E1,C1, S0 (psi)	E1,C2, S0 (psi)	E1,C1, S5 (psi)	% Diff E0,C0, S0	% Diff E1,C0, S0	% Diff E1,C1, S0	% Diff E1,C2, S0	% Diff E1,C1, S5	Min. % Diff.
G1-BF-1	Tension	1074	1417	---	---	---	1535	32	---	---	---	43	32
G1-BF-2	Tension	1461	1304	---	---	---	1406	11	---	---	---	4	4
G1-AVG	Tension	1267	1361	---	---	---	1471	7	---	---	---	16	7
G2-BF-1	Tension	495	460	469	520	556	570	7	5	5	12	15	5
G2-BF-2	Tension	581	377	383	437	499	529	35	34	25	14	9	9
G2-AVG	Tension	538	418	426	479	528	550	22	21	11	2	2	2
G2-BF-1	Compression	-568	-417	---	---	---	-522	27	---	---	---	8	8
G2-BF-2	Compression	-402	-483	---	---	---	-671	20	---	---	---	67	20
G2-AVG	Compression	-485	-450	---	---	---	-597	7	---	---	---	23	
G3-BF-1	Tension	1458	1178	1200	1332	993	1412	19	18	9	32	3	3
G3-BF-2	Tension	1155	1155	1176	1277	908	1351	0	2	11	21	17	0
G3-AVG	Tension	1307	1167	1188	1305	951	1382	11	9	0	27	6	0

Table 5.4 Bottom Flange Girder Stress Comparisons for SR 1 Over US 13, Pass 2

		Pass 2											
Gauge Location	Tension or Compression	Field Test (psi)	E0,C0, S0 (psi)	E1,C0, S0 (psi)	E1,C1, S0 (psi)	E1,C2, S0 (psi)	E1,C1, S5 (psi)	% Diff E0,C0, S0	% Diff E1,C0, S0	% Diff E1,C1, S0	% Diff E1,C2, S0	% Diff E1,C1, S5	Min. % Diff.
G1-BF-1	Tension	996	759	---	---	---	1342	24	---	---	---	35	24
G1-BF-2	Tension	1001	1201	---	---	---	970	20	---	---	---	3	3
G1-AVG	Tension	999	980	---	---	---	1156	2	---	---	---	16	2
G2-BF-1	Tension	414	204.9	199	234	266	352	51	52	43	36	15	15
G2-BF-2	Tension	421	356	359	426	509	372	16	15	1	21	12	1
G2-AVG	Tension	418	280	279	330	388	362	33	33	21	7	13	7
G2-BF-1	Compression	-449	-275	---	---	---	-272	39	---	---	---	39	39
G2-BF-2	Compression	-320	-394	---	---	---	-339	23	---	---	---	6	6
G2-AVG	Compression	-385	-334	---	---	---	-306	13	---	---	---	20	13
G3-BF-1	Tension	1244	799	802	903	860	952	36	36	27	31	23	23
G3-BF-2	Tension	945	802	806	892	762	912	15	35	6	19	4	4
G3-AVG	Tension	1094	801	804	898	811	932	15	27	18	26	15	15

Table 5.5 Bottom Flange Girder Stress Comparisons for SR 1 Over US 13, Pass 3

		Pass 3											
Gauge Location	Tension or Compression	Field Test (psi)	E0,C0, S0 (psi)	E1,C0, S0 (psi)	E1,C1, S0 (psi)	E1,C2, S0 (psi)	E1,C1, S5 (psi)	% Diff E0,C0, S0	% Diff E1,C0, S0	% Diff E1,C1, S0	% Diff E1,C2, S0	% Diff E1,C1, S5	Min. % Diff.
G1-BF-1	Tension	907	1158	---	---	---	1277	28	---	---	---	41	28
G1-BF-2	Tension	763	682	---	---	---	879	11	---	---	---	15	11
G1-AVG	Tension	835	920	---	---	---	1078	10	---	---	---	29	10
G2-BF-1	Tension	251	180	174	222	226	339	28	31	12	10	35	10
G2-BF-2	Tension	239	356	358	435	510	356	49	50	82	113	49	49
G2-AVG	Tension	245	268	266	329	368	348	9	9	34	50	42	9
G2-BF-1	Compression	-330	-259	---	---	---	-242	22	---	---	---	27	22
G2-BF-2	Compression	-262	-387	---	---	---	-376	48	---	---	---	44	44
G2-AVG	Compression	-296	-323	---	---	---	-309	9	---	---	---	4	4
G3-BF-1	Tension	1006	757	759	873	830	917	25	25	13	17	9	9
G3-BF-2	Tension	806	759	761	861	734	872	6	6	7	9	8	6
G3-AVG	Tension	906	758	760	867	782	894	16	16	4	14	1	1

Overall, it was determined that FEA E1, C1, S5 was the best approximation of the actual girder stresses. Of all the different models considered during calibration, Table 5.6 lists the model that best approximations the stresses at each location. Of the 3 passes and 12 combinations of gauge locations or average and tension or compression, there are 36 entries in the table of which 41.67 % are for FEA E1, C1, S5 as the best approximation. 63.9 % of the entries have E1 as the modulus of elasticity that is the best representation. Of the entries which contain E1 as the best representation, 78.3% have C1 as the amount of rigid links that are the best representation and 83% have S5 as the support conditions that are the best representation out of the E1, C1 versions. E0, C0, S0 is the version of the model that is the closest approximation of the neutral axis found for G1 and versions of the model while E1 and S0 generally match the best at other locations. in the field test results, but the E1, C1, S5 version of the model lowered the neutral axis from the preliminary version of the model (E0, C0, S0). For future work, it is suggested that E0, C1, S5 be investigated to see if the final version determined here in can be further optimized using the originally assumed elastic modulus value. Results for the cross-frames of this model will be discussed in Section 5.4.1.

Table 5.6 SR 1 Over US 13 Model Resulting in Lowest Percent Differences for Bottom Flange Girder Stresses

		Lowest % Difference		
Gauge Location	Tension or Compression	Pass 1	Pass 2	Pass 3
G1-BF-1	Tension	E0 C0 S0	E0 C0 S0	E0 C0 S0
G1-BF-2	Tension	E1 C1 S5	E1 C1 S5	E0 C0 S0
G1-AVG	Tension	E0 C0 S0	E0 C0 S0	E0 C0 S0
G2-BF-1	Tension	E1 C1 S0	E1 C1 S5	E1 C2 S0
G2-BF-2	Tension	E1 C1 S5	E1 C1 S0	E1 C1 S5
G2-AVG	Tension	E1 C2 S0	E1 C2 S0	E1 C0 S0
G2-BF-1	Compression	E1 C1 S5	E0 C0 S0	E0 C0 S0
G2-BF-2	Compression	E0 C0 S0	E0 C0 S0	E1 C1 S5
G2-AVG	Compression	E0 C0 S0	E1 C1 S5	E1 C1 S5
G3-BF-1	Tension	E1 C1 S5	E1 C1 S5	E1 C1 S5
G3-BF-2	Tension	E0 C0 S0	E1 C1 S5	E1 C0 S0
G3-AVG	Tension	E1 C1 S0	E1 C1 S5	E1 C1 S5

5.2.2 SR 299 Over SR 1

As with the SR 1 over US 13 bridge, once the field tests results for SR 299 over SR 1 were compared to its preliminary finite element model, changes in each of the three key parameters identified above (concrete elastic modulus, rigid link spacing, and boundary conditions) were made to calibrate a model that more accurately captured the observed stresses. For reasons described above, this process began by calibrating the girder stresses, which is discussed in this section.

For the SR 299 over SR 1 model, several different values for the modulus of elasticity were investigated. The preliminary model assumes a concrete strength of

5 ksi (E0). Model variations with 4 ksi strength concrete are represented as E1, while models with a 6 ksi strength concrete are represented as E2. These two values were chosen to investigate changing the stiffness of the model and to investigate raising and lowering the neutral axis of the girder. Since the observed NA position at G1 was significantly higher than theory while the position at G2 was significantly lower than theory.

Because spacing of rigid links at approximately 160 inches models most accurately captured the flexibility between the steel and girder components in the SR 1 over US 13 model, this spacing was again investigated for the SR 299 over SR 1 model. The variations of the model with rigid links spaced at approximately 160 inches are represented as C1. The preliminary model contains rigid links at every node along the centerline of the top flange of the girders (C0), which corresponds to a spacing ranging approximately between 5' and 8".

Finally, alternative support conditions were evaluated. The original support conditions (S0) had translation in the transverse and vertical directions constrained at the two supports at either end of the bridge with translation in the transverse, longitudinal, and vertical directions constrained at the support located at the center of the bridge between the two spans. For every support condition variation, the center node of the line of nodes along the bottom flange of the middle girder at the support located at the longitudinal center of the bridge, translation was constrained in all three directions and rotation was constrained in the longitudinal and vertical directions. The S1 support conditions had translation in the transverse and vertical directions constrained at the two nodes on either edge of the bottom flange where the support is located and had translation in the transverse direction constrained at the node in the center of the line of nodes on the bottom flange at the location of the support. This was assumed at all of the supports. These changes affect the end reactions and thus force distribution throughout the system. The variations of the model with these assumed support conditions are represented as S1. The support conditions described as S5 in Section 5.2.1 would be a better representation of the physical attributes of the bridge. This option was not evaluated due to time constraints. Other investigations included constraining rotation about the transverse axis in addition to the other constraints at every node in the original S0 (E2, C1, S3) and new support conditions S1 (E2, C1, S4). Note the label S2 was not utilized.

Several different variations of these three parameters were considered while investigating the calibration of this model. The differences between the different model variations are demonstrated by looking at Day 2, Pass 1 Loading Case 7, the truck position that creates the maximum stress for Girder location 2 since this is a location of maximum stress and corresponding load position. The first axle of the truck is approximately 70 ft onto the bridge from the east end at this position. The differences between the model variations at G1 and G2, the two girders instrumented under Day 2 loading, can be seen in Table 5.7 below. The load cases and positions considered for this bridge were unique from the previous bridge and were labeled based on an arbitrary numbering system created when stepping the truck load across the model. Since Pass 1 on Day 2 had the loading closest to the instrumentation on G1 and G2 (which were only fully instrumented) this was the situation which was chosen for investigation and in turn G3 was not considered in calibration since it was not instrumented on Day 2. The first variation, FEA S1, E1, C0, considered changing the support conditions and the modulus of elasticity of the concrete. The strength of the concrete was changed to 4 ksi and the new support conditions were assumed in order to change the stiffness of the model and change the stress distribution. The second variation, FEA S1, E2, C0, changed the strength of the concrete to 6 ksi, while assuming the new support conditions to investigate raising the neutral axis of the girders. In general, this lowered the stresses found in the girder locations which was the desired result and compared better with the field test results at most locations. Therefore, the next variation of the model, FEA S1, E2, C1, kept constant the modulus of elasticity and support conditions from the previous variation and introduced changing the spacing of the rigid links in order to increase the flexibility of the steel to concrete connection. Because in general the stress predicted by the finite element model was higher than the field test results, it was decided to investigate adding more restraint to the model to assess whether locked bearings in the actual structure may be increasing the fixity and reducing the positive bending stresses in the bridge. Degree of freedom four, or rotation about the transverse axis, was constrained at every node in the original and new support conditions. These two model variations are represented as FEA E2, C1, S3 for the original support conditions and FEA E2, C1, S4 for the new support conditions.

The results of this analysis are summarized in Table 5.7. The maximum stress values at Girder Locations 1 and 2 for each of the different model variations, in psi, are presented along with the maximum stress values from the field tests. The absolute value of the percent difference between each of the values from the different variations and the field test is also presented. All maximums for this case are in tension. In general, the percent difference at the bottom flange girder locations was greater than 40 % with percent differences ranging from 34% to 67%. The average bottom flange stresses compare best with the E2, C0, S1 version of the model. Another observation is that, in general, the web locations compare better with the field test than the bottom flange locations. The large differences between the two bottom flange locations at G2 in the model indicate that a significant amount of lateral bending is being captured.

Table 5.7 Girder Stress Comparisons for SR 299 Over SR 1

			Day 2 Pass 1 Case 7											
Gauge Location	Tension or Comp.	Field Test (psi)	E0,C0, S0 (psi)	E1,C0, S1 (psi)	E2,C0, S1 (psi)	E2,C1, S1 (psi)	E2,C1, S3 (psi)	E2,C1, S4 (psi)	% Diff E0,C0 S0	% Diff E1,C0 S0	% Diff E2,C0 S1	% Diff E2,C1 S1	% Diff E2,C1 S3	% Diff E2,C1 S4
G1-W-1	Tension	827	764	764	763	665	607	660	8	8	8	20	27	20
G1-W-2	Tension	181	764	764	763	665	607	660	---	---	---	---	---	---
G1-W-AVG	Tension	827	764	764	763	665	607	660	8	8	8	20	27	20
G1-BF-1	Tension	1093	1741	1727	1668	1806	1700	1795	59	58	53	65	56	64
G1-BF-2	Tension	1172	1806	1739	1678	1755	1645	1745	54	48	43	50	40	49
G1-BF-AVG	Tension	1132	1774	1733	1673	1781	1672	1770	57	53	**48**	57	48	56
G2-W-1	Tension	1010	1055	1110	1078	848	776	842	4	10	7	16	23	17
G2-W-2	Tension	---	1055	1110	1078	848	776	842	---	---	---	---	---	---
G2-W-AVG	Tension	1010	1055	1110	1078	848	776	842	4	10	7	16	23	17
G2-BF-1	Tension	1748	2342	2520	2397	2489	2337	2475	34	44	37	42	34	42
G2-BF-2	Tension	718	1166	1037	1040	1196	1153	1188	62	44	45	67	61	65
G2-BF-AVG	Tension	1233	1754	1779	1719	1842	1745	1831	42	44	**39**	49	42	49

As with SR 1 over US 13, the neutral axis position for several cases was calculated for the field test and the E0, C0, S0 base model and is included in Table 5.8. When a value was not calculated, it is marked with "---" in the table. The neutral axis position was calculated in the same way described in Section 5.2.1. The theoretical values for the neutral axis position for each of the locations were also calculated based on the girder geometry for both 4 ksi and 5 ksi and are included in the same table. The depth of the web in this girder is 54 inches and the total depth of section (including the deck) is approximately 66 inches. Thus, the calculated value for G3 is suspicious.

Table 5.8 NA Positions for SR 299 Over SR 1

	Field Test NA Estimates (inches)		E0,C0,S0 Estimates (inches)		Theoretical NA Values (inches)	
	Pass 1	Pass 2	Pass 1	Pass 2	4 ksi	5ksi
G1	51.39	---	51.39	---	46.52	47.61
G2	38.22	---	---	---	46.52	47.61
G3	90.11	65.59	---	50.17	46.52	47.61

In order to better understand the behavior of this bridge because of the large differences between the stresses predicted by the model and the stresses found during the field test, demonstrated in Table 5.7, calculations were performed by hand in an effort to compare these results to theory. The hand calculations used the method of consistent deformations to perform an indeterminate analysis of the moment at Girder location 1 when the middle axle of the triaxle dump truck was placed longitudinally immediately over the Girder location 1. This was compared with the FEA results from Load Case 7 described previously in this section. The distribution factor for the bridge was calculated to be 0.435 according to the AASHTO (2010)

Specifications and was applied to the loading. This was found to be higher than distribution factors calculated from the model that will be discussed later in this section. Virtual work was used to calculate the displacements necessary to use this method of analysis. A copy of the hand calculations including the distribution factor calculation can be found in Appendix C. The moment found using the method of consistent deformation was divided by the section modulus, assuming a concrete strength of 5 ksi, to determine the stress. The result of the hand calculations was a stress of 2.08 ksi at Girder location 1. This compared much closer to the FEA results, ranging between 1.67 ksi and 1.78 ksi, than to stresses collected during the field test, 1.09 ksi. A summary of this comparison is in Table 5.9, showing that the average of the two girder locations is on average within approximately 16.5% of the hand calculations. It is expected for the hand calculations to be higher than the FEA because of conservatism that is inherent in the calculation of the distribution factor.

Table 5.9 Comparison to Hand Calculations

	Pass 1									
Gauge Location	Field Test (psi)	Hand Calcs (psi)	E0,C0, S0 (psi)	E1,C0, S1 (psi)	E2,C0,S1 (psi)	E2,C1, S1 (psi)	% Diff E0,C0,S0	% Diff E1,C0,S1	% Diff E2,C0,S1	% Diff E2,C1,S1
G1-BF-1	1093	2079	1741	1727	1668	1806	16	17	20	13
G1-BF-2	1172		1806	1739	1678	1755	13	16	19	16
G1-AVG	**1132**		**1773**	**1733**	**1673**	**1781**	**15**	**17**	**20**	**14**

The dead load stresses in the model were also compared to the dead load stress according to theory. In two variations of the model, the truck loading was removed from the model and it was reanalyzed with only dead load on the structure. Girder location 1, the same location considered in the hand calculations for live load mentioned in the previous paragraph, was used to determine the stresses due to dead load only. It was determined using the same hand calculation procedure as described for the live load stresses that this stress was approximately 9.5 ksi. This calculated stress was within 8 % of the stresses found in the dead load analysis of the finite element model. A comparison can be found in Table 5.10 below. The stress from the FEA S1, E2, C1 dead load only model was within 4 % of the theoretical dead load stress.

Table 5.10 Dead Load Comparison

Gauge Location	Theoretical DL Stress (psi)	E0,S0,C0 DL Only (psi)	S1, E2 ,C1 DL Only (psi)	% Diff E0,S0,C0 DL Only	% Diff E2,S1,C1 DL Only
G1-BF-1	9500	10236	9895	8	4
G1-BF-2		10131	9923	7	4
G2-BF-1	---	10937	10268	---	---
G2-BF-2		9687	9903	---	---

In an effort to figure out why the finite element model for SR 299 over SR 1 was not comparing as well to the field test as the SR 1 over US 13 model, several characteristics of the model were checked to assure accuracy. First, the load position of the triaxle dump truck on the model was double checked with the position of the truck during field tests. From observations and notes taken in the field, it was determined that the load position of the truck in the model matched fairly well with the positioning during the field tests. Small changes to the load position could possibly be made, but it was decided that this was not what was causing large differences between the model and the field tests since the transverse position of the truck would change by less than 1 ft farther from the instrumented locations. Second, the distribution factor of the model was calculated by dividing the stress of a particular girder by the sum of stress values at all of the girders. The distribution factors for each girder location were calculated using the positive stress values for all girders during the pass and load position causing the maximum stress in the girder location of interest. The data for these calculations are included in Table 5.11, where the pass for each is indicated since it varies slightly between the two days. These values are approximately half of the values previously computed using AASHTO methods. If this value were used in the hand calculations, they would match the field test results relatively well. Thus the differences in loading attributes should be explored further in future work.

Table 5.11 SR 299 Over SR 1 Distribution Factors

Girder Location	Day	Pass	Distribution Factor
G3	1	2	0.288
G1	2	1	0.224
G2	2	1	0.217

5.3 Selected Girder Stress Model Results

5.3.1 SR 1 Over US 13

FEA E1, C1, S5 was chosen as the final calibrated model for SR 1 over US 13. On average, all bottom flange results for the SR 1 over US 13 model are within 20 % of the field test results as shown in Table 5.12 which presents the percent difference between the FEA and the field test for all girder locations, for each of the passes, in tension and compression. Both tension and compression are considered for Girder Location 2 where the bottom flange experiences both stress states, in other locations were compression is not experienced the entry is denoted by “---“. On average, the bottom flange results for Pass 1 are within 12% of the field test results, for Pass 2 are within 16% of the field test results, and for Pass 3 are within 19% of the field test results. The truck load is positioned closest to the instrumented girder locations in Pass 1 which on average is the best match with the field test results. A higher percent difference is expected between the field test and the FEA for Girder Location 2 in compression because at this location the concrete is in tension and the finite element model does not account for the differing response in tension. Interestingly, in this situation, the correlation improves as the truck passes move farther from the gauge site.

Table 5.12 Comparison of Girder Stresses in FEA E1, C1, S5 to Field Test of SR 1 Over US 13

Gauge Location	Tension or Comp.	Pass 1 Field Test (psi)	Pass 1 E1,C1, S5 (psi)	Pass 1 % Diff	Pass 2 Field Test (psi)	Pass 2 E1,C1, S5 (psi)	Pass 2 % Diff	Pass 3 Field Test (psi)	Pass 3 E1,C1, S5 (psi)	Pass 3 % Diff
G1-AVG	Tension	1267	1471	16	999	1156	16	835	1078	29
G1-AVG	Comp.	---	---	---	---	---	---	---	---	---
G2-AVG	Tension	538	550	2	418	362	13	245	348	42
G2-AVG	Comp.	-485	-597	23	-385	-306	20	-296	-309	4
G3-AVG	Tension	1307	1381	6	1094	932	15	906	894	1
G3-AVG	Comp.	---	---	---	---	---	---	---	---	---
Average				**12**			**16**			**19**

The change between the S1 support conditions and the S5 support conditions was found to be very small. Both of these support conditions contain constraint of translation in transverse direction at the center node of the line of nodes on the bottom flange where the support is located and contain constraint of translation in the vertical direction at the outside nodes on the line of nodes on the bottom flange where the support is located. The original S0 support conditions constrained translation in the transverse and vertical directions at all nodes on the line of nodes on the bottom flange where the support is located. A common feature of S1 and S5 that differs from S0 is that longitudinal constraint at the center pier support is provided for all girders in S0 but only the center girder in S1 and S5.

5.3.2 SR 299 Over SR 1

After investigating several different variations of the SR 299 over SR 1 model, there was still no model that achieved an acceptable approximation of the field test girder stresses. As indicated in Section 5.2.2, hand calculations based on theoretical expectations of steel bridge behavior compared well with the finite element analysis results for dead load and live load. The load position was checked as well as the distribution factor and both were determined not to be the source of the differences between the model and field tests. Therefore, it was determined that there is something unexplained about the bridge that has not been identified and is not being captured by the finite element model. Although a final version of the SR 299 over SR 1 model was not chosen, results from the cross-frame locations are presented in Section 5.4.2. Future work to determine what has not been identified should be considered and is discussed in Chapter 6.

5.4 Alternative Cross-frame Stress Models

The primary objective of creating these finite element models was to develop a finite element model that would accurately capture cross-frame forces. The girder locations were first used to calibrate the models with the field tests and insure the global bending response was accurately captured before the cross-frame forces were further investigated. The following subsections examine the cross-frame forces from the calibrated models.

5.4.1 SR 1 Over US 13

The cross-frame data from the FEA E1, C1, S5 model was compared to the field test results with two different cross-frame connections. The first was with the cross-frames connected to the stiffeners via merged nodes, simulating a fixed connection. This was the method of connection used in all of the previous bridge models discussed in the previous sections. The second was with the cross-frames connected to the stiffeners via rigid links which linked the translational degrees of freedom of the two nodes, simulating a pinned connection. The cross-frame data from these models was analyzed by looking at the section points on the beam-type elements comprising the cross-frame members. ABAQUS defines section points at the top and bottom of the beam elements. However, the orientation used to establish "top" and "bottom" is unknown. Thus, data for the model was collected at both of these section points and was averaged in two different ways to determine which assumption of the orientation would yield the most accurate results. The averages of the field test data considered an average of the two gauges placed at the center of both legs of the angle. This assumes a constant stress throughout the concentric leg of the angle and a linear distribution of stress is assumed throughout the eccentric leg of the angle to account for shear lag, where more of the load is carried by the connected leg of the angle resulting in a nonuniformity of stress and flexural bending of the members. This same stress distribution is assumed in the FEA, but two different calculations were performed based on probable definitions of top and bottom in the analysis. "Case 1" considered an average between the top and bottom section points which assumes one section point is at the end of the concentric leg and the other is in the plane of the eccentric leg. "Case 2" considered an average between the top section point and the average of the top and bottom section points assuming the top is in the plane of the concentric leg and the bottom is at the end of the eccentric leg. Therefore, a constant stress was assumed throughout the concentric leg of the angle and an average of the two section points was taken to determine the average of the linear stress distribution along the eccentric leg of the angle. However, the bottom section point stresses are consistently higher than the top section point stresses, suggesting that the position of the bottom section point is closer to the concentric leg. Thus, a third averaging case considering this should be included in future work.

The model with the pinned connection for the cross-frames is consistently a better match to the field test data than the model where the cross-frames are connected with a fixed connection. Specifically, in 78 % of the averages of cross-frame gauge locations considered, the pinned connection is a better match with the field test data. Also the Case 1 average, which is an average of the top and bottom section points, is a better match with the field test data than the Case 2 average in 86 % of the cross-frame gauge locations considered. The pinned cross-frames also appear to better represent the actual amount of bending in the cross-frames based on the difference between top and bottom section points. The complete set of cross-frame data for Pass 1 for this bridge is presented below. Tables 5.13 presents the data for Cross-frame 12-3, Table 5.14 presents the data for Cross-frame 12-4, Table 5.15 presents the data for Cross-frame 14-3, Table 5.16 presents the data for Cross-frame 4-4, and Table 5.17 presents the data for Cross-frame 11-3. It includes the maximum stresses recorded during the field test at each location which was converted from strain by multiplying by the modulus of elasticity of steel, the section point values for the fixed and pinned connection cases, both averages of section points, and the differences between those averages and the field test data. The eccentric leg of the angle is denoted with an asterisk. For the sake of conciseness here, the full set of cross-frame data for all passes and both days of testing is included in Appendix D.

Table 5.13 Cross-frame 12-3 Data for SR 1 over US 13 Day 1 Pass 1

			Section Points FEA E1,C1,S5 Fixed						Section Points FEA E1 C1 S5 Pinned					
Gauge Location	σ_{MAX} (psi)	σ_{Avg} (psi)	Botto m (psi)	Top (psi)	Avg Case 1 (psi)	% Diff	Avg Case 2 (psi)	% Diff	Bottom (psi)	Top (psi)	Avg Case 1 (psi)	% Diff	Avg Case 2 (psi)	% Diff
12-3-B	1062	**621**	244	-240	2	100	-119	119	276	93	**184**	**70**	139	78
12-3-B*	180													
12-3-D	458	**504**	244	-216	14	97	-101	120	264	20	**142**	**72**	81	84
12-3-D*	549													
12-3-H	658	**658**	756	10	383	42	197	70	808	153	**481**	**27**	317	52
12-3-I	1391	**746**	1195	495	845	-13	670	10	1102	725	**914**	**-22**	819	-10
12-3-I*	101													
12-3-J	1315	**688**	1360	-716	322	53	-197	129	1238	-242	**498**	**28**	128	81
12-3-J*	61													

Table 5.14 Cross-frame 12-4 Data for SR 1 over US 13 Day 1 Pass 1

			Section Points FEA E1,C1,S5 Fixed						Section Points FEA E1 C1 S5 Pinned					
Gauge Location	σ_{MAX} (psi)	σ_{Avg} (psi)	Bottom (psi)	Top (psi)	Avg Case 1 (psi)	% Diff	Avg Case 2 (psi)	% Diff	Bottom (psi)	Top (psi)	Avg Case 1 (psi)	% Diff	Avg Case 2 (psi)	% Diff
12-4-A	-2467	**-1489**	-2710	-1091	-1901	-28	-1496	0	-2730	-2566	**-2648**	**-78**	-2607	-75
12-4-A*	-510													
12-4-C	-2915	**-1598**	-2921	497	-1212	24	-358	78	-2946	-863	**-1904**	**-19**	-1383	13
12-4-C*	-281													
12-4-G	2850	**2850**	2833	962	1897	33	1430	50	2828	1935	**2381**	**16**	2158	24
12-4-I	-167	**121**	100	-348	-124	202	-236	295	139	-508	**-185**	**252**	-347	386
12-4-I*	410													
12-4-J	245	**-357**	-863	1779	458	228	1119	414	-721	1533	**406**	**214**	970	372
12-4-J*	-958													

Table 5.15 Cross-frame 14-3 Data for SR 1 over US 13 Day 1 Pass 1

			Section Points FEA E1,C1,S5 Fixed						Section Points FEA E1 C1 S5 Pinned					
Gauge Location	σ_{MAX} (psi)	σ_{Avg} (psi)	Bottom (psi)	Top (psi)	Avg Case 1 (psi)	% Diff	Avg Case 2 (psi)	% Diff	Bottom (psi)	Top (psi)	Avg Case 1 (psi)	% Diff	Avg Case 2 (psi)	% Diff
14-3-B	1299	**1299**	-648	-193	-420	132	-307	124	-645	-110	**-378**	**129**	-244	119
14-3-F	918	**972**	1071	473	772	21	622	36	1215	548	**881**	**9**	714	27
14-3-F*	1027													
14-3-H	1422	**1123**	1175	-595	290	74	-153	114	1321	-480	**421**	**63**	-29	103
14-3-H*	823													
14-3-I	2453	**1302**	2050	-849	601	54	-124	110	2034	-361	**836**	**36**	238	82
14-3-I*	151													
14-3-J	2491	**1425**	2108	-1162	473	67	-345	124	2113	-893	**610**	**57**	-142	110
14-3-J*	360													

Table 5.16 Cross-frame 4-4 Data for SR 1 Over US 13 Day 2 Pass 1

			Section Points FEA E1, C1, S5 Fixed						Section Points FEA E1, C1, S5 Pinned					
Gauge Location	σ_{MAX} (psi)	σ_{Avg} (psi)	Bottom (psi)	Top (psi)	Avg Case 1 (psi)	% Diff	Avg Case 2 (psi)	% Diff	Bottom (psi)	Top (psi)	Avg Case 1 (psi)	% Diff	Avg Case 2 (psi)	% Diff
4-4-A	-2979	**-1655**	-2716	3374	329	120	1852	212	-2072	1725	**-173**	**90**	776	147
4-4-A*	-332													
4-4-C	-3133	**-1661**	-2731	3437	353	121	1895	214	-2111	1993	**-59**	**96**	967	158
4-4-C*	-190													
4-4-E	3300	**2287**	2451	-3037	-293	113	-1665	173	2187	-1569	**309**	**86**	-630	128
4-4-E*	1275													
4-4-G	4218	**1972**	2456	-3004	-274	114	-1639	183	2173	-1292	**441**	**78**	-425	122
4-4-G*	-274													
4-4-I	1162	**938**	508	-1302	-397	142	-850	191	-1250	1300	**25**	**97**	663	29
4-4-I*	714													
4-4-J	1052	**43**	411	-792	-190	543	-491	1244	404	-790	**-193**	**550**	-492	1246
4-4-J*	-966													

Table 5.17 Cross-frame 11-3 Data for SR 1 Over US 13 Day 2 Pass 1

			Section Points FEA E1, C1, S5 Fixed						Section Points FEA E1, C1, S5 Pinned					
Gauge Location	σ_{MAX} (psi)	σ_{Avg} (psi)	Bottom (psi)	Top (psi)	Avg Case 1 (psi)	% Diff	Avg Case 2 (psi)	% Diff	Bottom (psi)	Top (psi)	Avg Case 1 (psi)	% Diff	Avg Case 2 (psi)	% Diff
11-3-B	1355	**1355**	1757	-1512	122	91	-695	151	1635	-1241	**197**	**85**	-522	139
11-3-F	-1540	**-1540**	-1376	-1424	-1400	9	-1412	8	-1388	-1473	**-1431**	**7**	-1452	6
11-3-H	-1384	**-784**	-1761	1742	-10	99	866	210	-1766	1525	**-120**	**85**	702	190
11-3-H*	-184													
11-3-I	419	**311**	202	240	221	29	230	26	152	-110	**21**	**93**	-44	114
11-3-I*	203													
11-3-J	478	**19**	234	-439	-102	643	-271	1537	179	-343	**-82**	**536**	-213	1229
11-3-J*	-440													

On average, in 73% of the cross-frame locations studied, the field test average magnitudes are greater than the stress magnitudes captured by the finite element model for the Case 1 average. The exception is at the locations where stresses are highest where the model is conservative. Some of the cross-frame locations matched fairly well, while others matched poorly. The field tests show that a large amount of bending is occurring in the cross-frames. In an effort to determine which locations were matching well, each of the instrumented cross-frame locations was ranked from highest to lowest magnitude stress for both the field test average and Case 1 average from the pinned connection model. These ranking are compared in Table 5.18 for each pass for all cross-frame locations. Cross-frames where only one gauge was placed on the concentric leg of the angle are denoted with an asterisk and since these gauge locations are not averaged with a lower eccentric leg stress value, higher results are expected at these locations. The FEA data at these locations continues to be an average of the top and bottom section points.

The results in Table 5.18 show that Cross-frame locations 12-4-A, 12-4-C, 12-4-G, and 11-3-F are consistently toward the top of the rankings. All of these locations are on inclined members on the side of the cross-frame framing into Girder 3 in the negative bending region of Girder 3; this is a logical result since this is where cross-frames are needed to brace the compression flange. Cross-frame locations 4-4-I, 4-4-J, and 11-3-I are also consistently toward the bottom of the rankings.

When analyzing all of the cross-frame data, several different observations were made. For Cross-frame locations 12-3-B and 12-4-A, which are both top corner locations on either side of Girder location 2, the percent difference between the pair of gauges stays consistent at approximately 85% for 12-3-B and approximately 79% for

12-4-A for all three passes. This trend also occurs in Cross-frame location 4-4-A which is also a top corner location where the percent difference between the pair of gauges stays consistent at approximately 88%. It should be noted that for each of these cross-frame locations the percent difference between the top and bottom section point values also stays fairly consistent between passes, although it is not consistent with the percent differences between the pairs of field test gauges. Further evaluation of this discrepancy could shed light on the relative contributions of bending and shear lag in the cross-frames. Furthermore, it is noted that the member forces in Cross-frame 4-4 are significantly under predicted by the model. Given the close proximity of this cross-frame to the support, this may point to further refinements needed on this aspect of the model.

Table 5.18 Average Cross-frame Stresses Ranking

	Pass 1		Pass 2		Pass 3	
Gauge Location	FT Avg.	Pinned Case 1 Avg.	FT Avg.	Pinned Case 1 Avg.	FT Avg.	Pinned Case 1 Avg.
12-3-B	20	19	13	5	9	6
12-3-D	21	21	14	1	14	1
12-3-H*	19	10	17	10	10	10
12-3-I	17	5	16	18	18	22
12-3-J	18	9	20	15	23	19
12-4-A	8	1	6	2	4	2
12-4-C	6	3	3	4	5	4
12-4-G*	1	2	2	7	11	7
12-4-I	24	18	24	9	22	8
12-4-J	22	13	15	14	16	12
14-3-B*	12	14	1	6	1	5
14-3-F	14	6	25	8	21	9
14-3-H	13	12	19	13	26	13
14-3-I	11	7	5	12	6	14
14-3-J	9	8	8	11	8	11
4-4-A	5	20	9	21	12	21
4-4-C	4	24	11	24	15	24
4-4-E	2	15	7	20	13	20
4-4-G	3	11	12	16	17	17
4-4-I	15	25	21	25	25	25
4-4-J	25	17	22	19	19	16
11-3-B*	10	16	4	17	3	18
11-3-F*	7	4	10	3	2	3
11-3-H	16	22	18	23	7	23
11-3-I	23	26	23	26	20	26
11-3-J	26	23	26	21	24	15

*Gauge placed only on concentric leg of angle

The cross-frame locations were also investigated as bottom flange groupings, meaning the gauge locations that framed into the bottom corner of a cross-frame (for example, the two gauges on the bottom portion of the inclined angle at 14-3-H and the two gauges on the same side of the bottom chord at 14-3-J). Of the two gauges, only the gauge on the concentric leg of the angle was considered for this analysis. The data from the gauges at these locations was summed for both the field test and FEA E1, C1, S5 pinned model and is presented in the following tables. The percent difference between the field test and the FEA for these groupings was calculated. Table 5.19 presents the groupings for Pass 1, Table 5.20 presents the groupings for Pass 2, and Table 5.21 presents the groupings for Pass 3. They present the maximum stress from the field test (σ_{Max}), bottom and top section point values for FEA E1, C1, S5 pinned model, the Case 1 average of the section points, and the percent difference between the Case 1 average and the field test maximum. The percent difference between the Case 1 average and the field test of the bottom flange groupings is high in this analysis with the groupings for Pass 1 on average 82% different, the groupings for Pass 2 on average 107% different, and the groupings for Pass 3 on average 43% different.

Table 5.19 Bottom Flange Gauge Groupings, SR 1 Over US 13 Pass 1

	Pass 1				
Gauge Location	σ_{MAX} (psi)	Bottom (psi)	Top (psi)	Avg. Case 1 (psi)	% Diff
12-3-H	658	808	153	480.5	
12-3-J	1315	1238	-242	498	
BF 12-3	1973			979	50
12-4-G	2850	2828	1935	2381.5	
12-4-I	-167	139	-508	-184.5	
BF 12-4	2683			2197	18
14-3-H	1422	1321	-480	420.62	
14-3-J	2491	2113	-893	610	
BF 14-3	3913			1031	74
4-4-G	4218	2173	-1292	440.5	
4-4-I	1162	-1250	1300	25	
BF 4-4	5380			466	91
11-3-H	-1766	1525	1564	1544.61	
11-3-J	179	-343	-341	-342.126	
BF 11-3	-1587			1202	176

Table 5.20 Bottom Flange Gauge Groupings, SR 1 Over US 13 Pass 2

	Pass 2				
Gauge Location	σ_{MAX} (psi)	Bottom (psi)	Top (psi)	Avg. Case 1 (psi)	% Diff
12-3-H	-678	-2080	219	-931	
12-3-J	1121	556	219	388	
BF 12-3	442			-543	223
12-4-G	1979	1534	1251	1393	
12-4-I	-836	-1189	-1002	-1096	
BF 12-4	1143			297	74
14-3-H	192	-800	-447	-624	
14-3-J	3012	2179	-493	843	
BF 14-3	3204			219	93
4-4-G	2571	1870	-1096	387	
4-4-I	236	329	-349	-10	
BF 4-4	2807			377	87
11-3-H	-1325	-2709	2428	-141	
11-3-J	475	671	-1083	-206	
BF 11-3	-850			-347	59

Table 5.21 Bottom Flange Gauge Groupings, SR 1 Over US 13 Pass 3

	Pass 3				
Gauge Location	σ_{MAX} (psi)	Bottom (psi)	Top (psi)	Avg. Case 1 (psi)	% Diff
12-3-H	-1246	-2172	232	-970	
12-3-J	869	320	255	288	
BF 12-3	-377			-683	-81
12-4-G	1188	1364	1157	1261	
12-4-I	-1136	-1456	-976	-1216	
BF 12-4	52			45	14
14-3-H	-659	-826	-384	-605	
14-3-J	2868	1968	-422	773	
BF 14-3	2209			168	92
4-4-G	1747	1791	-1048	372	
4-4-I	-355	-914	983	35	
BF 4-4	1393			406	71
11-3-H	-2342	-2762	2563	-100	
11-3-J	469	-1529	2408	440	
BF 11-3	-1873			340	118

5.4.2 SR 299 Over SR 1

Although a final version of the SR 299 over SR 1 model was never chosen, the cross-frame data for model C1, E2, S1 Day 2 Pass 1 is presented in Table 5.22. The values at computed for the longitudinal position that produces the maximum at each location. When comparing an average of the absolute values of the percent differences between the field test and the FEA for Pass 1 (the pass where the load is closest to the instrumentation) for the cross-frames for SR 1 over US 13 to the an average of the absolute values of the percent differences between the field test and the FEA for Pass 1 for the cross-frames for SR 299 over SR 1, as expected, the cross-frames for SR 1 over US 13 match better with the field test than the cross-frames for SR 299 over SR1. This day and pass was chosen for study due to the load location for the pass being closest to the gauges installed. The data presented is based on 6 ksi concrete, rigid links spaced at approximately 160 inches, and new support conditions which constrain the vertical direction at the two nodes on either edge of the bottom flange where the support is located and constrain translation in the transverse and vertical directions at the node in the center of the line of nodes on the bottom flange at the location of the support. As with the cross-frame data for SR 1 over US 13, section points along the beam element comprising the cross-frame location are considered. As before, two different cases for averaging the section points were calculated. Case 1 considers the average of the top and bottom section points, while Case 2 considers an average of the top section point and an average of the top and bottom section points for the reasons discussed in Section 5.4.1. As with the previous bridge, at most locations, the Case 1 average is a better match than the Case 2 average. It was determined in Section 5.2.2 that there is something unexplained about the bridge that has not been identified and is not being captured by the finite element model or the theoretical expectation of bridge behavior. Future work to determine what has not been identified should be considered and is discussed in Chapter 6. Thus, no effort was made to achieve a better match to the cross-frame forces predicted by the field test in the modeling at this time. Table 5.22 presents the field tests values, the top and bottom section point values, both Case 1 and Case 2 averages, and the percent difference between each case and the field test average. The eccentric leg of the angle is denoted with an asterisk.

Table 5.22 Cross-frame Data for SR 299 Over SR 1 Day 2 Pass 1

Gauge Location	σ_{MAX} (psi)	$\sigma_{MAX-AVG}$ (psi)	Section Points FEA S1, E2, C1: Bottom (psi)	Top (psi)	Avg. Case 1 (psi)	% Diff	Avg. Case 2 (psi)	% Diff
12-4-B	1523	797	183	-249	-33	104	-141	118
12-4-B*	71							
12-4-D	1411	981	135	84	110	89	97	90
12-4-D*	552							
12-4-G	1303	793	672	983	828	-4	905	-14
12-4-G*	283							
12-4-H	1396	649	903	-994	-46	107	-520	180
12-4-H*	-98							
12-5-A	-1365	-664	-724	1115	195	129	655	199
12-5-A*	37							
12-5-C	-1104	-743	-560	891	165	122	528	171
12-5-C*	-382							
12-5-E	1509	560	943	-1409	-233	142	-821	247
12-5-E*	-389							
12-5-F	1231	691	773	-173	300	57	64	91
12-5-F*	151							
8-4-B	-329	-113	-729	-444	-586	-421	-515	-358
8-4-B*	104							
8-4-D	-212	24	-719	-778	-749	3181	-764	3242
8-4-D*	261							
8-4-G	154	110	364	190	277	-152	233	-112
8-4-G*	66							
8-4-H	210	154	413	-230	91	41	-69	145
8-4-H*	98							

*Denotes eccentric leg

For SR 299 over SR 1, removing the cross-frames on the 134’ span from the model was investigated. In general, this caused an increase in stresses at the girder locations studied.

5.5 Conclusion

The truck load positioning that caused the maximum stress at each girder location was determined by stepping the truck loading across the model in 10 feet or less increments. Once the maximum position was discovered, calibration of the models began by comparing the stresses at the locations corresponding to each of the bottom flange girder locations that were instrumented to the field test data. Maximum positions of the truck loading were verified each time the model was altered. Different parameters of the model were then changed in order to attempt to best capture the actual behavior of each bridge. The three main parameters that were changed to assess global behavior via the girder stresses were the modulus of elasticity (E) of the concrete, the spacing of the rigid links used in the model to simulate composite action, and the support conditions.

For the SR 1 over US 13 bridge, model variation E1, C1, S5 was chosen as the final calibrated version of the model. There was less than a 20% difference between the E1, C1, S1 model and the field test data for each of the bottom flange locations in all three truck passes. This model had a concrete strength of 4 ksi (E1), rigid links spaced at approximately 160 inches (C1), and support conditions (S5) that assumed constraint of the vertical direction at every node along the bottom flange where the supports were located and constraint in the transverse direction at the center node of the line of nodes on the bottom flange where the abutments and pier support were located. When analyzing the cross-frame data for this bridge, the cross-frame connection in the E1, C1, S5 model was investigated as a fixed or pinned connection. The cross-frames with a pinned connection compared better with the field test data in 78% of the locations studied, yet the percent difference between this case and the field test was still often high for several cross-frames. Section points along the beam element cross-section representing the cross-frame in the model were also considered. It was discovered that the best match to the field test data was an average (Case 1) between the top and bottom section points which suggested ABAQUS oriented one of the section points at the edge of the concentric angle and the other section point in the plane of the eccentric angle.

For the SR 299 over SR 1 bridge, no model was chosen as the final calibrated version of the model. It was determined that the finite element model was responding according to theory, but something unexplained about the bridge had not been identified and was causing a different behavior. Future work should be considered to identify this behavior. Also, the bottom section point stresses are consistently higher than the top section point stresses, suggesting that the position of the bottom section point is closer to the concentric leg. Thus, a third averaging case considering this should be included in future work.

Chapter 6

CONCLUSION

6.1 Summary

The objectives of this thesis were to quantify the forces in cross-frames in skewed steel I-girder bridges through field testing and to also calibrate a finite element model that accurately captures those forces. Cross-frames are an important secondary member in steel I-girder bridges providing lateral-load resistance, improving live-load distribution, and reducing the buckling length of the compression flanges of the steel girders. While it is known that bridges have the capacity to easily sustain loads greater than their design loads, a codified method for quantifying this reserve capacity that accounts for the three-dimensional behavior does not exist. Cross-frames are a critical component in maximizing steel bridge reserve capacity. Furthermore, it is also known that the role of cross-frames becomes more significant in skewed and curved bridges and also that skew influences reserve capacity.

This research involved both field testing and finite element analysis. Two bridges of varying skews in the state of Delaware were chosen based on parameters such as skew, cross-frame type, and cross-frame spacing. Preliminary finite element models for the two bridges of varying skews chosen for study were created and analyzed.

The field testing aspect of this research was described in Chapter 4. Field tests were conducted on two different bridges, SR 1 over US 13, a 65 degree skew bridge approximately 5 miles south of the Chesapeake & Delaware Canal in Delaware, and SR 299 over SR 1, a 32 degree skew bridge located in the Middletown-Odessa area of Delaware. BDI ST-350 strain transducers and their associated structural testing system were used to instrument both bridges over four separate days of testing. Strain transducers were clamped on cross-frame and bottom flange locations, while they were bonded to web locations. Instrumentation layouts for both bridges were created based on a preliminary finite element analysis then slightly adjusted based on the instrumentation available. Over four days of field testing, eleven cross-frames and six girder cross-sections were tested between both bridges. Data was recorded each day for different passes of a weighed triaxle dump truck provided by DelDOT. Ultimately, the field testing of both bridges was a success and a large amount of useful data was gathered.

The field testing was then used to calibrate finite element models to accurately capture the behavior of both bridges using finite element analysis. Preliminary finite element models of both bridges were altered in an effort to most accurately reflect the actual behavior of both bridges. The load and position of the DelDOT triaxle dump truck used in field testing was placed in the preliminary finite element models. It was stepped across the bridge in increments of 10’ or less to find the truck position causing the maximum stress for each of the girder and cross-frame locations where strain gauges exist in the field testing to begin the calibration process. Three main parameters were considered when making changes to the preliminary finite element models. These were the modulus of elasticity of the concrete, the spacing of rigid links used to simulate composite action, and the support conditions. A final calibrated model (FEA E1, C1, S5) was determined for SR 1 over US 13. It had a concrete strength of 4 ksi, rigid links spaced at approximately 160 inches, and different support conditions that constrained the vertical direction at the two nodes on either edge of the bottom flange where the support is located and constrained the transverse and vertical directions at the node in the center of the line of nodes on the bottom flange at the location of the support. On average, all bottom flange results for the final finite element model were within 20% of the field test results. On average, in 73% of the cross-frame locations studied the field test average magnitudes are greater than the stress magnitudes captured by the finite element model. The exception are the locations where the highest stresses are recorded, here the model predictions are conservative. The SR 299 over SR 1 bridge proved to be a bigger challenge in the calibration process. After following the same calibration process used for the SR 1 over US 13 bridge, an acceptable model was not obtained. The predicted behavior of the structure was computed by hand according to theory and it was found that the FEA results were in good agreement with theoretical expectations. Thus, it was determined that there was something unexplained about the bridge that had not been identified and was not being captured by the finite element model or hand calculations. Future work to determine what has not been identified is needed and is discussed in Section 6.3.

6.2 Results

Two bridges of varying skews, SR 1 over US 13 and SR 299 over SR 1, both located in New Castle County, Delaware, were selected for field testing. Cross-frames and girder locations were instrumented and the bridges were load tested with a weighed truck. Overall between the two bridges, the field tests captured data for 11 cross-frames and 6 girder locations. For the bridge with less skew, SR 299 over SR 1, the maximum bottom flange stress was 1.7 ksi while the maximum cross-frame stress is of similar magnitude, 1.5 ksi. For the more-heavily skewed bridge, SR 1 over US

13, the maximum bottom flange stress was 1.5 ksi while the maximum cross frame stress is more than double this value, 3.6 ksi which occurs in the inclined member of the cross-frame near the maximum positive moment location. This suggests that the potential for cross-frame yielding is an important consideration in determining the reserve capacity of steel bridges.

In an effort to calibrate finite element models for each bridge, comparison of stresses at bottom flange locations was chosen as initial metric for comparing the FEA and the field tests. The final finite element model (E1, C1, S5) for SR 1 over US 13 predicted stresses at bottom flange girder locations within 20% of the field test results under all truck passes and instrumented locations. Hand calculations of the expected stress in the bottom flange according to the American Association of State Highway and Transportation Officials specifications matched the finite element model for SR 299 over SR 1 well, but the bridge behavior captured during the field testing differs from conventional expectations. Therefore, a final finite element model for this bridge was not chosen and future work is needed to identify the source of the unexplained behavior and more accurately calibrate the model.

The data from the calibrated model for the SR 1 over US 13 bridge was compared to the field test results in two different ways, one simulating a fixed cross-frame connection and the other simulating a pinned cross-frame connection, in order to determine the best approximation of the cross-frame connection. Cross-frame data for the final calibrated model, FEA E1, C1, S5 with pinned cross-frame connections (which was determined to be the best approximation of the actual cross-frame connection), of the SR 1 over US 13 bridge was presented in Section 5.4 as well as in Appendix D. Data was collected by looking at the different section points that

ABAQUS defines along the cross-section of the beam elements that comprise the cross-frames. This section point data was averaged in two different ways in order to evaluate the orientation of the section points assumed by ABAQUS, which suggested that ABAQUS specified the top of the element to be at the end of the concentric leg of the angle and the bottom of the element to be in the plane of the eccentric leg of the angle. However, since the bottom section point typically displays the highest stress, other means of synthesizing the data should be evaluated in future work. These averages are used to determine the average stress on the cross-section, which can be compared to the field test data by assuming a uniform stress in the concentric leg and linear stress distribution in the eccentric leg in all cases.

From the collected data, it was determined that the model with the pinned connection cross-frames was a better representation of the field test data than the model where the cross-frames have a fixed connection 78% of the time. This seems to produce results that better mimic the large amount of bending in the cross-frames that was observed in the field test data. The Case 1 average, where the top and bottom section points were averaged was a better match to the field test data than the Case 2 average in 86% of the cross-frame locations studied. It was also determined that in 73% of the cross-frame locations studied the averages from the field test data were greater in magnitude than the stresses predicted by the finite element models. The exception are the locations where the highest stresses are recorded, here the model predictions are conservative. For future analysis of the data, it may be beneficial to note the improved accuracy of the data as the transverse position of the load is closer to the location being analyzed. Other smaller observations and trends in the data are presented in Section 5.4. In general, bottom flange girder stresses compare better with the field test than the cross-frame stresses. Cross-frame locations 12-4-A, 12-4-C, 12-4-G, and 11-3-F are consistently exhibit high stresses in all three passes. The highest magnitude force observed in a cross-frame for the field tests was 3.6 ksi, while the highest magnitude stress observed in a cross-frame for the final calibrated model was 3.3 ksi, a 10% error. For future analysis of the data, it may be beneficial to look at how the data compares with the field test when the load is positioned closer to the instrumented locations.

Although no final calibrated model was determined for the SR 299 over SR 1 bridge, cross-frame data from the FEA S1, E2, C1 variation of the model is presented in Section 5.4 because it is currently the best approximation of the field test data at the bottom flange locations. Because an acceptable match between the bottom flange stresses was never determined with this model (average bottom flange girder stresses for the E2, C1, S1 model are approximately 40 to 50% different than the field test results), the pinned versus fixed cross-frame connection was not considered for this model. Data for the cross-frames was presented in Section 5.4 in a similar manner as described above for the SR 1 over US 13 bridge. In general, the stresses at the bottom flange girder locations predicted by the FEA are higher than the maximum bottom flange stresses from the field tests. Future work to continue the calibration process for the SR 299 over SR 1 model is discussed in Section 6.3.

6.3 Future Work

The calibration of the preliminary finite element models, as described in Chapter 5, consisted of a trial and error process guided by comparisons of neutral axis positions and bottom flange stresses to determine the version of the model that best captured the response of the bridge recorded by the field test data. A careful system for organizing all the data that is generated by this type of work is critical.

Future work is needed in the calibration of the SR 299 over SR 1 model, the 32 degree skew bridge located in the Middletown-Odessa area of Delaware. As described in Chapter 5, work done calibrating the model thus far has not captured some unexplained phenomenon that is being represented in the field test data. Hand calculations have been conducted and have demonstrated that the finite element model is performing according to theory. Distribution factor calculations were also performed and were found to be different between the model and the field test and further evaluating this discrepancy is a suggested starting point for future work. Since the pinned versus fixed cross-frame connection was never investigated for this bridge, this is an important parameter to consider. Further investigation into this unexplained behavior is needed in order to finish the calibration process for the SR 299 over SR 1 model. Both bridge models also model concrete the same in tension and compression; therefore concrete strength in tension is overestimated. This could be refined in future work.

It is also recommended to consider bridges with a smaller number of girders when considering bridges to study using FEA. The SR 1 over US 13 bridge model with 5 girders was much easier to model and manage in terms of data and computer memory than the SR 299 over SR 1 bridge model with 11 girders.

In order to quantify the influence of cross-frames on a bridge's reserve capacity, a parametric study will be conducted. In the parametric study, several factors such as lateral bracing layout (e.g., staggered or not staggered, perpendicular to girders or parallel to skew), lateral bracing configuration (X or K type cross-frames), and bridge skew should be varied and the resulting cross-frame forces and influence of cross-frames on the bridge's reserve capacity will be determined. This will be done by changing those factors in the calibrated models for SR 1 over US 13 and SR 299 over SR 1. From the results of the parametric study, general conclusions regarding the influences of cross-frames on reserve capacity will be quantified. Additionally, cross-frames significantly influence a bridge's response to vehicular impacts to girders, for example a truck violating the allowable bridge clearance. Quantification of this effect is also lacking. A select subset of the bridge models already developed will be subjected to a loading representative of a truck strike. The positioning of this load can also be varied and the resulting cross-frame forces and structural response will be studied. From this, a recommendation about whether cross-frames are beneficial or detrimental in this situation can be offered.

REFERENCES

American Association of State Highway and Transportation Officials. (2010). *AASHTO LRFD Bridge Design Specifications, 5th Edition.* American Association of State Highway and Transportation Officials, Washington, D.C.

Azizinamini, A., Kathol, S., and Beacham, M. (1995). "Influence of Cross Frames on Load Resisting Capacity of Steel Girder Bridges." Eng.J.-Amer.Inst.Steel Constr., 32(3), 107-116.

Bechtel, Andrew J. (2008). “Destructive Testing and Ultimate Capacity of Skewed Simple Span Bridges.” Thesis. University of Delaware.

Bishara, A. G., and Elmir, W. E. (1990). "Interaction between Cross Frames and Girders." J.Struct.Engrg.Journal of Structural Engineering, 116(5).

Bridge Diagnostics. (2006). “BDI Strain Transducer ST-350 specifications sheet.” Bridge Diagnostics, Inc.

Fasl, Jeremiah, Romage, Michelle, Helwig, Todd, Herman, Reagan, and Frank, Karl. (2009). “Field Measurements on Steel Girder Bridge with Skewed Supports Utilizing Lean-On Bracing.” ASCE Proceedings of 2009 Structural Congress. Vol. 341, 1-10.

Fell, B. V., and Kanvinde, A. M. (2010). "Tensile forces for seismic design of braced frame connections - Experimental results." *Journal of Constructional Steel Research,* 66(4), 496-503.

Google Maps. (2012). <www.googlemaps.com>. (April 13, 2012).

Hartman, A. S., Hassel, H. L., Adams, C. A., Bennett, C. R., Matamoros, A. B., and Rolfe, S. T. (2010). "Effects of Cross-Frame Placement and Skew on Distortion-Induced Fatigue in Steel Bridges." *Transportation Research Record: Journal of the Transportation Research Board,* 2200(-1), 62-68.

Liu, J., and Chajes, M. J. (2008). "Lateral-torsional buckling study of a continuous, skewed, steel bridge during deck placement." *Bridge Structures,* 4(1), 15-22.

Michaud, K. (2011). “Evaluating Reserve Capacity Through Destructive Testing of a Decommissioned Bridge.” Thesis. University of Delaware.

Quadrato C., Battistini A., Frank K., Helwig T., and Engelhardt M. (2010). "Improved cross-frame connection details for steel bridges with skewed supports." (2200).

Ross, J. H. (2007). “Evaluating Ultimate Bridge Capacity Through Destructive Testing of Decommissioned Bridges.” Thesis. University of Delaware.

Schluter IV, E. (2001). “Influence and Design of Intermediate Cross Frames in Composite Steel Bridges.” Thesis. University of Delaware.

Tedesco, J. W., Stallings, J. M., and Tow, D. R. (1995). "Finite element method analysis of bridge girder-diaphragm interaction." Computers & Structures., 56(2-3), 461.

Wang, W., Battistini, A., Helwig, T., Engelhardt, M., and Frank, K. (2011). “Staggered bracing in skewed steel bridge.” Structural Stability Research Council, Conference Proceedings, 70-81.

Wang L., and Helwig T.A. (2008). "Stability bracing requirements for steel bridge girders with skewed supports." *J Bridge Eng Journal of Bridge Engineering*, 13(2), 149-157.

Appendix A

FIELD TEST LABELS

The labeling system used for the field tests conducted for SR 299 over SR 1 and SR 1 over US 13 are presented herein. As stated in Chapter 4, the field tests were carried out with the help of DelDOT over four days using BDI ST-350 strain transducers. The following diagrams indicate the locations of the strain gauges as well as their corresponding identification number of the strain gauge placed in that location. The diagrams for the testing of SR 299 over SR 1 are presented first, followed by the diagrams for the testing of SR 1 over US 13. Girder locations that were instrumented on multiple days are presented side by side and are presented first for each bridge followed by the cross-frames. In a few instances, the note “did not balance” with the gauge number indicates the gauge did not zero during the balancing process when no live load was on the bridge (e.g., Figure A-6). In these cases, the note “NB” appears with the gauge location in the tables.

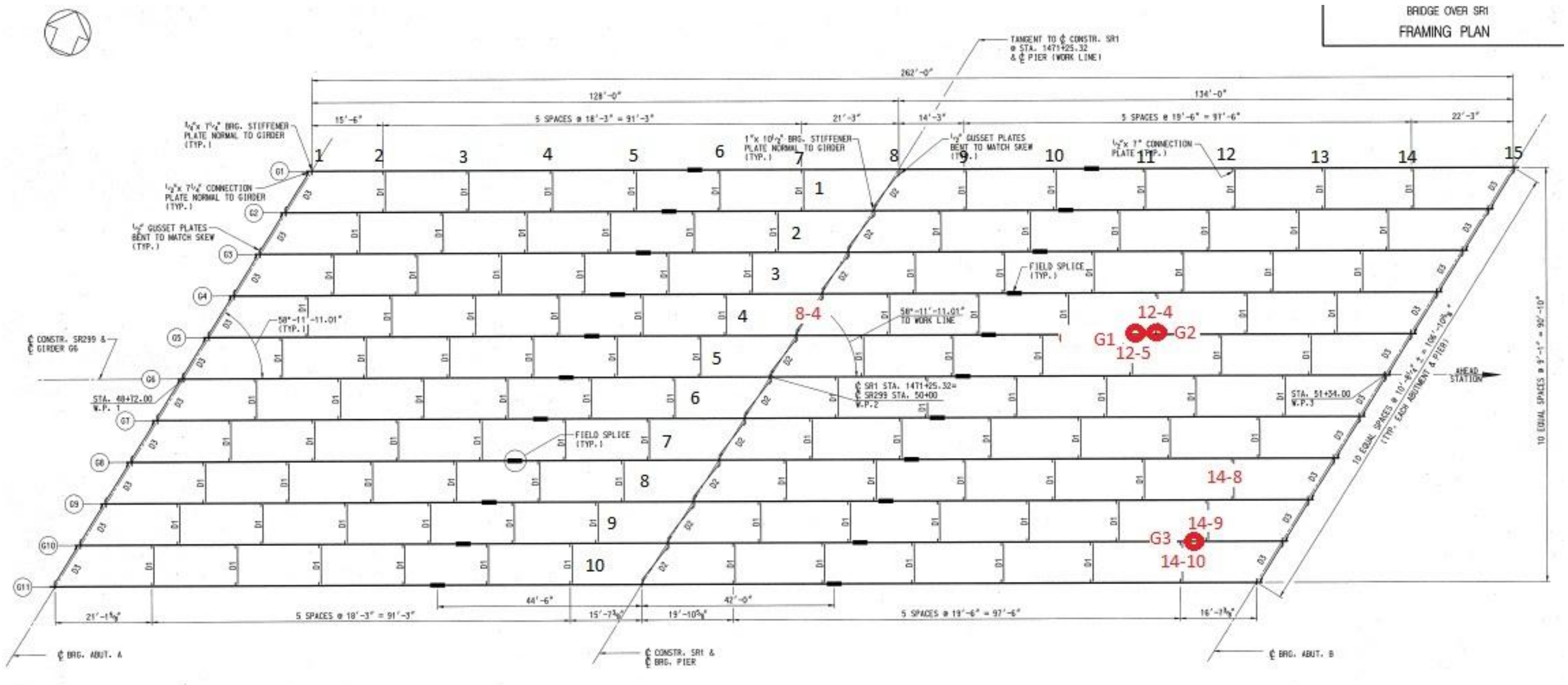

Figure A-1 SR 299 Over SR 1 Instrumentation Layout

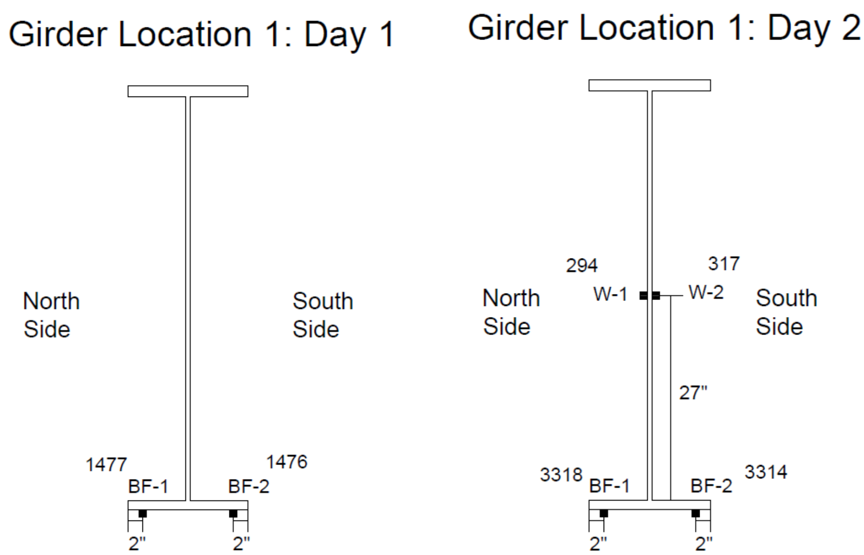

Figure A-2 SR 299 Over SR 1 Girder Location 1, Day 1 & 2

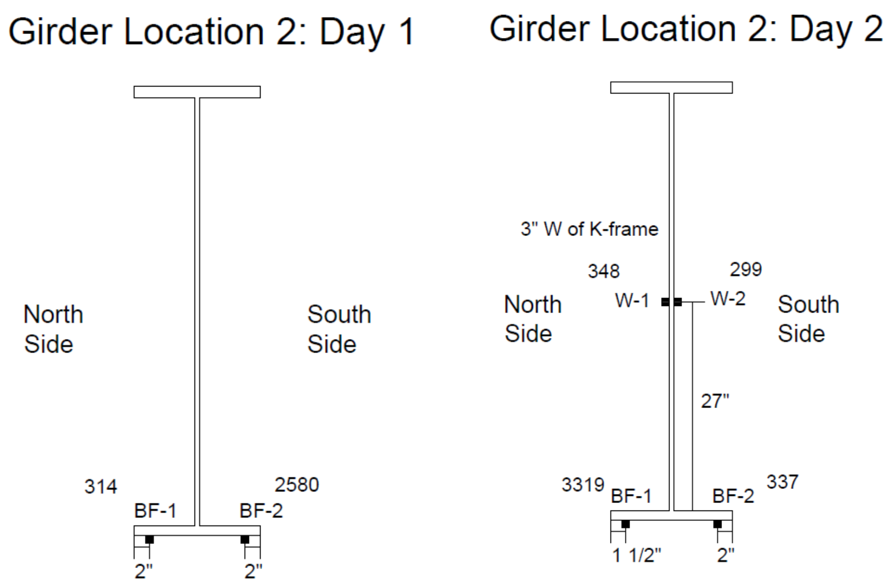

Figure A-3 SR 299 Over SR 1 Girder Location 2, Day 1 & 2

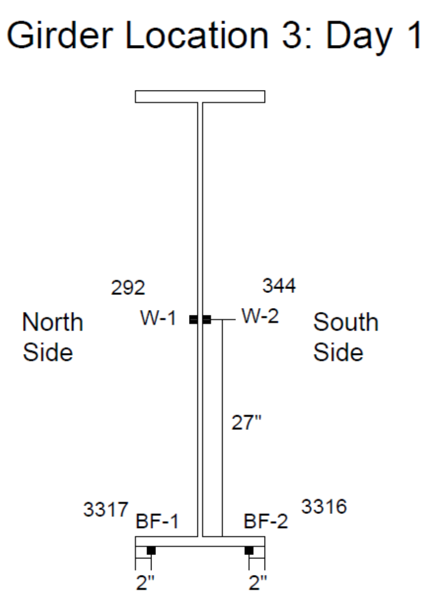

Figure A-4 SR 299 Over SR 1 Girder Location 3

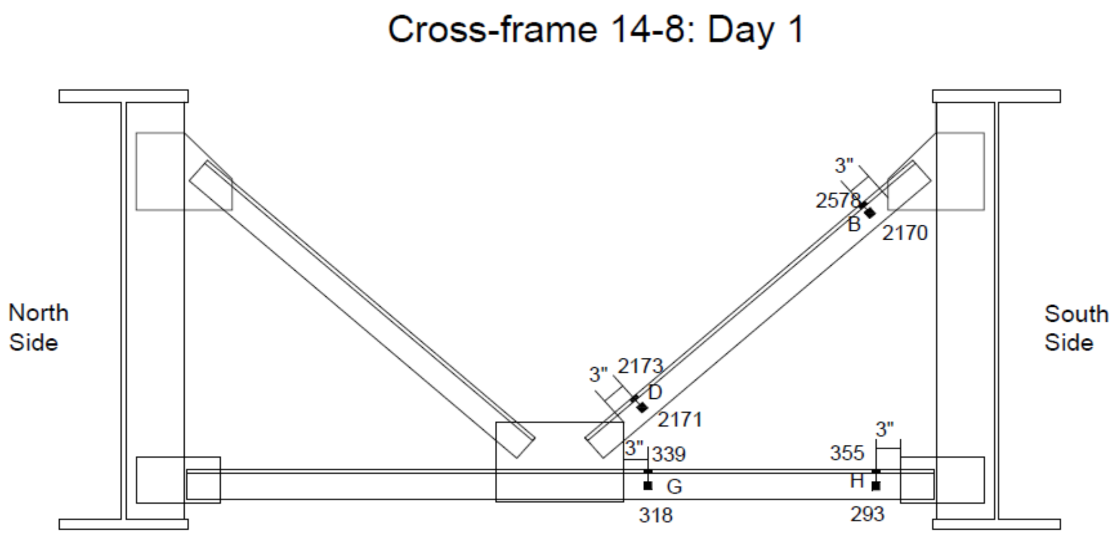

Figure A-5 SR 299 Over SR 1 Cross-frame 14-8

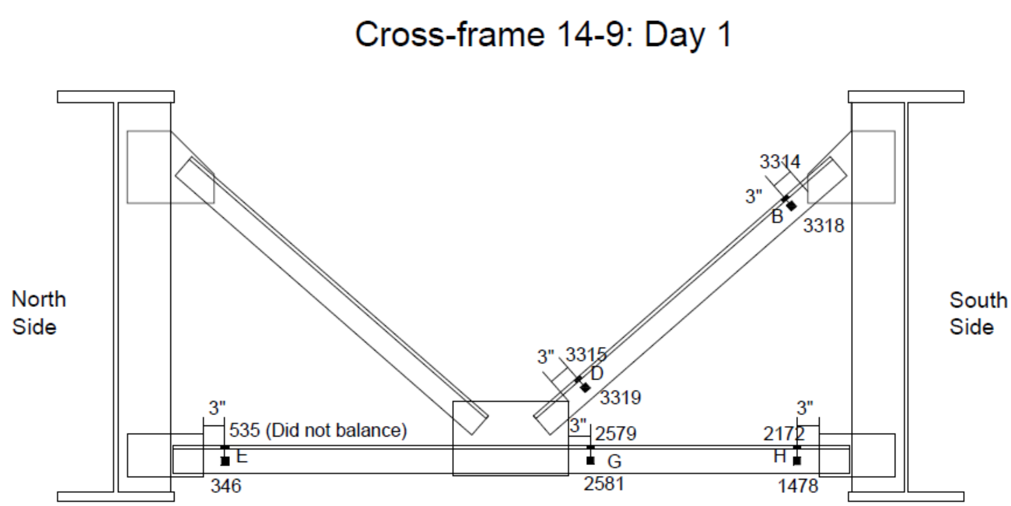

Figure A-6 SR 299 Over SR 1 Cross-frame 14-9

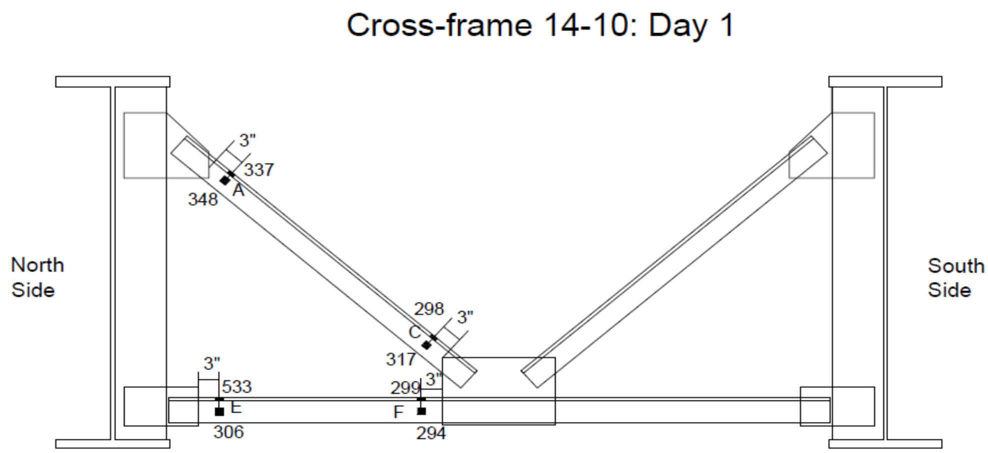

Figure A-7 SR 299 Over SR 1 Cross-frame 14-9

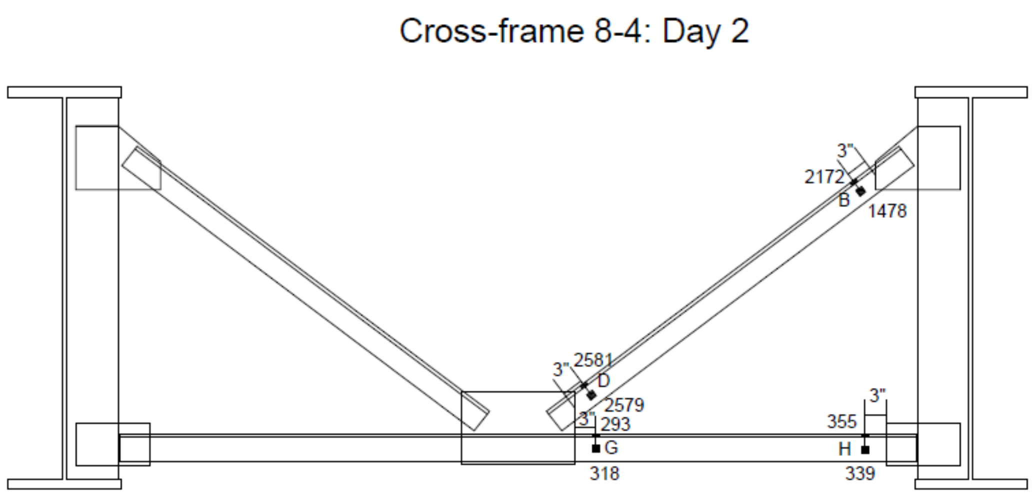

Figure A-8 SR 299 Over SR 1 Cross-frame 8-4

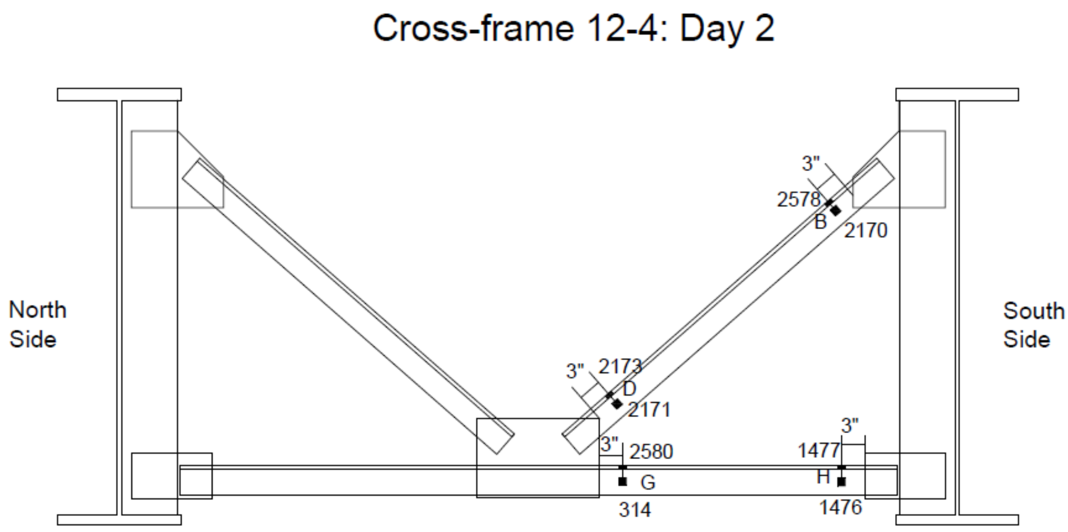

Figure A-9 SR 299 Over SR 1 Cross-frame 12-4

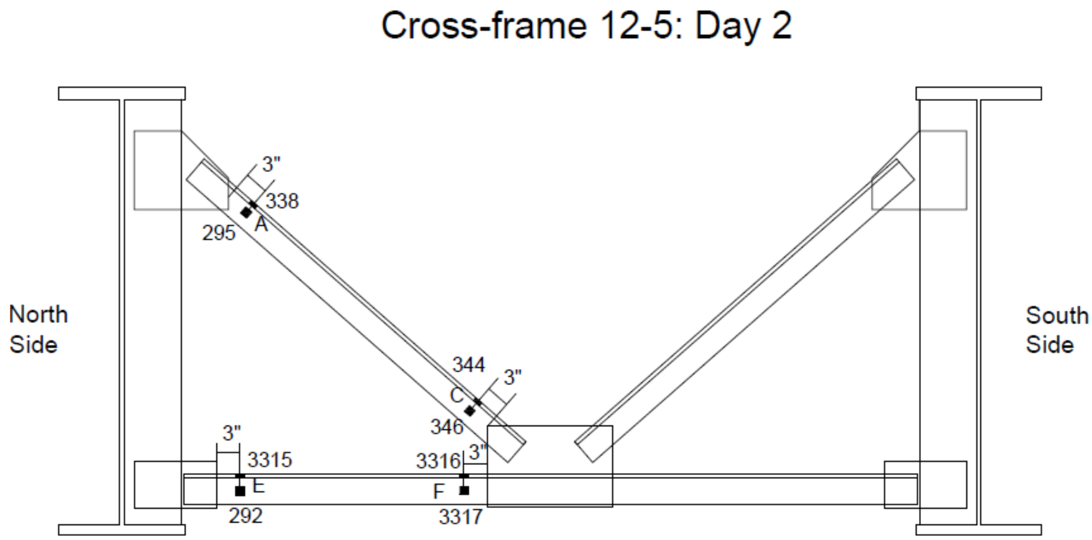

Figure A-10 SR 299 Over SR 1 Cross-frame 12-5

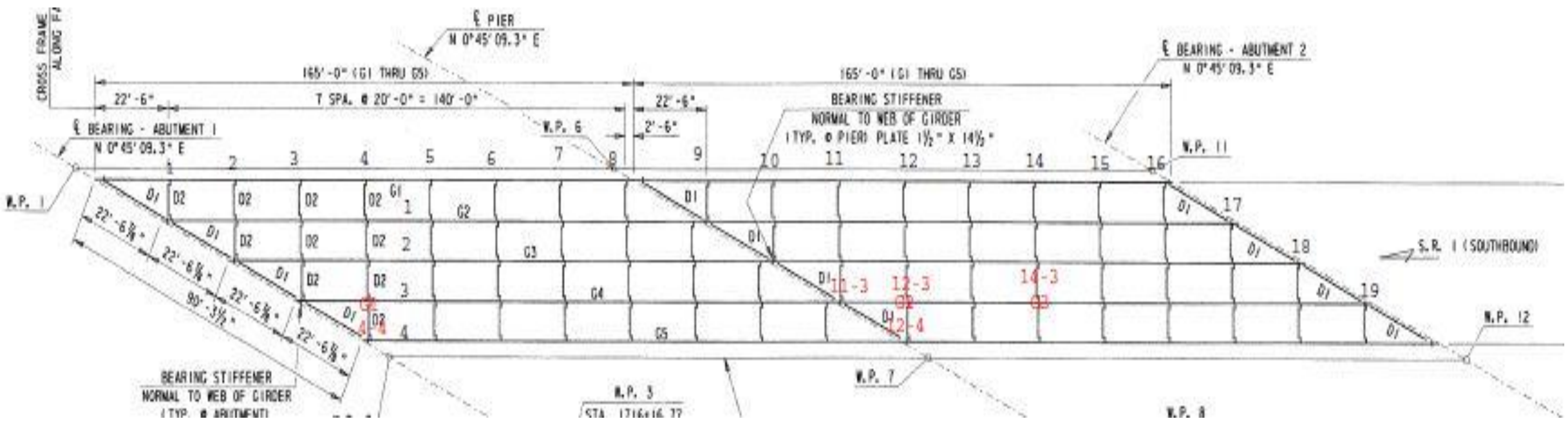

Figure A-11 SR 1 Over US 13 Instrumentation Layout

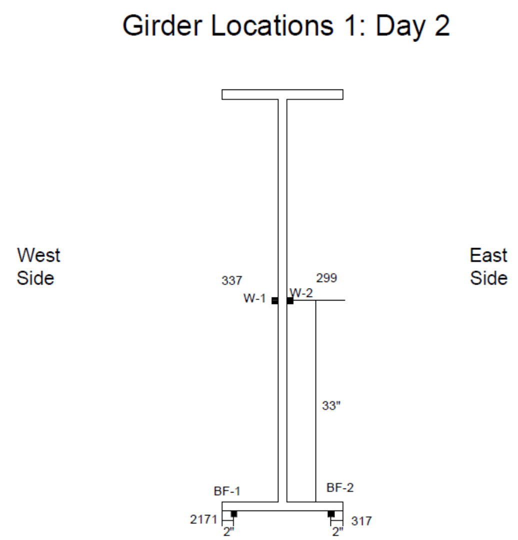

Figure A-12 SR 1 Over US 13 Girder Location 1

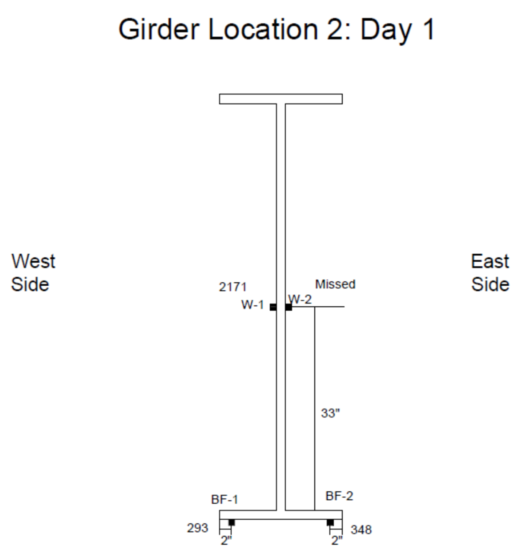

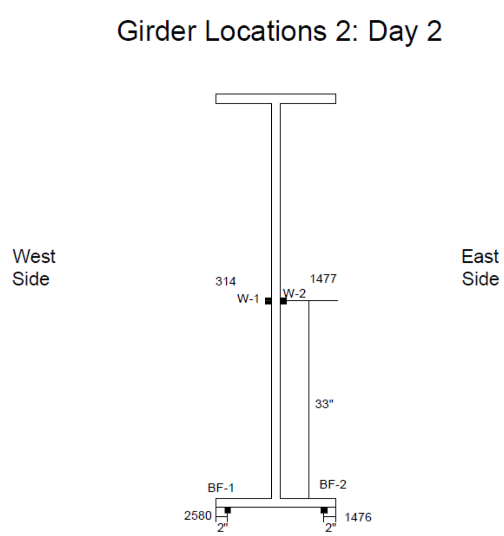

Figure A-13 SR 1 Over US 13 Girder Location 2, Day 1 & 2

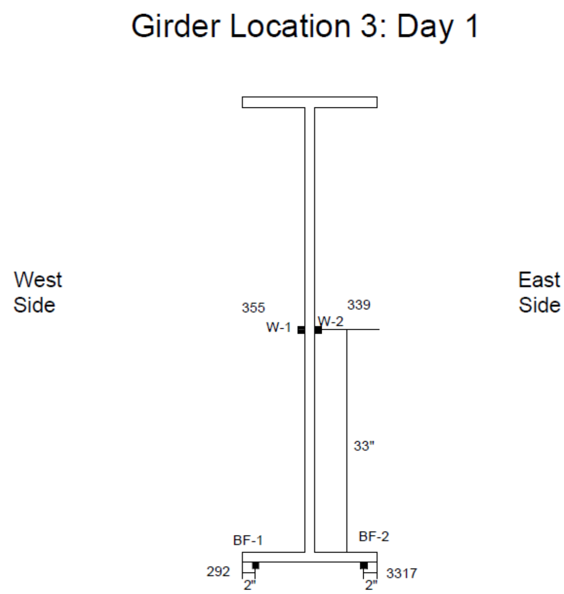

Figure A-14 SR 1 Over US 13 Girder Location 3

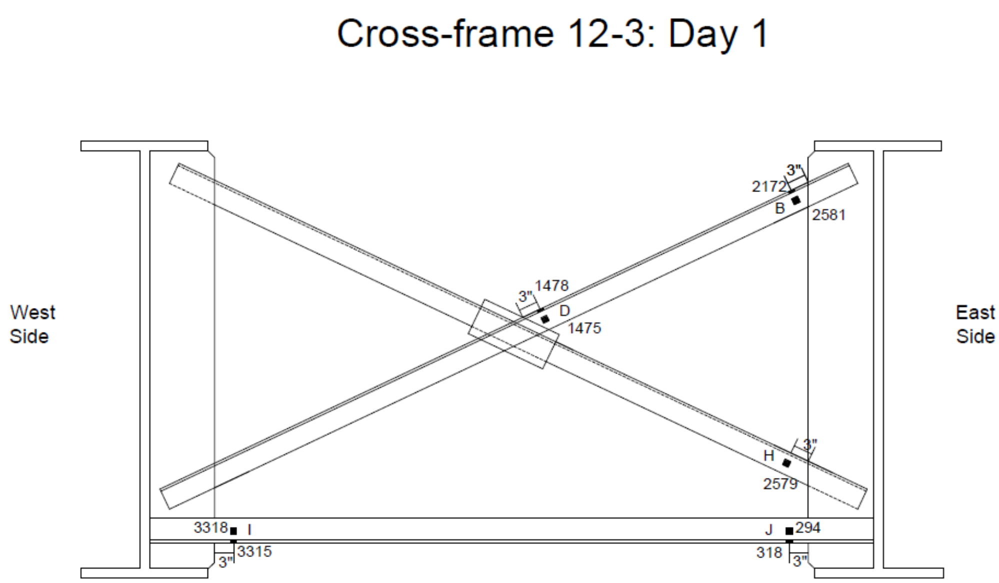

Figure A-15 SR 1 Over US 13 Cross-frame 12-3

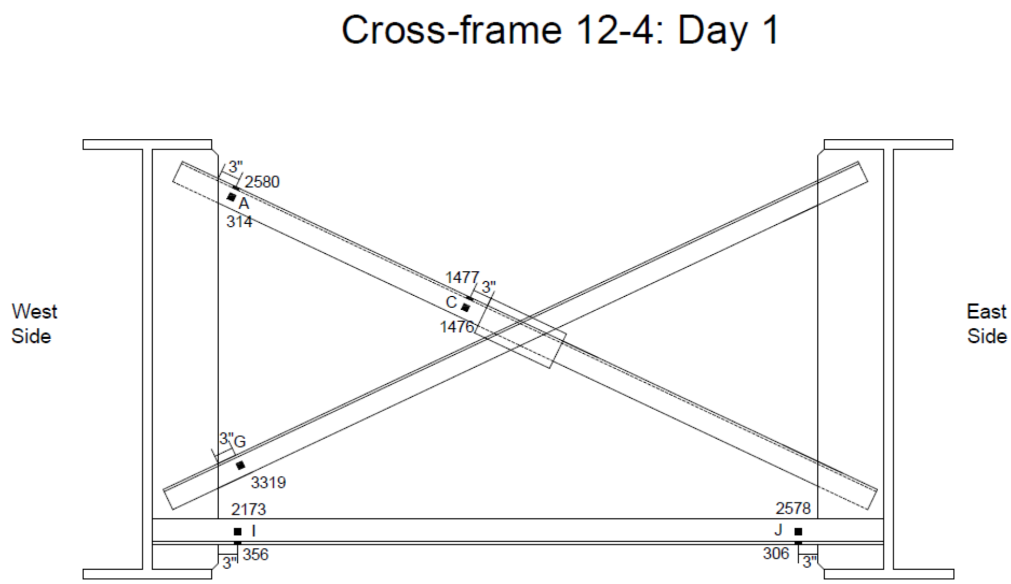

Figure A-16 SR 1 Over US 13 Cross-frame 12-4

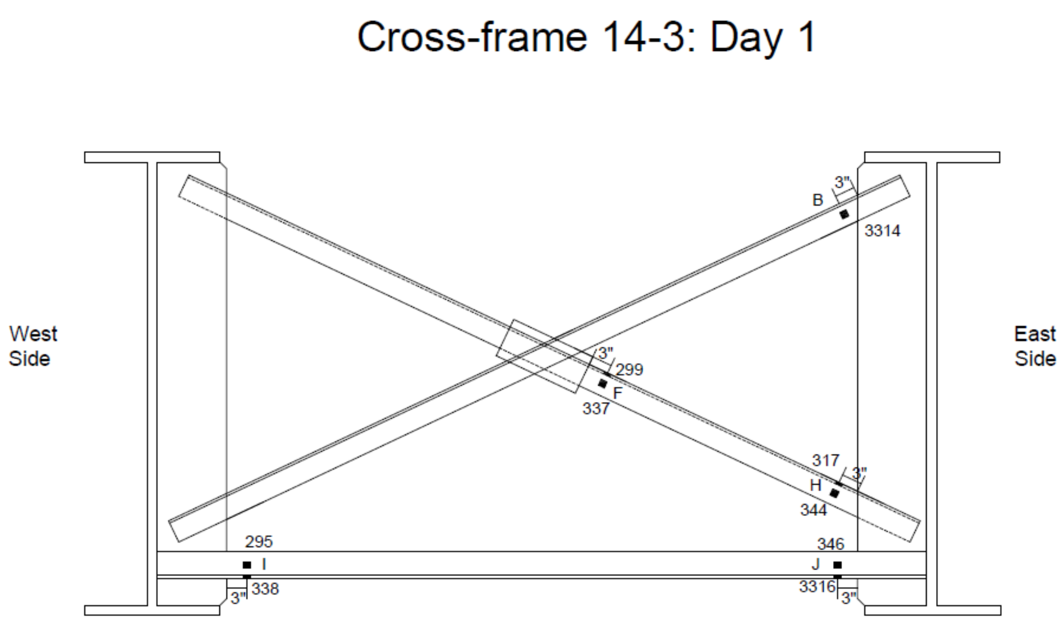

Figure A-17 SR 1 Over US 13 Cross-frame 14-3

Cross-frame 4-4: Day 2

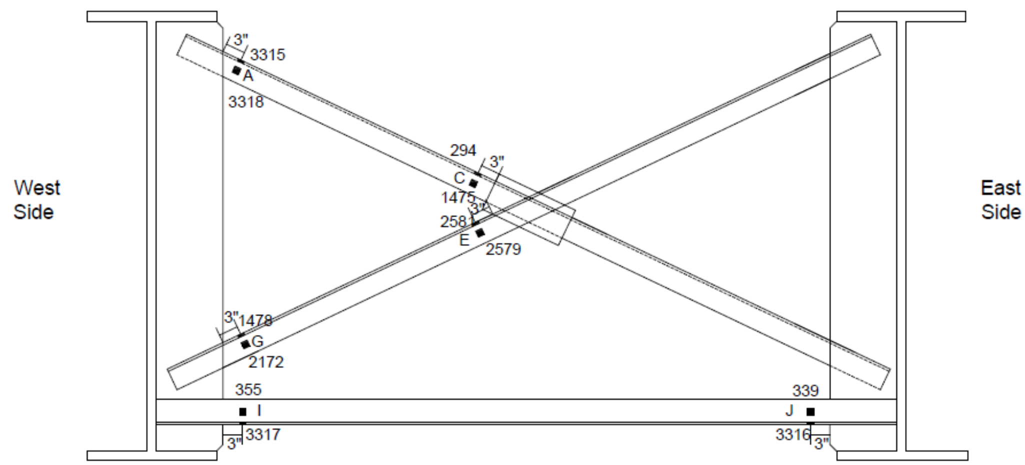

Figure A-18 SR 1 Over US 13 Cross-frame 4-4

Cross-frame 11-3: Day 2

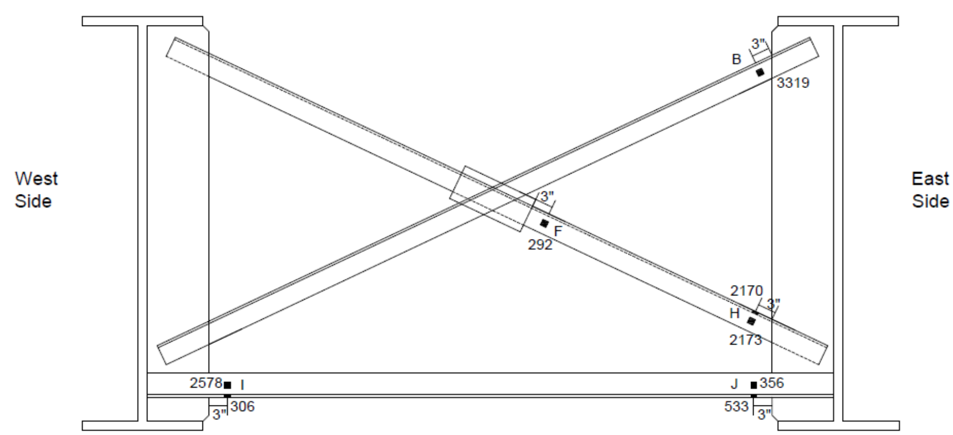

Figure A-19 SR 1 Over US 13 Cross-frame 11-3

Appendix B

FIELD TEST DATA

The balanced field test data for SR 299 over SR 1 and SR 1 over US 13 are presented herein. As stated in Section 4.5, the field test data was processed in MATLAB using the "smooth" function to take a moving average of the data and downsampled to create graphs. The strain versus time plots are presented in this appendix. The x-axis represents time in seconds and the y-axis represents microstrain. The data for SR 299 over SR1 is presented first followed by the data for SR 1 over US 13. Girder locations are presented first for each bridge followed by the cross-frames. Data from different truck passes are presented on different plots. The note "NB" next to a gauge location indicates that the gauge did not balance. Note for SR 299 over SR 1, Pass 1 and Pass 2 are presented in the same plots for Day 2. Approximately 40 seconds corresponds to the end of Pass 1.

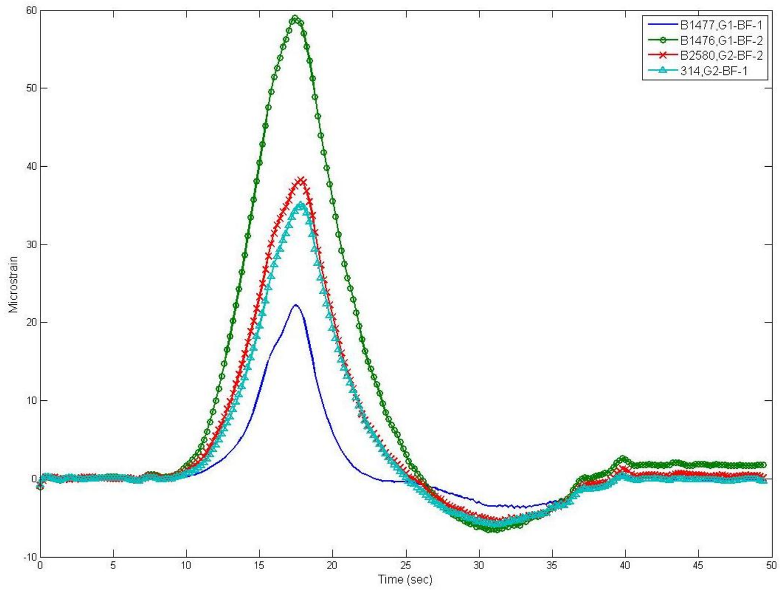

Figure B-1 SR 299 Over SR 1 Day 1 Pass 1 Girder Locations 1 & 2

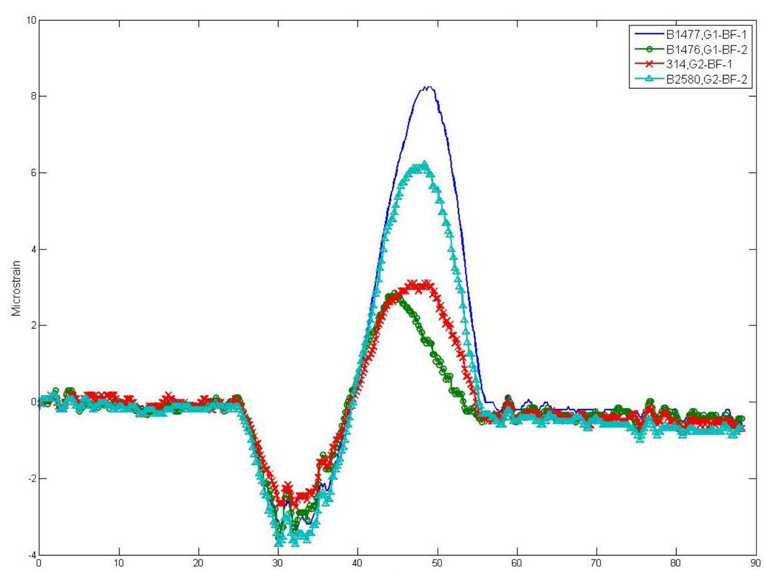

Figure B-2 SR 299 Over SR 1 Day 1 Pass 2 Girder Locations 1 & 2

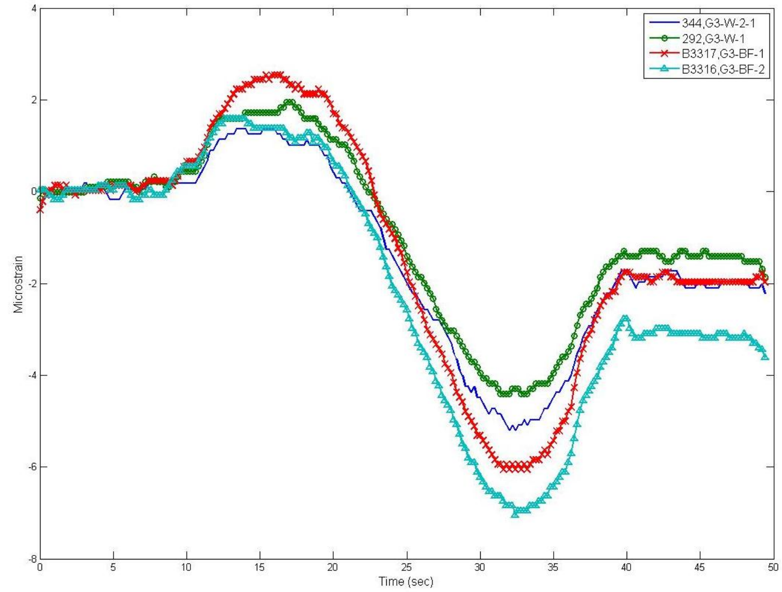

Figure B-3 SR 299 Over SR 1 Day 1 Pass 1 Girder Location 3

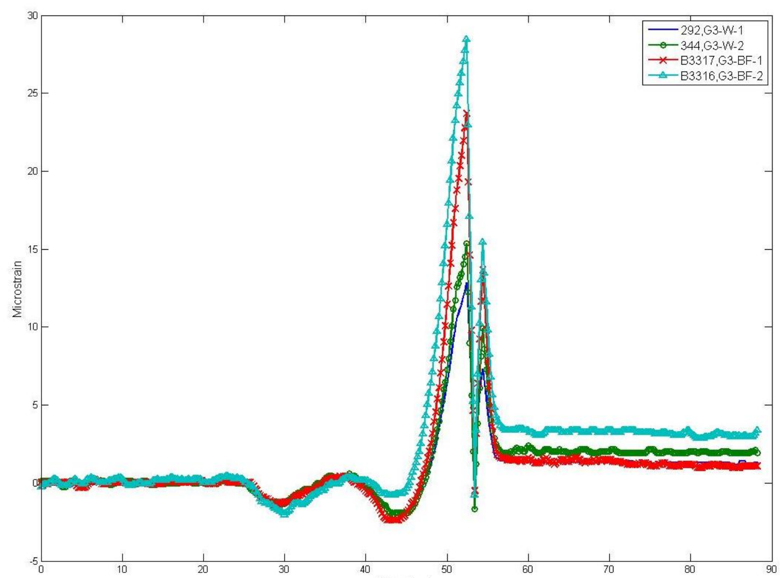

Figure B-4 SR 299 Over SR 1 Day 1 Pass 2 Girder Location 3

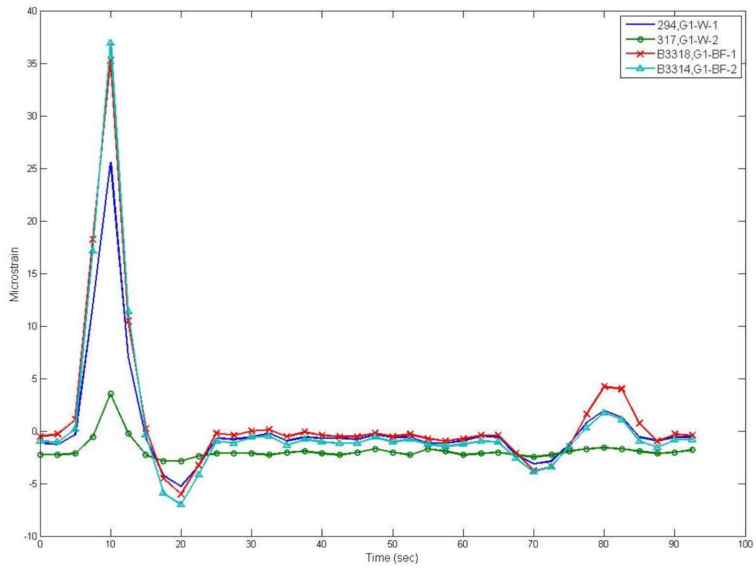

Figure B-5 SR 299 Over SR 1 Day 2 Pass 1&2 Girder Location 1

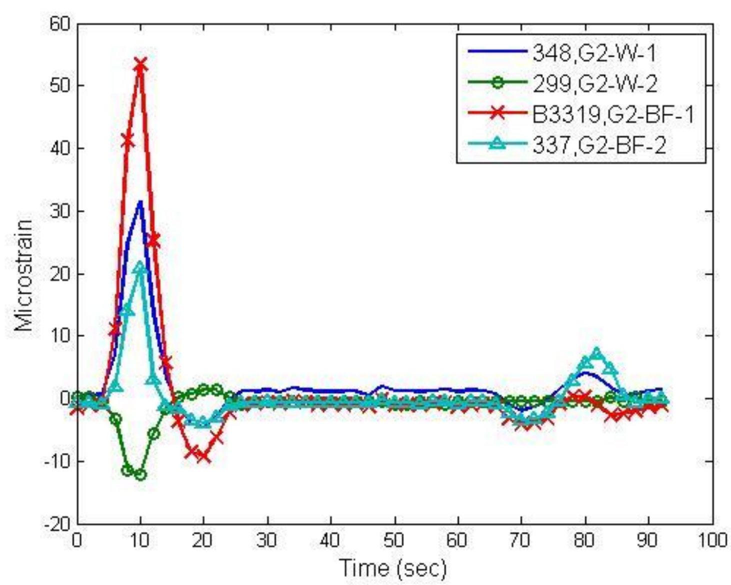

Figure B-6 SR 299 Over SR 1 Day 2 Pass 1&2 Girder Location 2

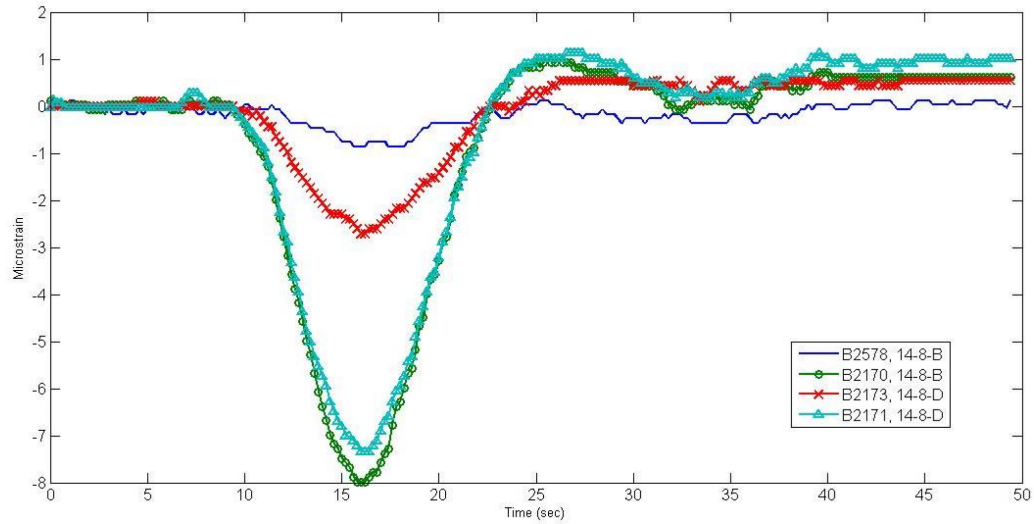

Figure B-7 SR 299 Over SR 1 Day 1 Pass 1 Cross-frame 14-8, 1 of 2

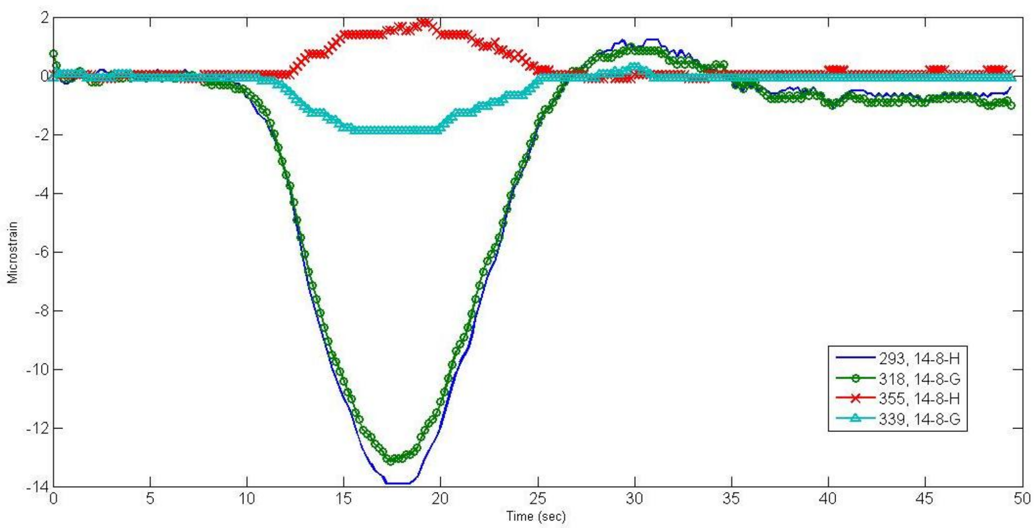

Figure B-8 SR 299 Over SR 1 Day 1 Pass 1 Cross-frame 14-8, 2 of 2

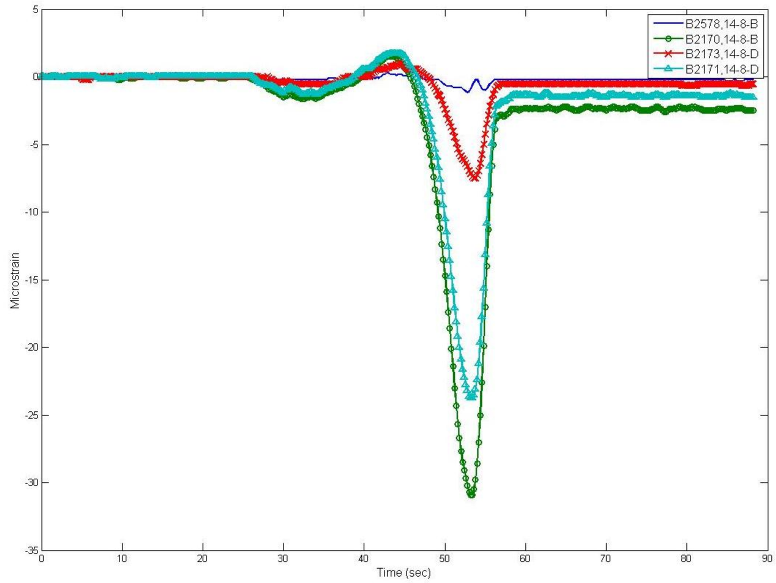

Figure B-9 SR 299 Over SR 1 Day 1 Pass 2 Cross-frame 14-8, 1 of 2

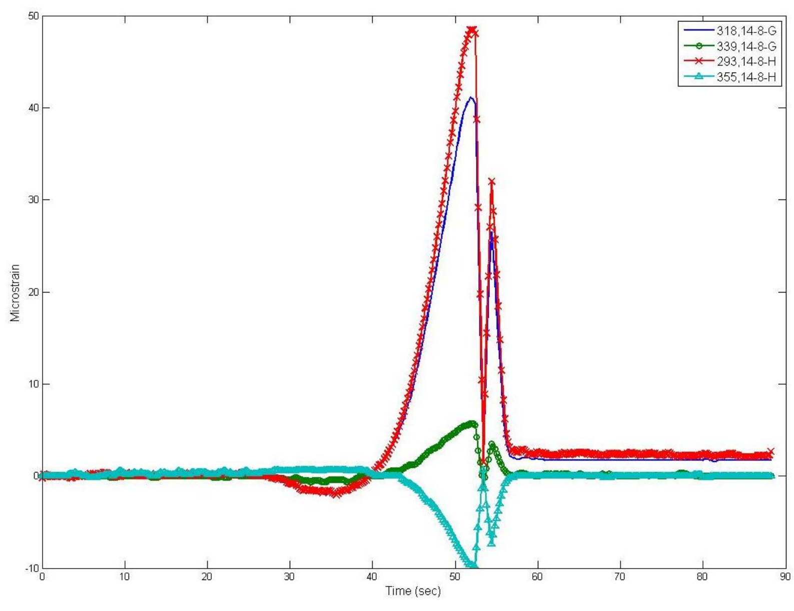

Figure B-10 SR 299 Over SR 1 Day 1 Pass 2 Cross-frame 14-8, 2 of 2

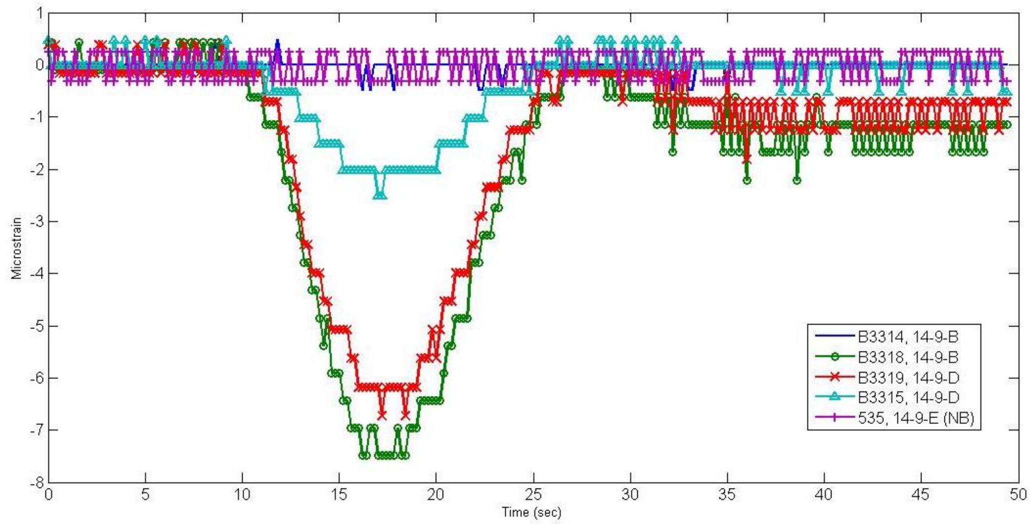

Figure B-11 SR 299 Over SR 1 Day 1 Pass 1 Cross-frame 14-9, 1 of 2

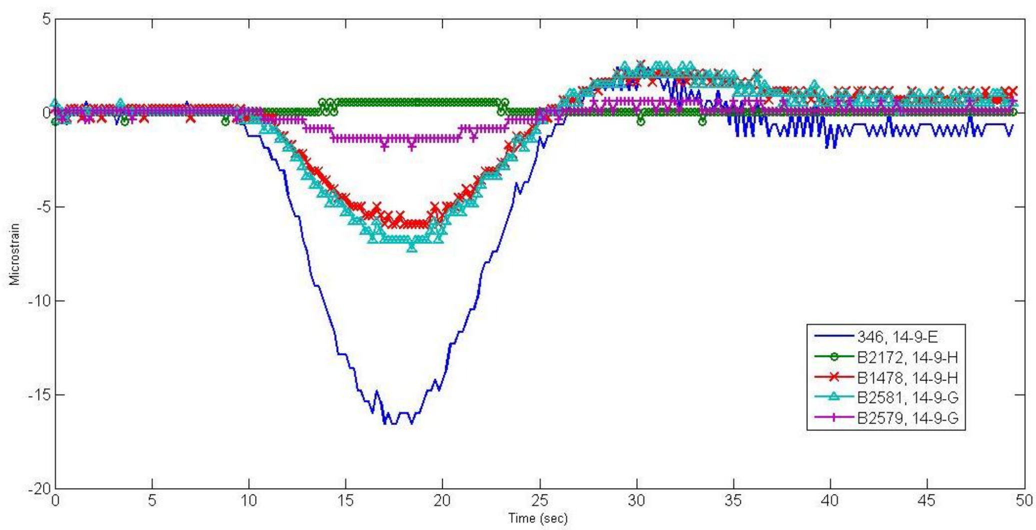

Figure B-12 SR 299 Over SR 1 Day 1 Pass 1 Cross-frame 14-9, 2 of 2

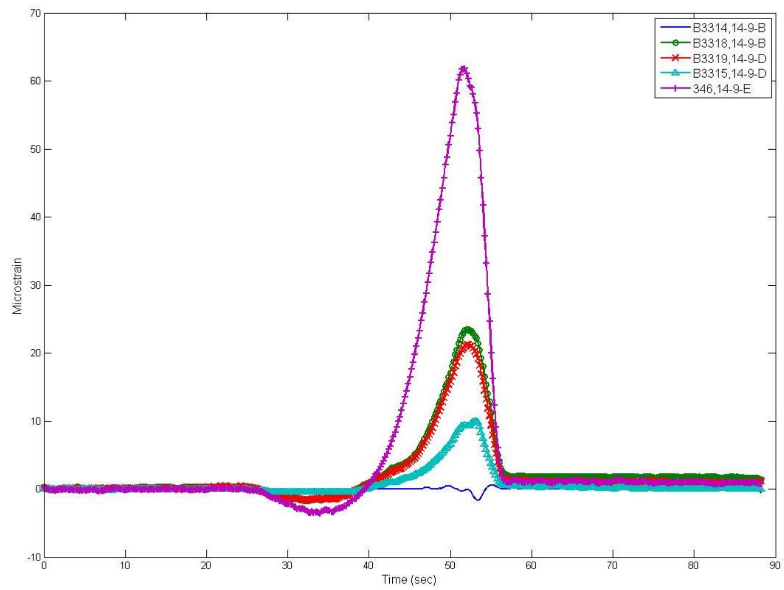

Figure B-13 SR 299 Over SR 1 Day 1 Pass 2 Cross-frame 14-9, 1 of 2

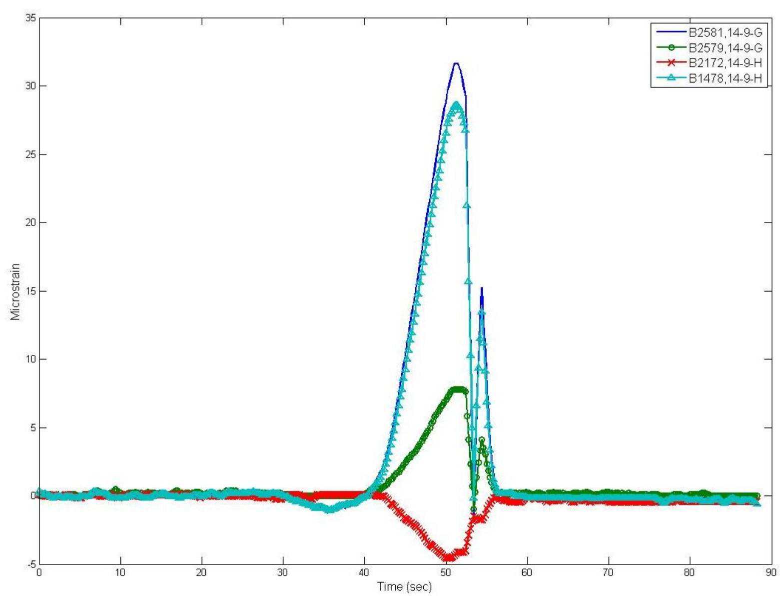

Figure B-14 SR 299 Over SR 1 Day 1 Pass 2 Cross-frame 14-9, 2 of 2

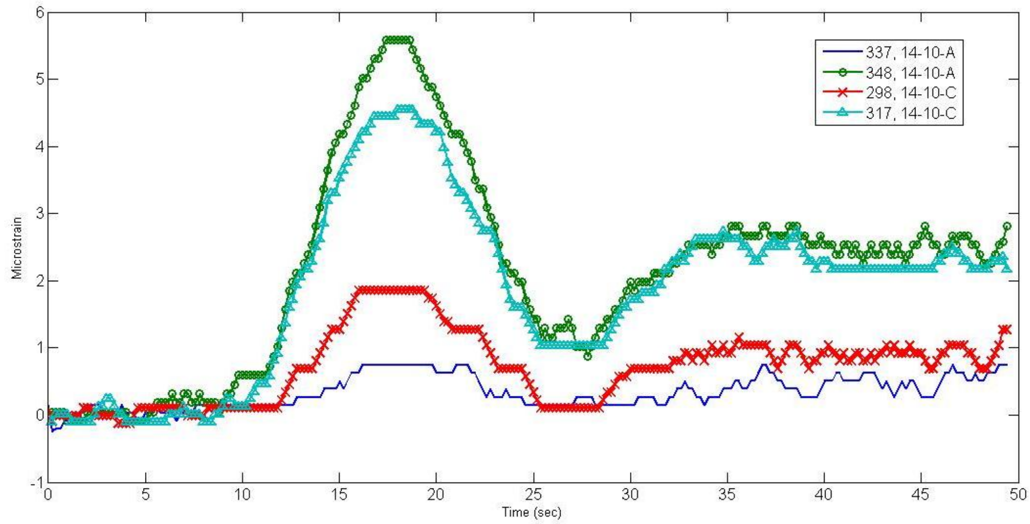

Figure B-15 SR 299 Over SR 1 Day 1 Pass 1 Cross-frame 14-10, 1 of 2

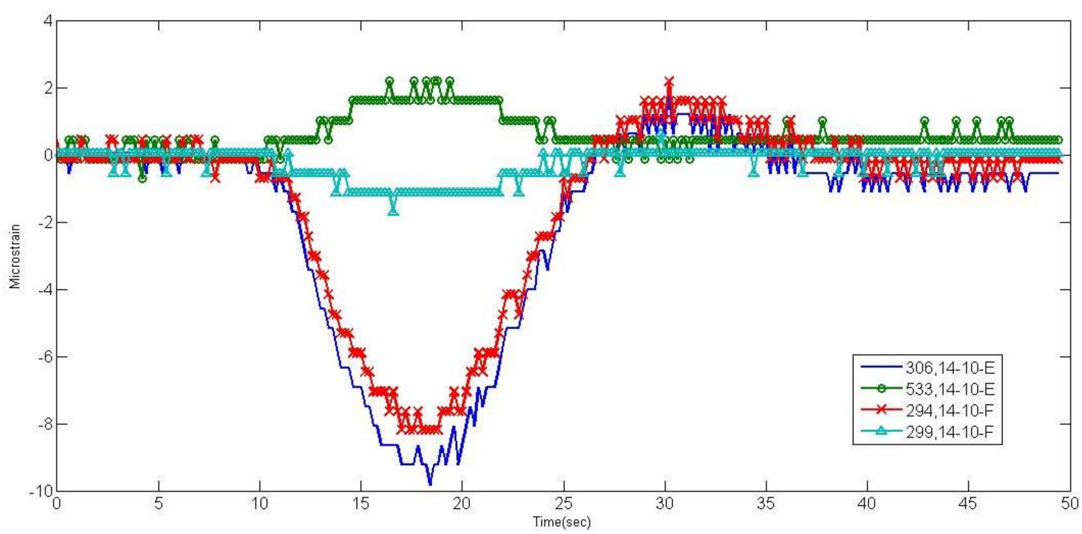

Figure B-16   SR 299 Over SR 1 Day 1 Pass 1 Cross-frame 14-10, 2 of 2

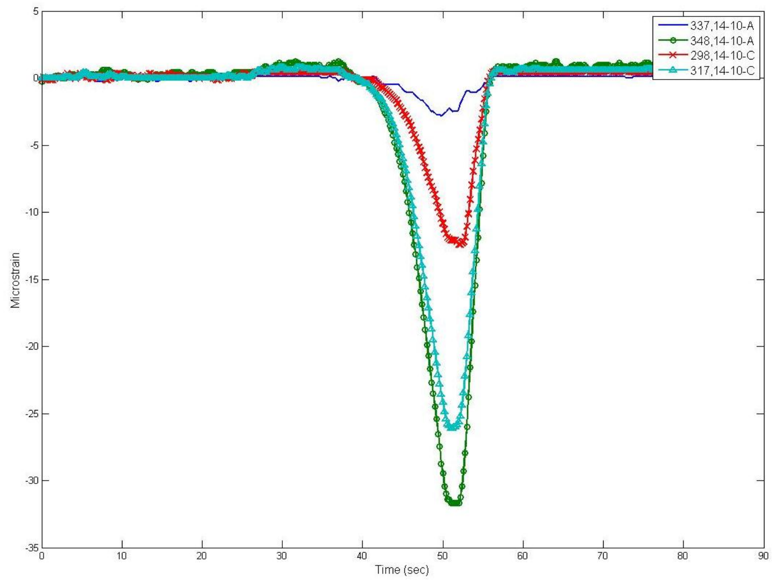

Figure B-17 SR 299 Over SR 1 Day 1 Pass 2 Cross-frame 14-10, 1 of 2

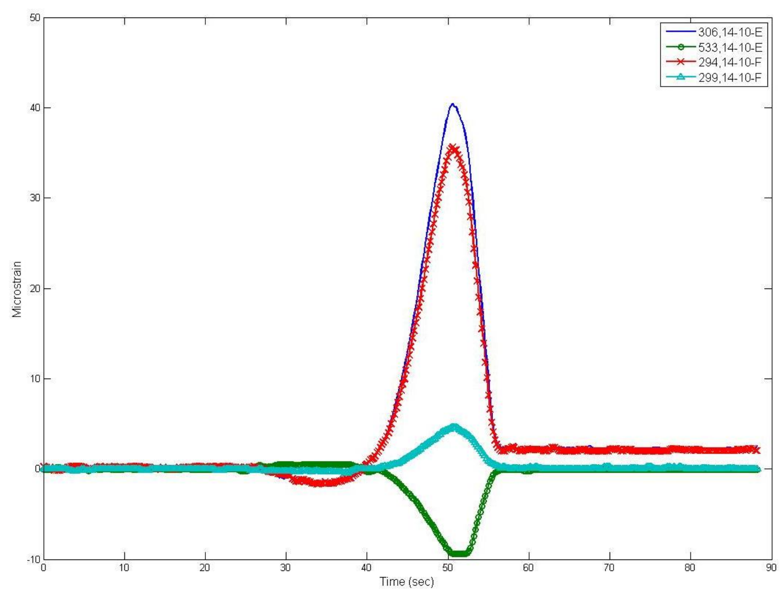

Figure B-18 SR 299 Over SR 1 Day 1 Pass 2 Cross-frame 14-10, 2 of 2

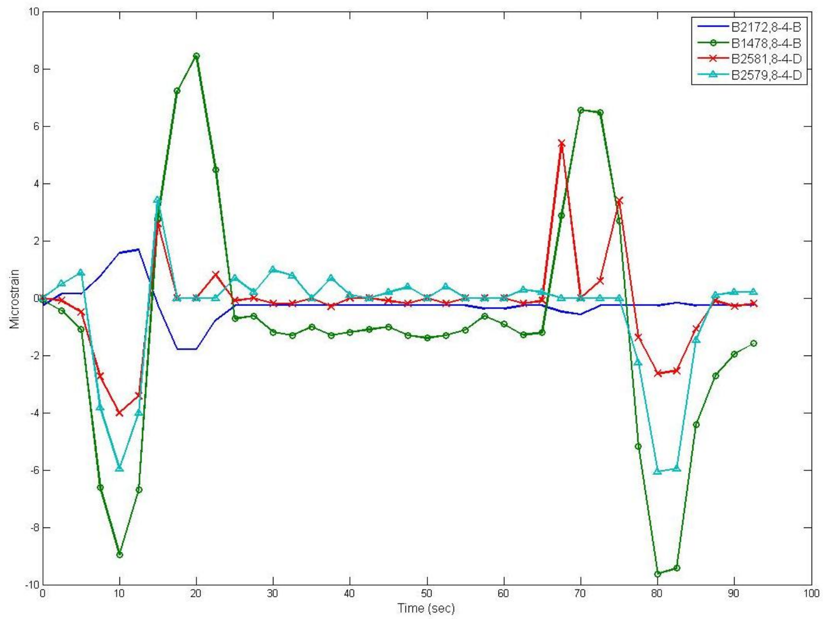

Figure B-19 SR 299 Over SR 1 Day 2 Pass 1&2 Cross-frame 8-4, 1 of 2

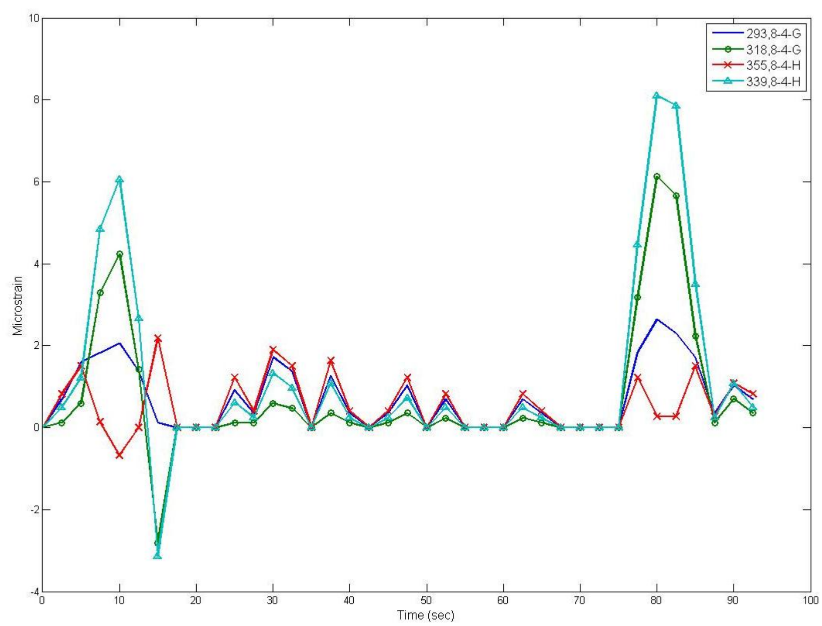

Figure B-20 SR 299 Over SR 1 Day 2 Pass 1&2 Cross-frame 8-4, 2 of 2

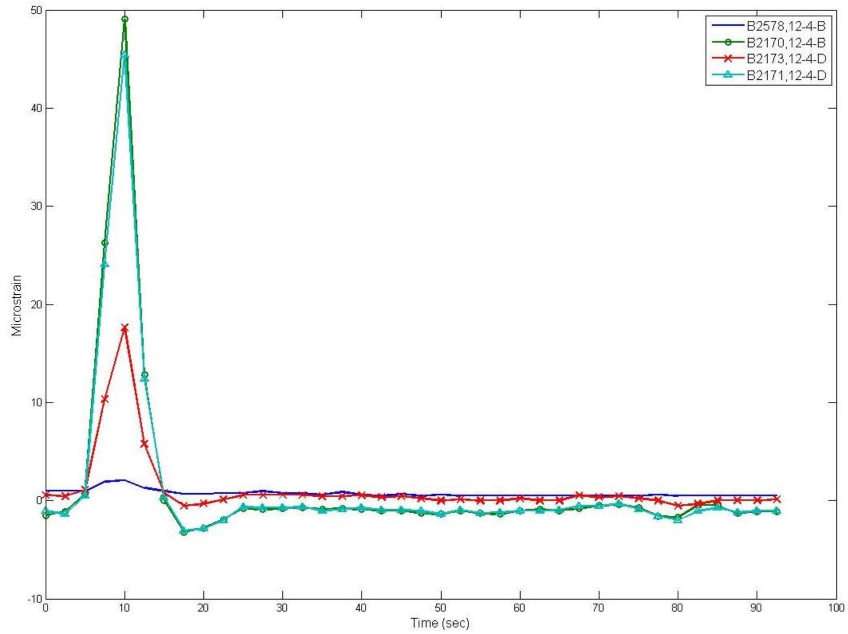

Figure B-21 SR 299 Over SR 1 Day 2 Pass 1&2 Cross-frame 12-4, 1 of 2

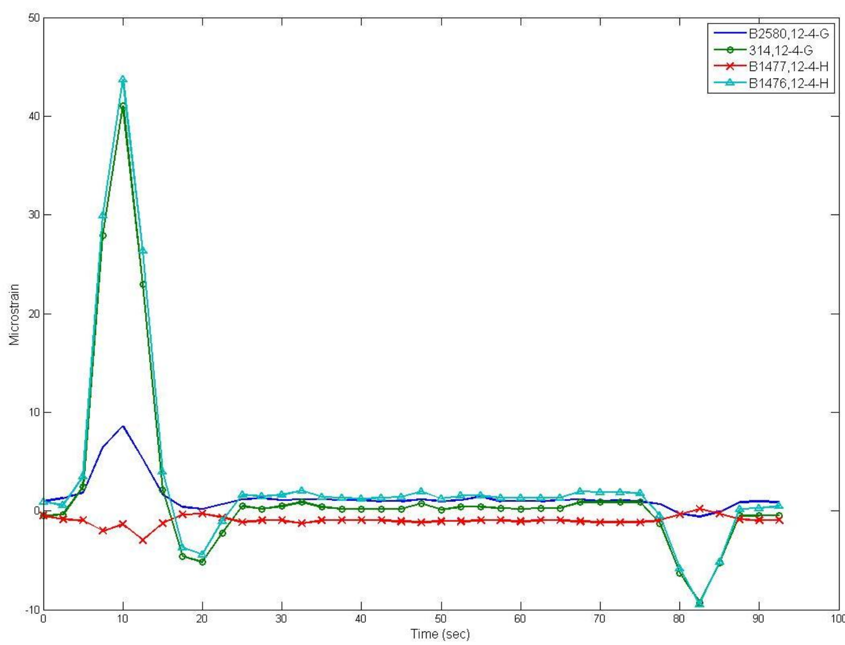

Figure B-22 SR 299 Over SR 1 Day 2 Pass 1&2 Cross-frame 12-4, 2 of 2

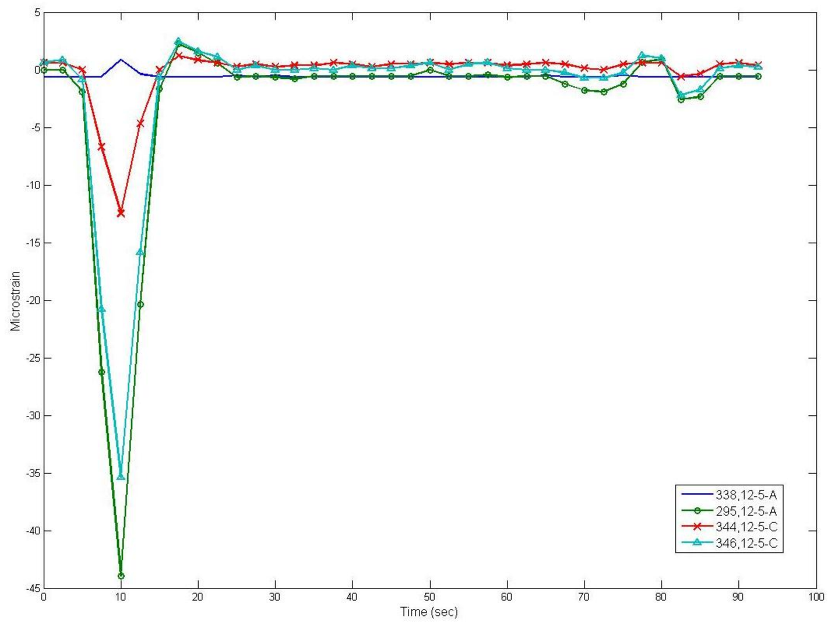

Figure B-23 SR 299 Over SR 1 Day 2 Pass 1&2 Cross-frame 12-5, 1 of 2

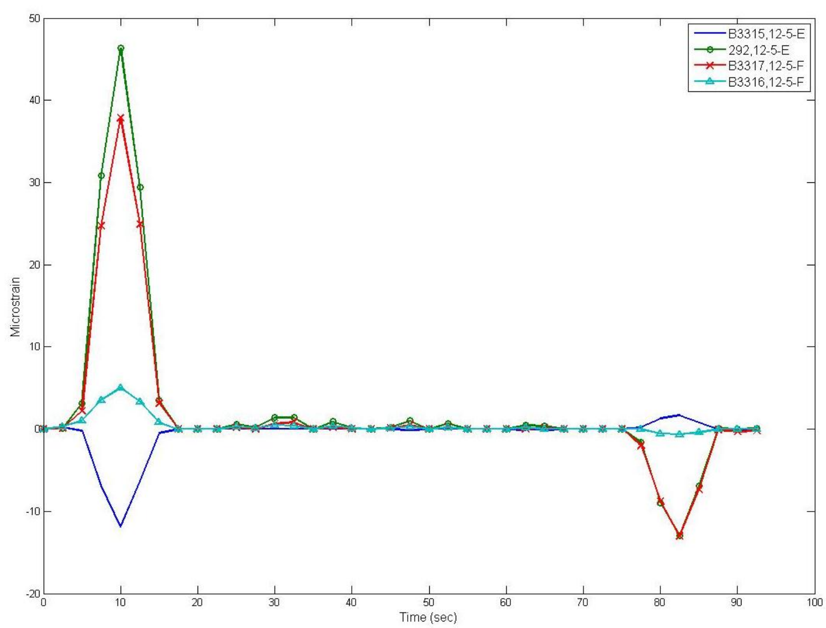

Figure B-24 SR 299 Over SR 1 Day 2 Pass 1&2 Cross-frame 12-5, 2 of 2

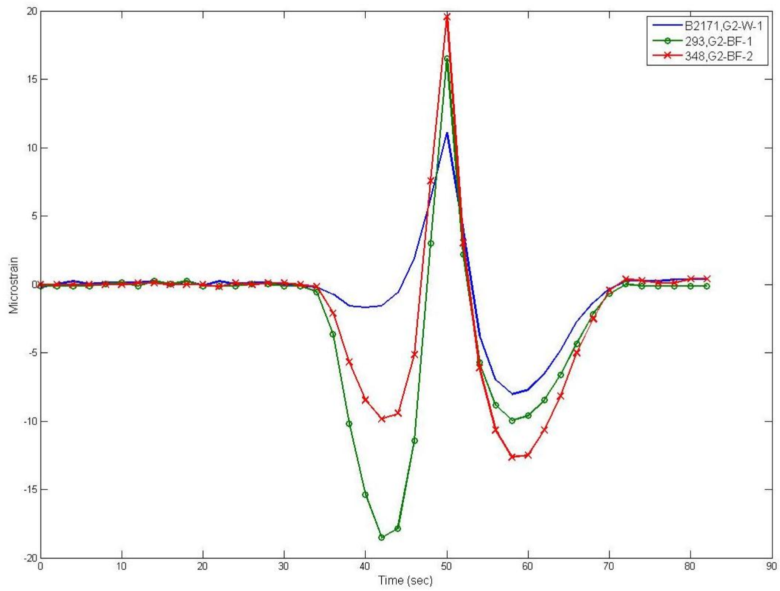

Figure B-25 SR 1 Over US 13 Day 1 Pass 1 Girder Location 2

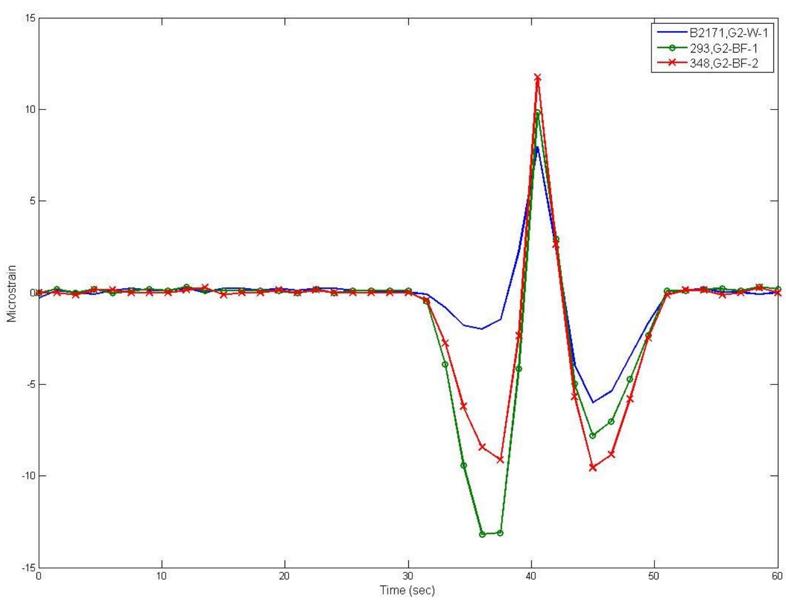

Figure B-26 SR 1 Over US 13 Day 1 Pass 2 Girder Location 2

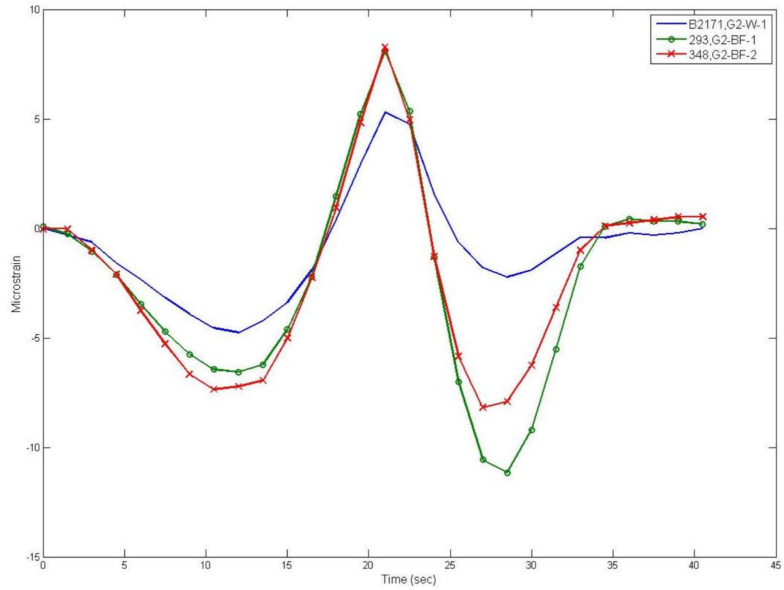

Figure B-27 SR 1 Over US 13 Day 1 Pass 3 Girder Location 2

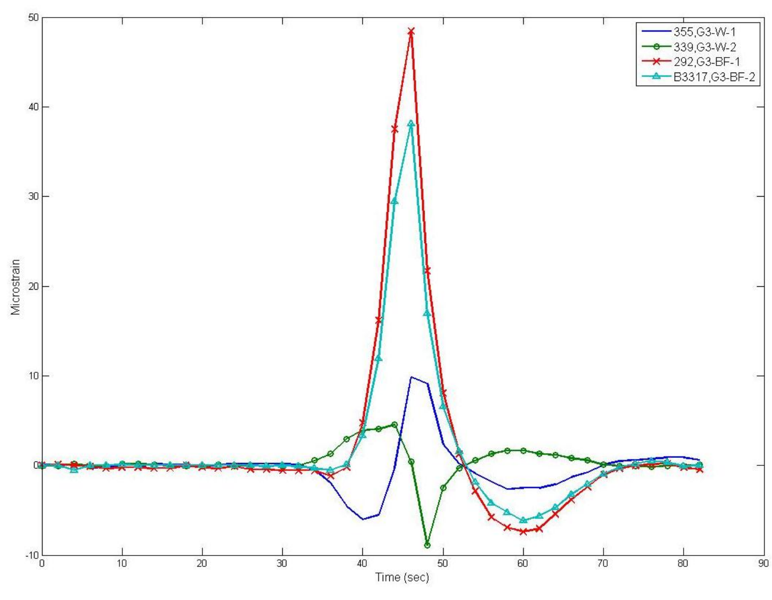

Figure B-28 SR 1 Over US 13 Day 1 Pass 1 Girder Location 3

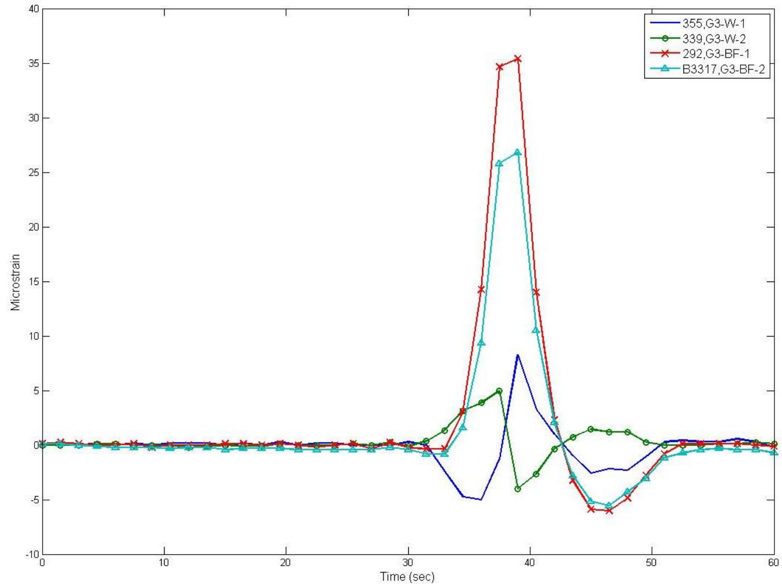

Figure B-29 SR 1 Over US 13 Day 1 Pass 2 Girder Location 3

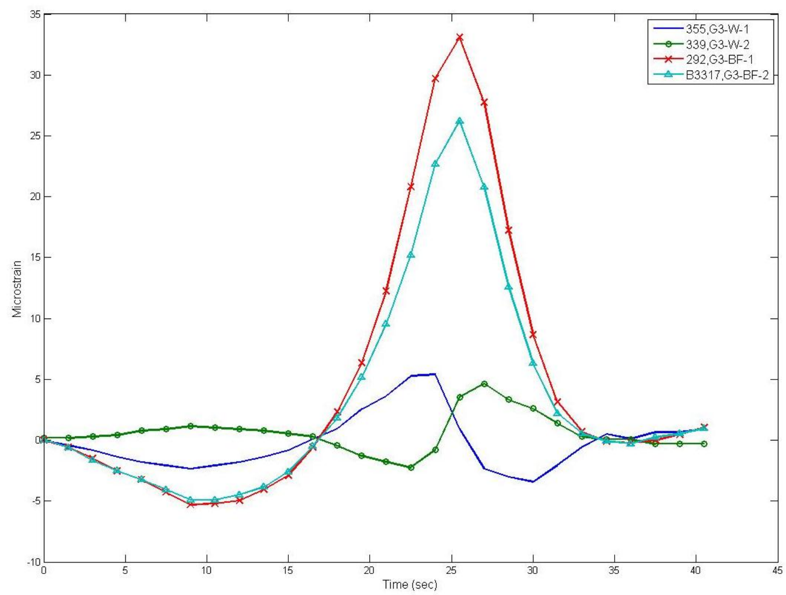

Figure B-30 SR 1 Over US 13 Day 1 Pass 3 Girder Location 3

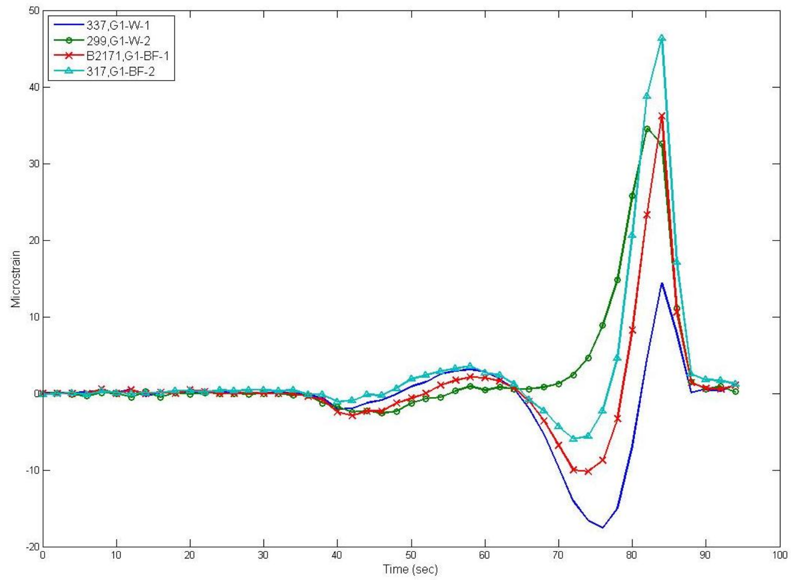

Figure B-31 SR 1 Over US 13 Day 2 Pass 1 Girder Location 1

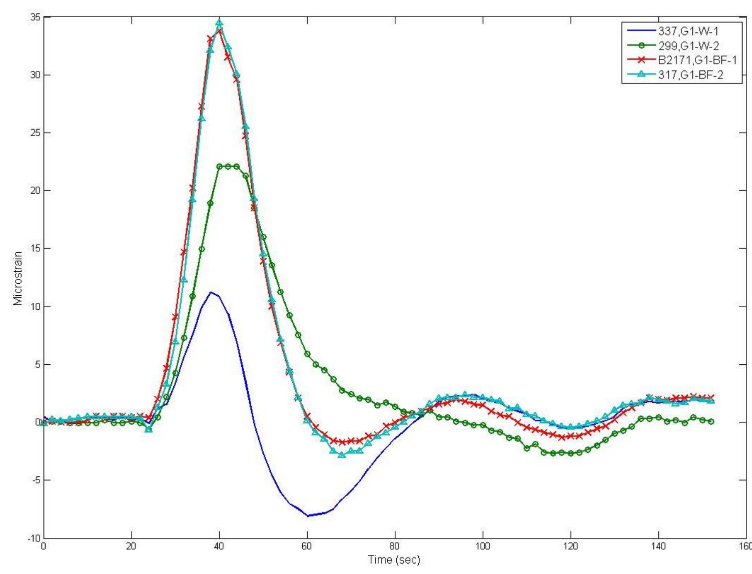

Figure B-32 SR 1 Over US 13 Day 2 Pass 2 Girder Location 1

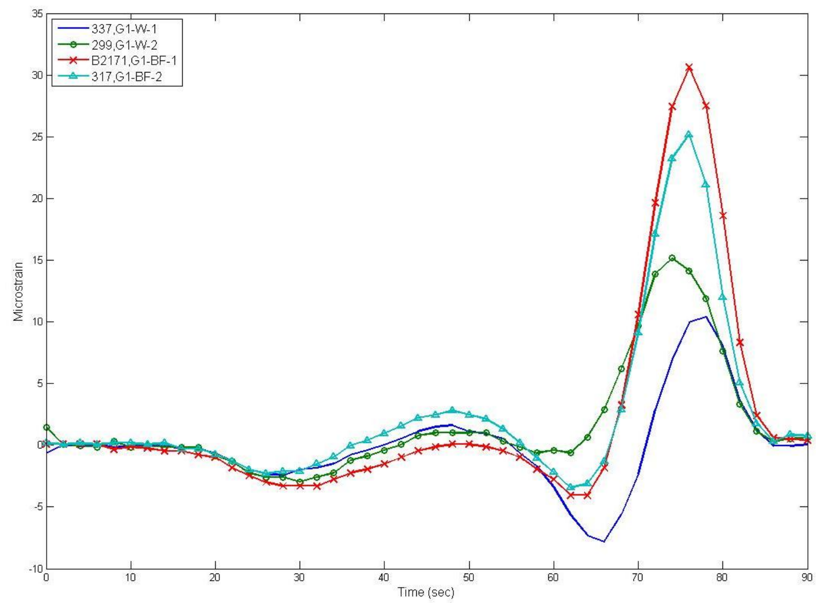

Figure B-33 SR 1 Over US 13 Day 2 Pass 3 Girder Location 1

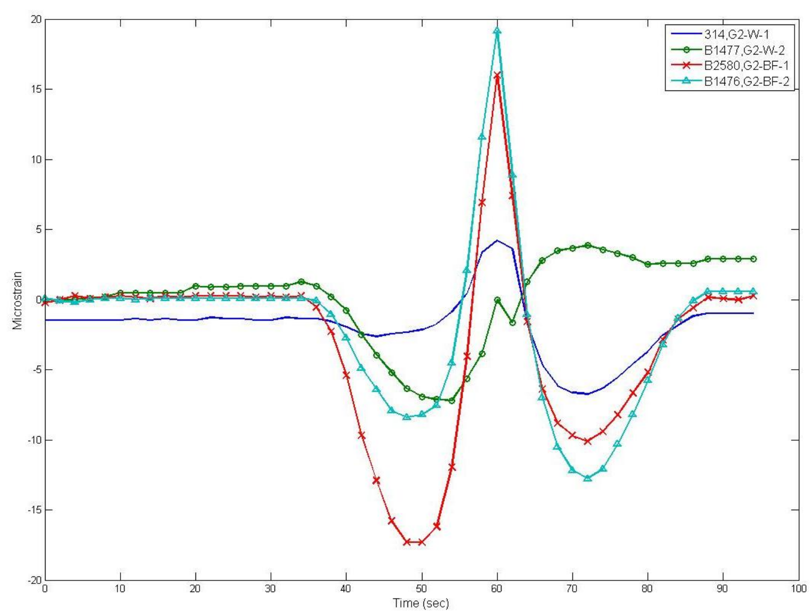

Figure B-34 SR 1 Over US 13 Day 2 Pass 1 Girder Location 2

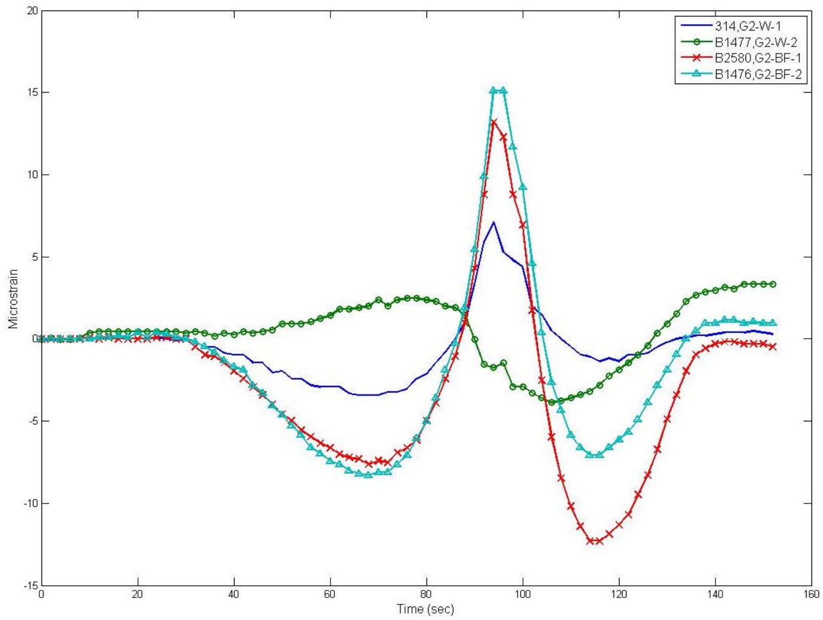

Figure B-35 SR 1 Over US 13 Day 2 Pass 2 Girder Location 2

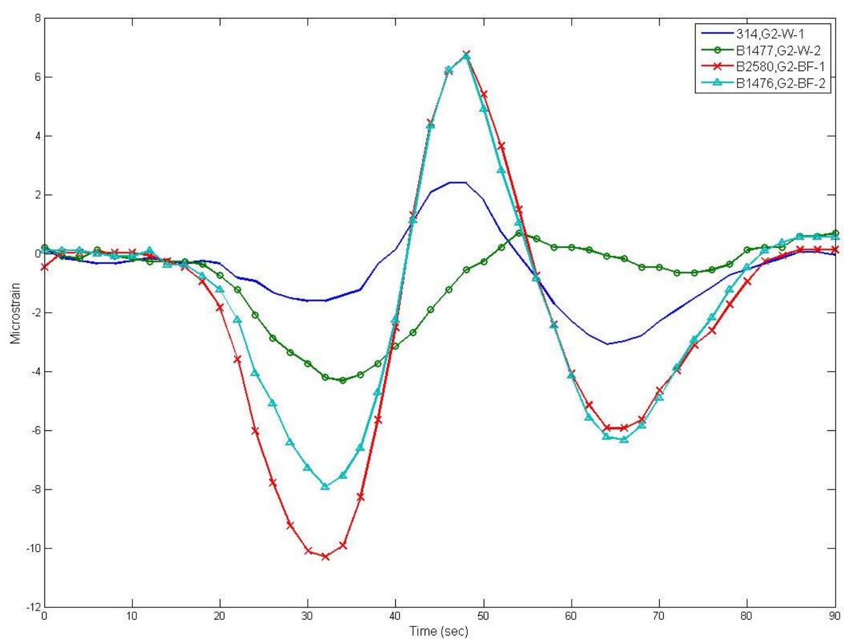

Figure B-36 SR 1 Over US 13 Day 2 Pass 3 Girder Location 2

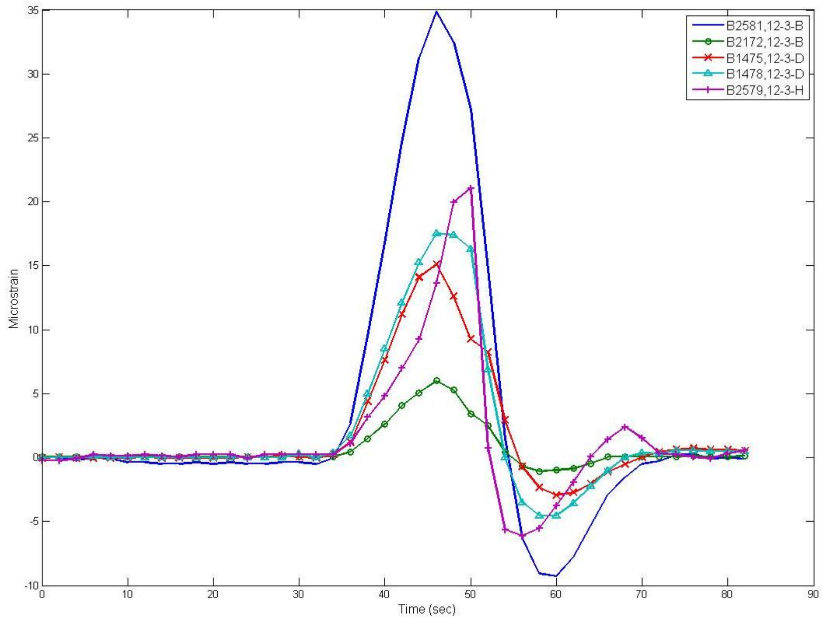

Figure B-37 SR 1 Over US 13 Day 1 Pass 1 Cross-frame 12-3, 1 of 2

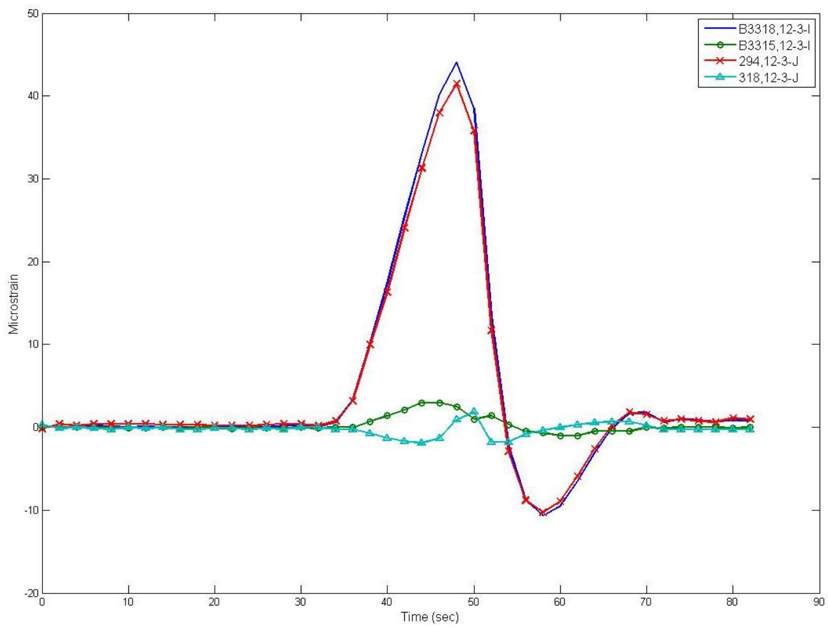

Figure B-38 SR 1 Over US 13 Day 1 Pass 1 Cross-frame 12-3, 2 of 2

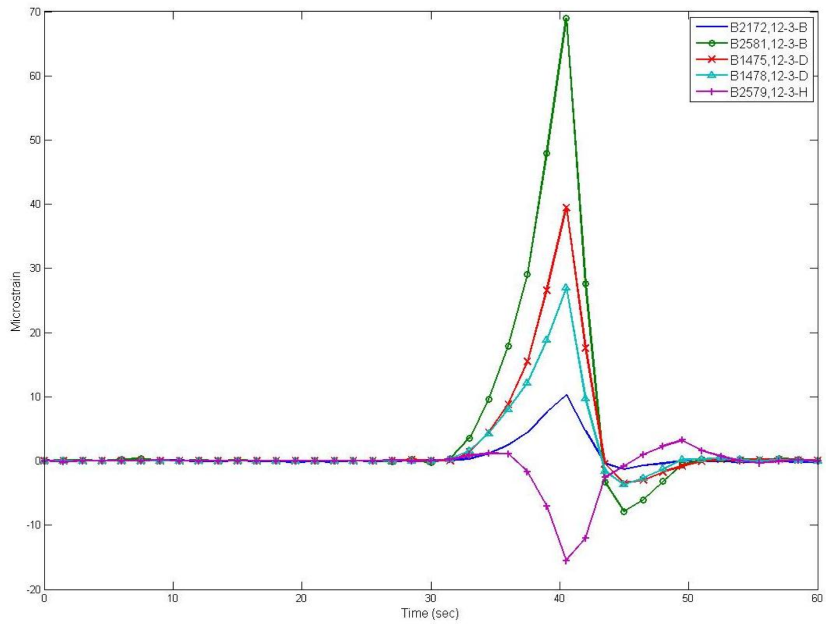

Figure B-39 SR 1 Over US 13 Day 1 Pass 2 Cross-frame 12-3, 1 of 2

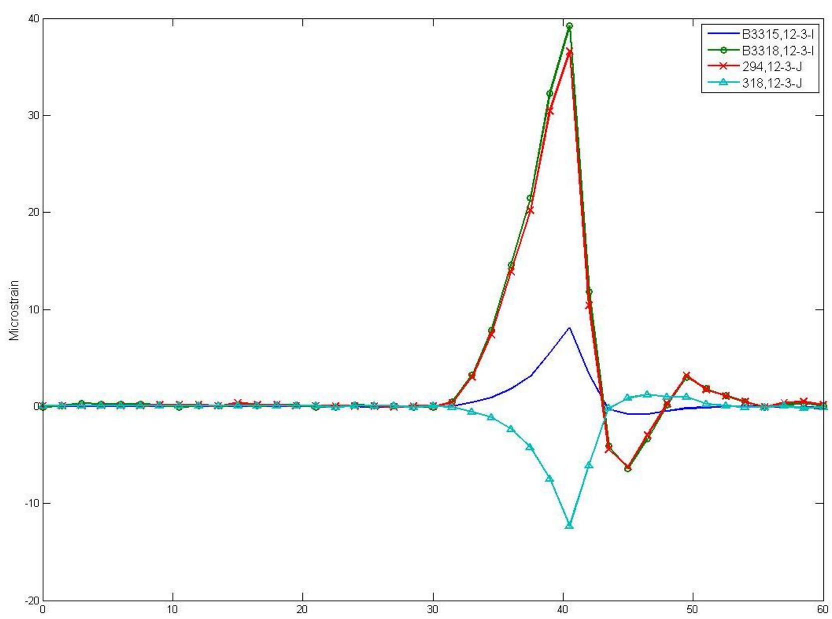

Figure B-40 SR 1 Over US 13 Day 1 Pass 2 Cross-frame 12-3, 2 of 2

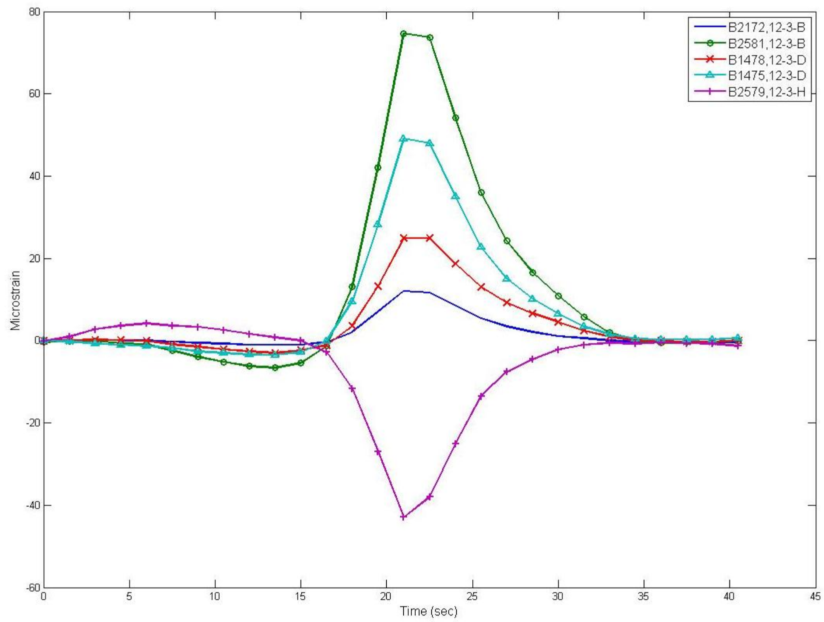

Figure B-41 SR 1 Over US 13 Day 1 Pass 3 Cross-frame 12-3, 1 of 2

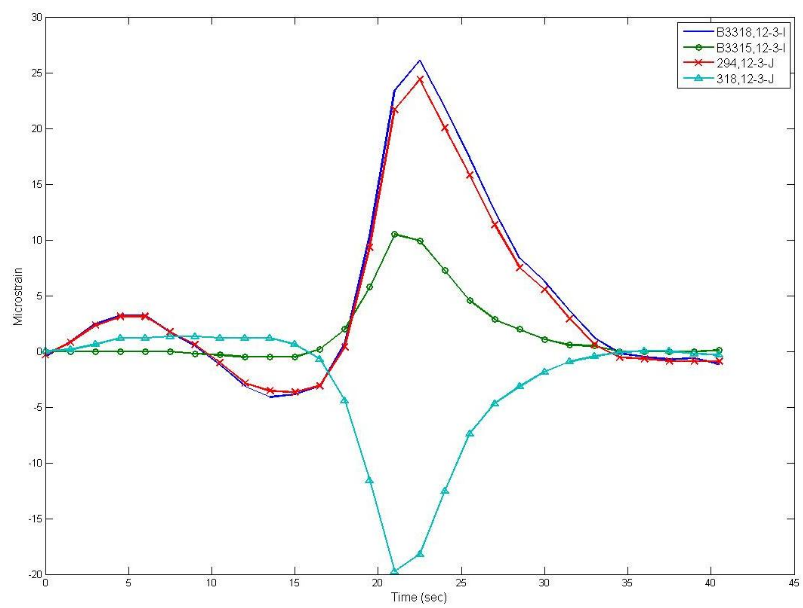

Figure B-42 SR 1 Over US 13 Day 1 Pass 3 Cross-frame 12-3, 2 of 2

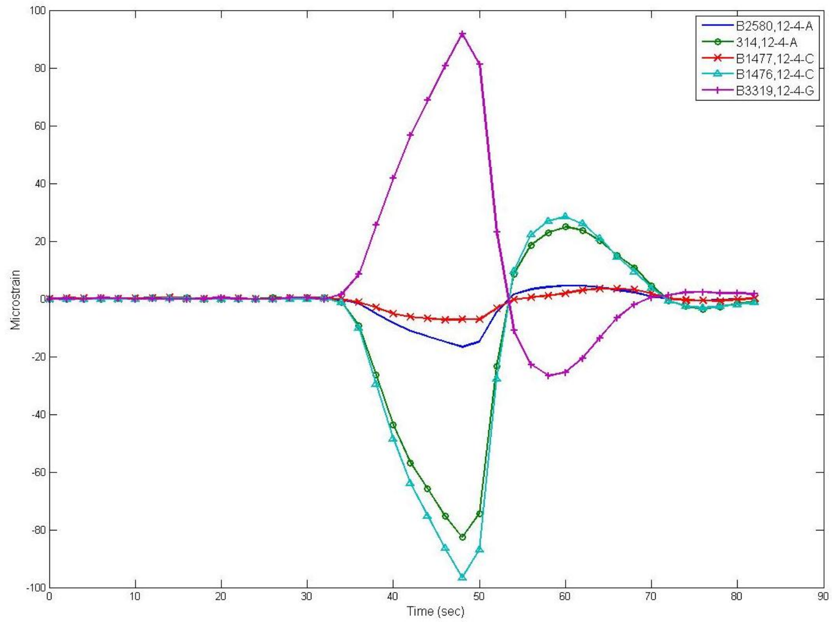

Figure B-43 SR 1 Over US 13 Day 1 Pass 1 Cross-frame 12-4, 1 of 2

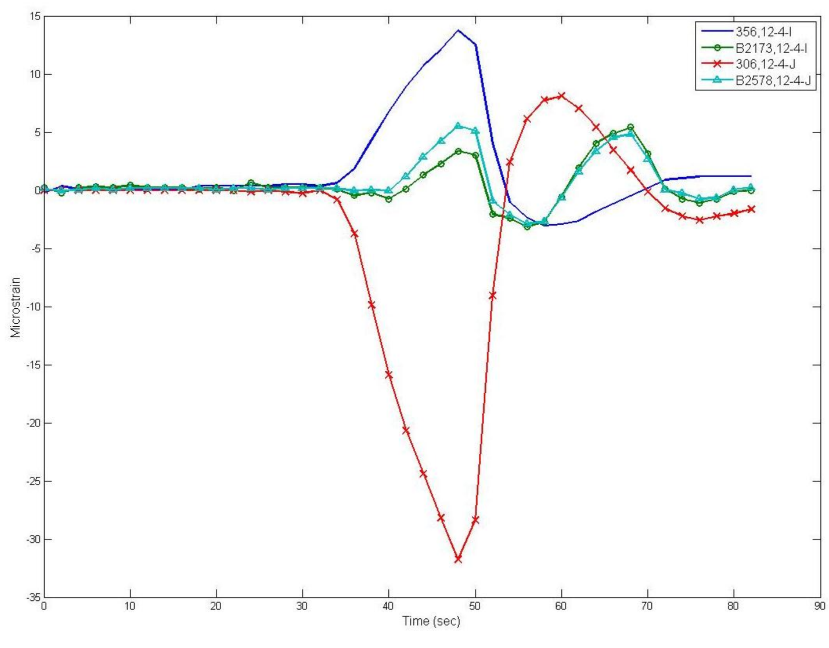

Figure B-44 SR 1 Over US 13 Day 1 Pass 1 Cross-frame 12-4, 2 of 2

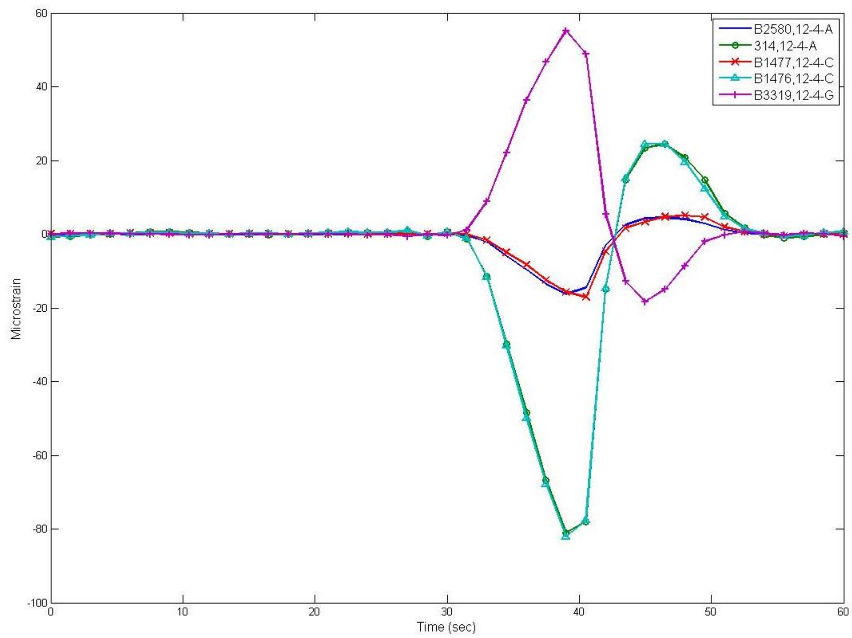

Figure B-45 SR 1 Over US 13 Day 1 Pass 2 Cross-frame 12-4, 1 of 2

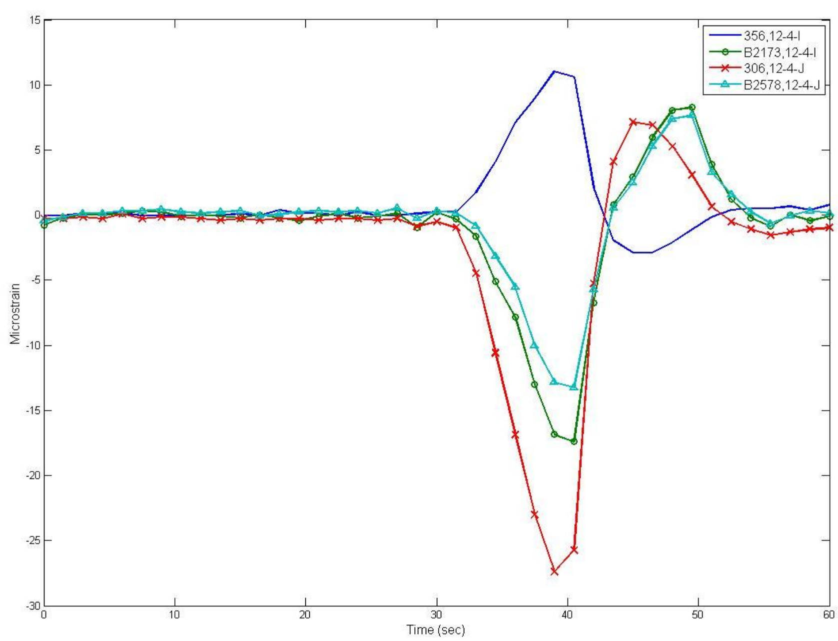

Figure B-46 SR 1 Over US 13 Day 1 Pass 2 Cross-frame 12-4, 2 of 2

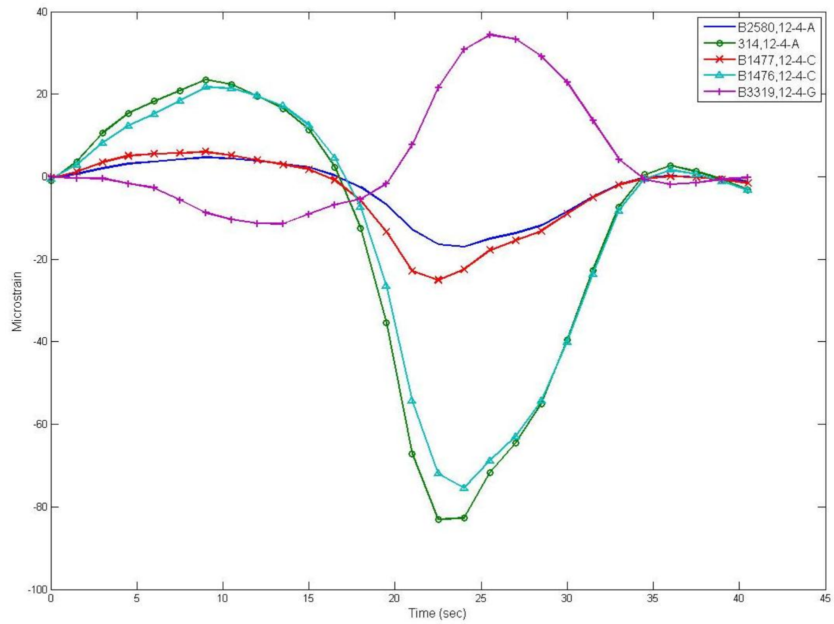

Figure B-47 SR 1 Over US 13 Day 1 Pass 3 Cross-frame 12-4, 1 of 2

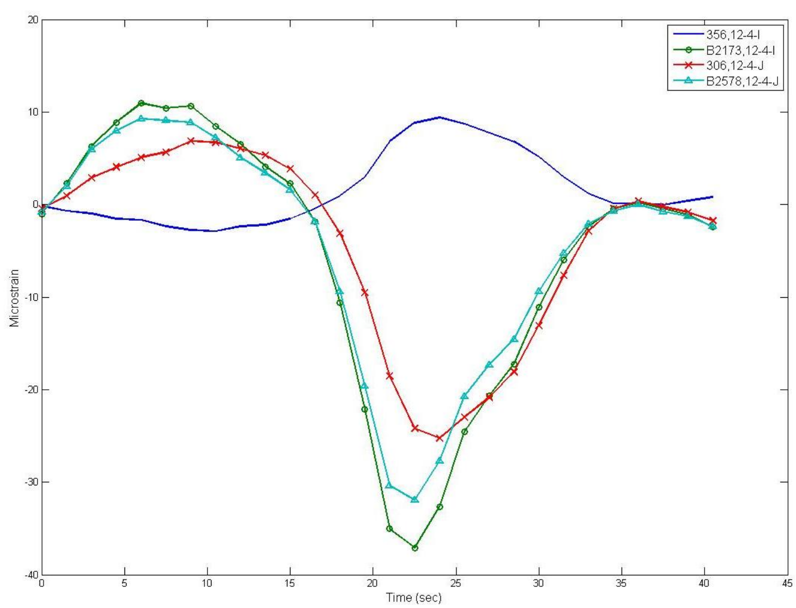

Figure B-48 SR 1 Over US 13 Day 1 Pass 3 Cross-frame 12-4, 2 of 2

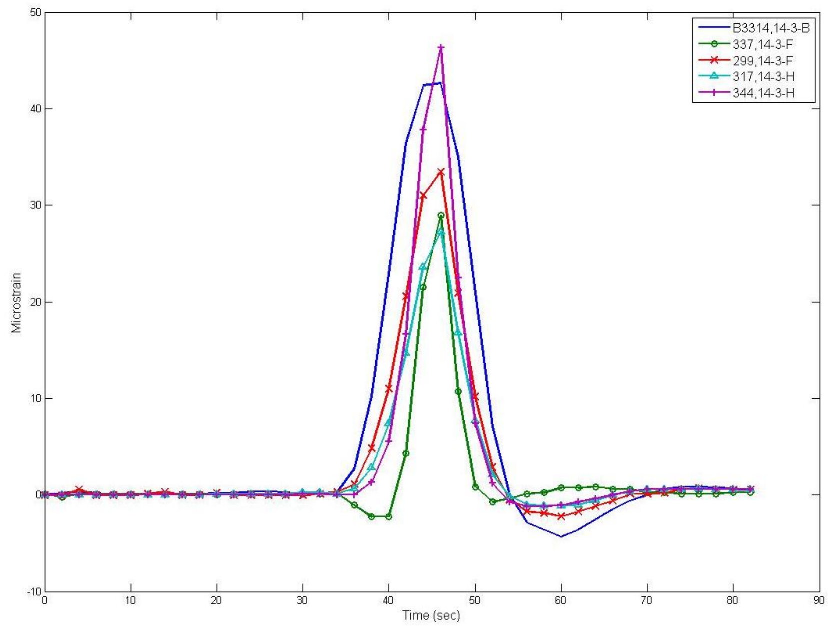

Figure B-49 SR 1 Over US 13 Day 1 Pass 1 Cross-frame 14-3, 1 of 2

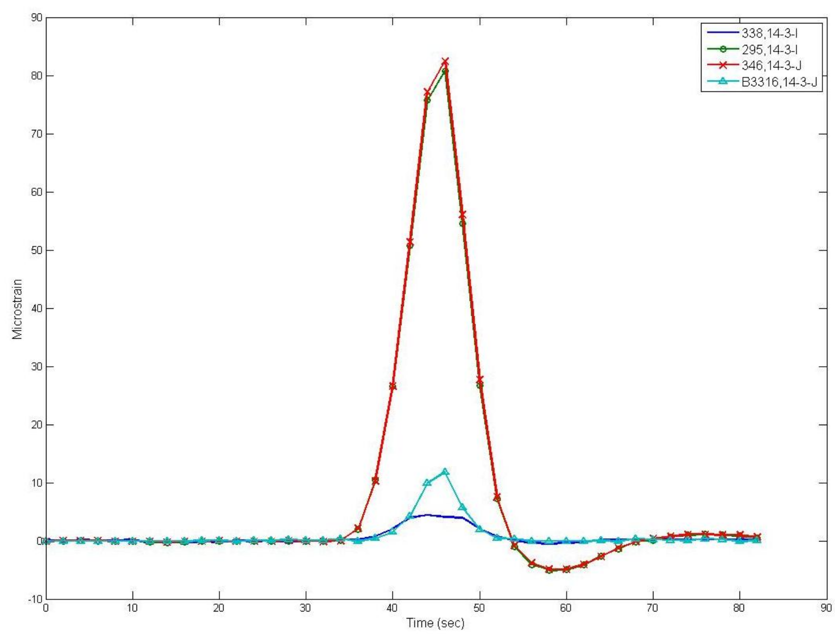

Figure B-50 SR 1 Over US 13 Day 1 Pass 1 Cross-frame 14-3, 2 of 2

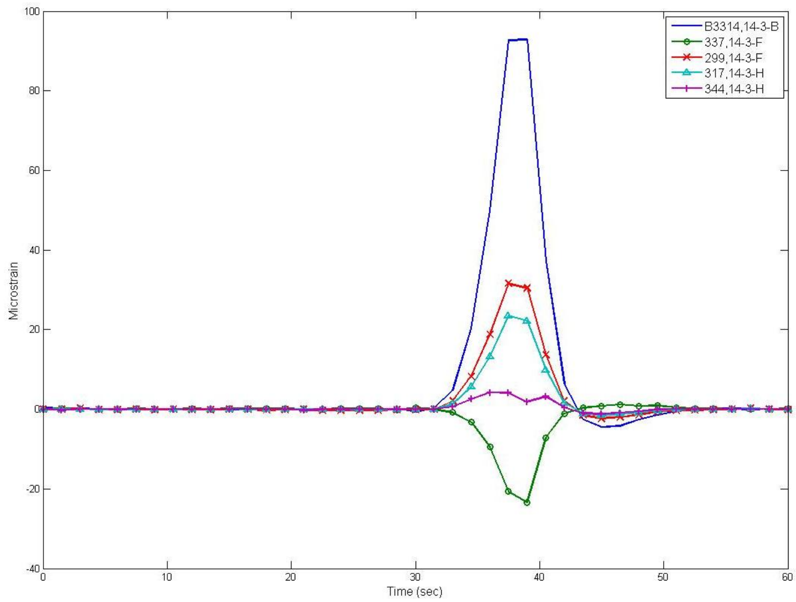

Figure B-51 SR 1 Over US 13 Day 1 Pass 2 Cross-frame 14-3, 1 of 2

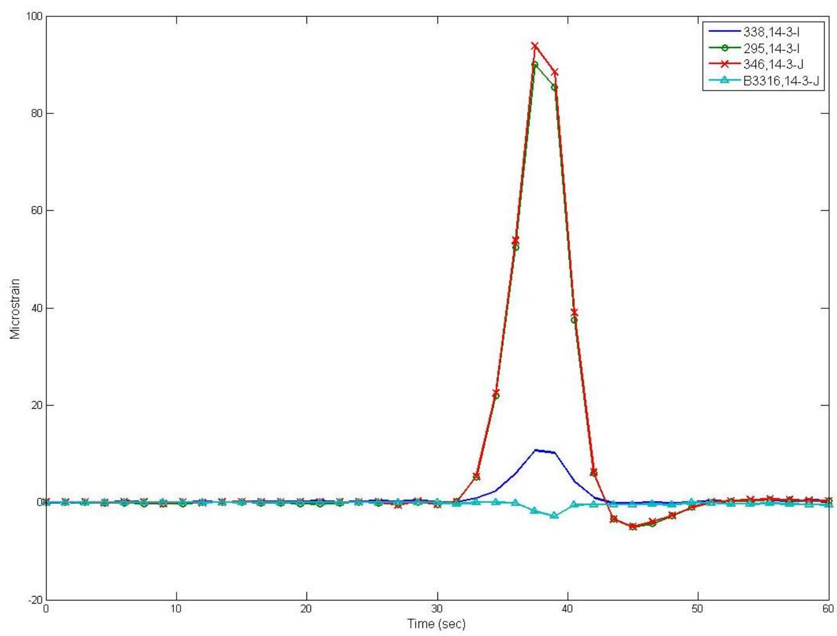

Figure B-52 SR 1 Over US 13 Day 1 Pass 2 Cross-frame 14-3, 2 of 2

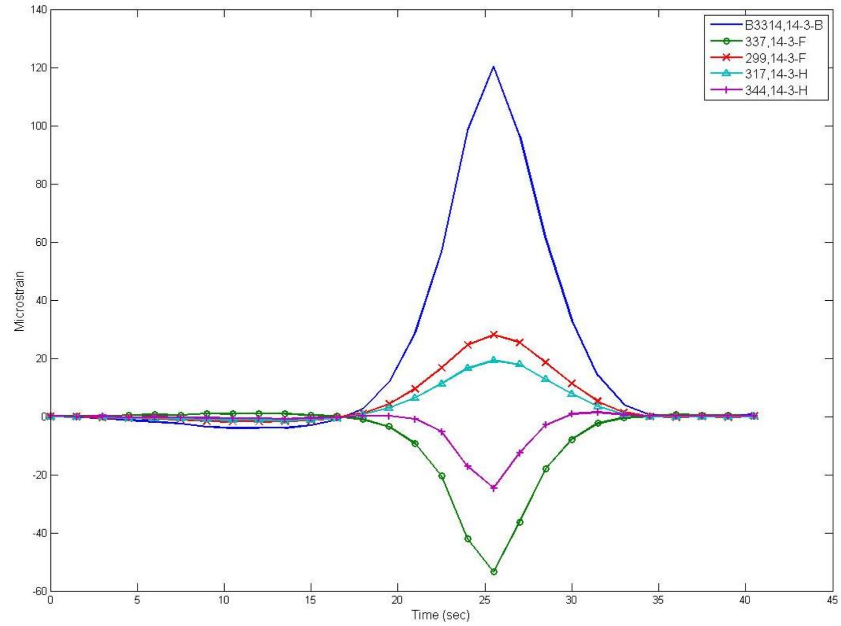

Figure B-53 SR 1 Over US 13 Day 1 Pass 3 Cross-frame 14-3, 1 of 2

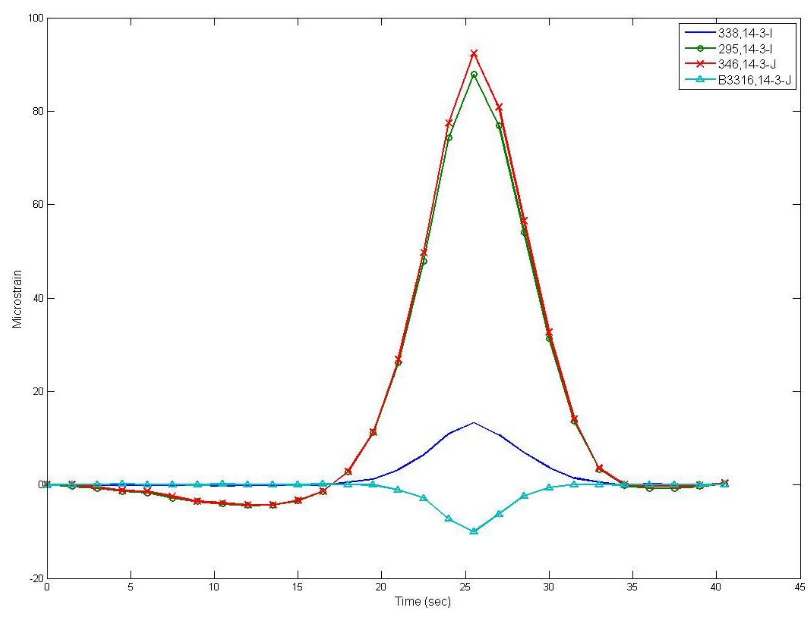

Figure B-54 SR 1 Over US 13 Day 1 Pass 3 Cross-frame 14-3, 2 of 2

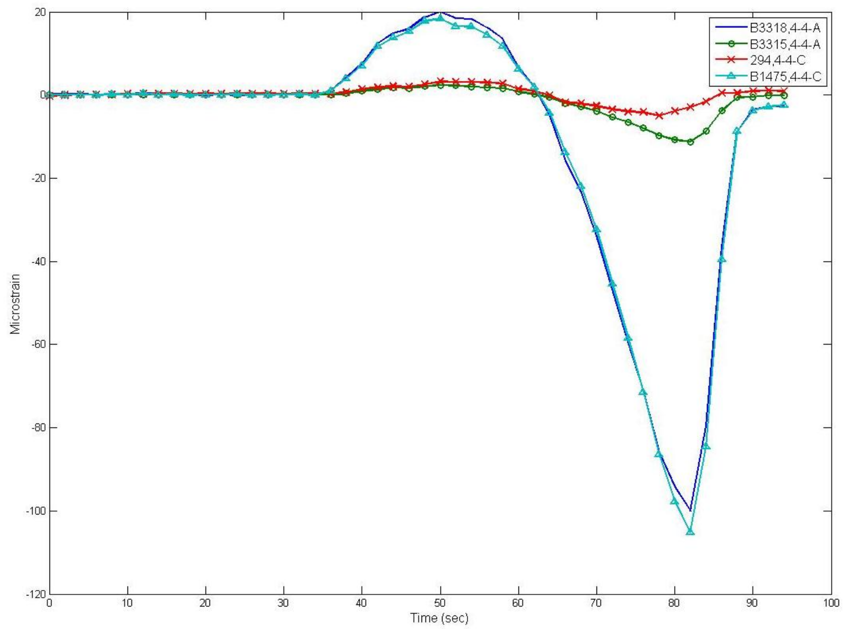

Figure B-55 SR 1 Over US 13 Day 2 Pass 1 Cross-frame 4-4, 1 of 3

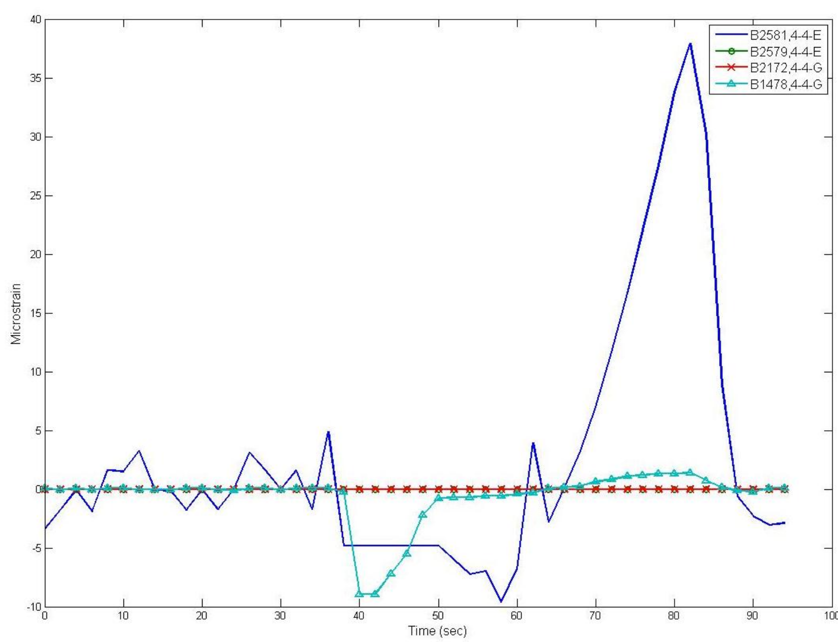

Figure B-56 SR 1 Over US 13 Day 2 Pass 1 Cross-frame 4-4, 2 of 3

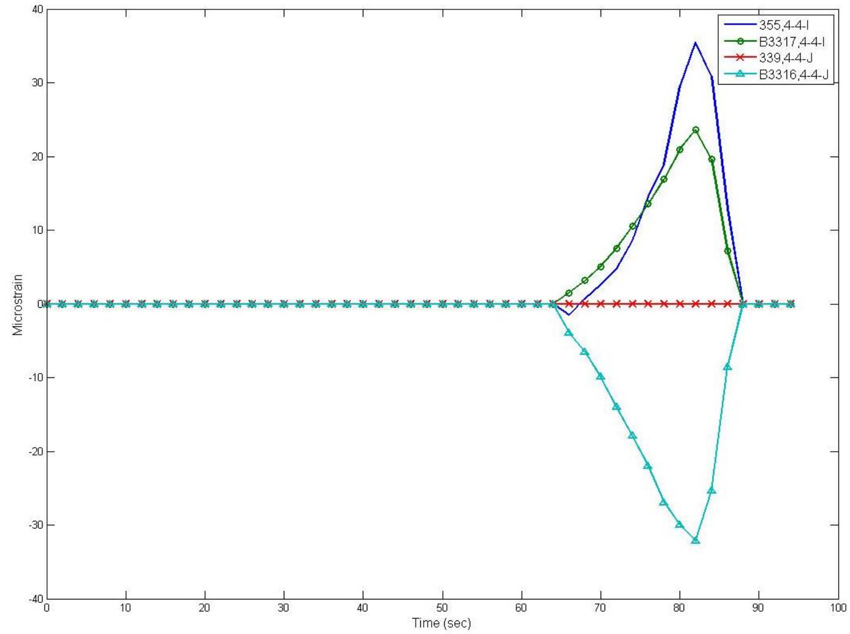

Figure B-57 SR 1 Over US 13 Day 2 Pass 1 Cross-frame 4-4, 3 of 3

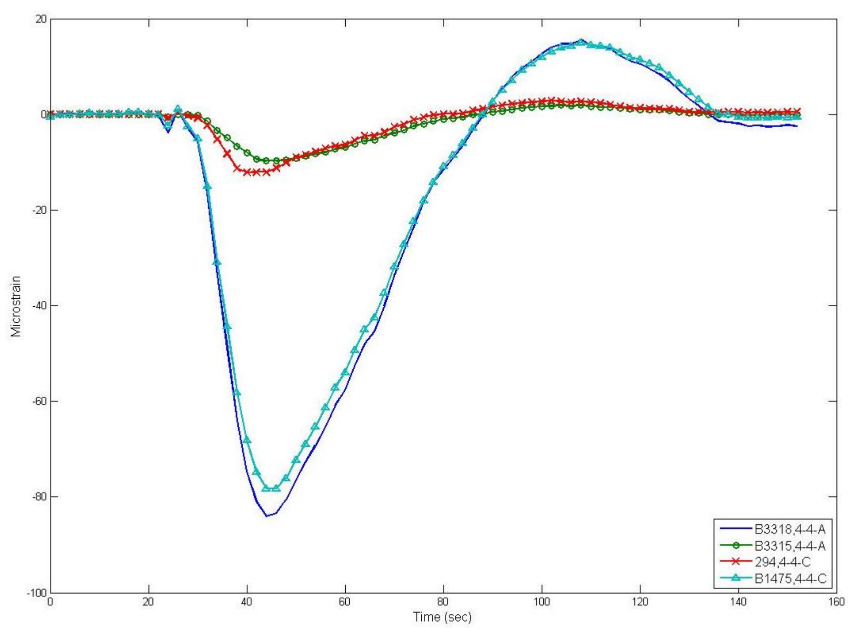

Figure B-58 SR 1 Over US 13 Day 2 Pass 2 Cross-frame 4-4, 1 of 3

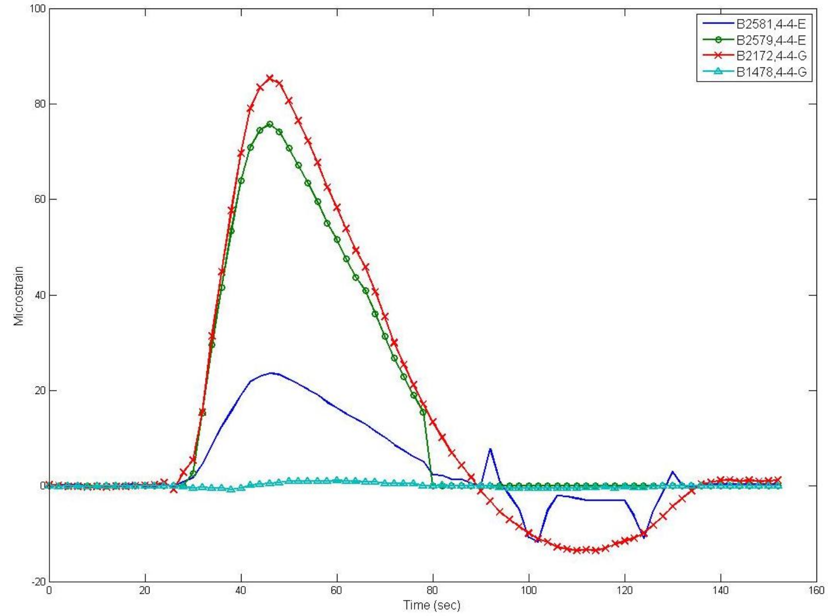

Figure B-59 SR 1 Over US 13 Day 2 Pass 2 Cross-frame 4-4, 2 of 3

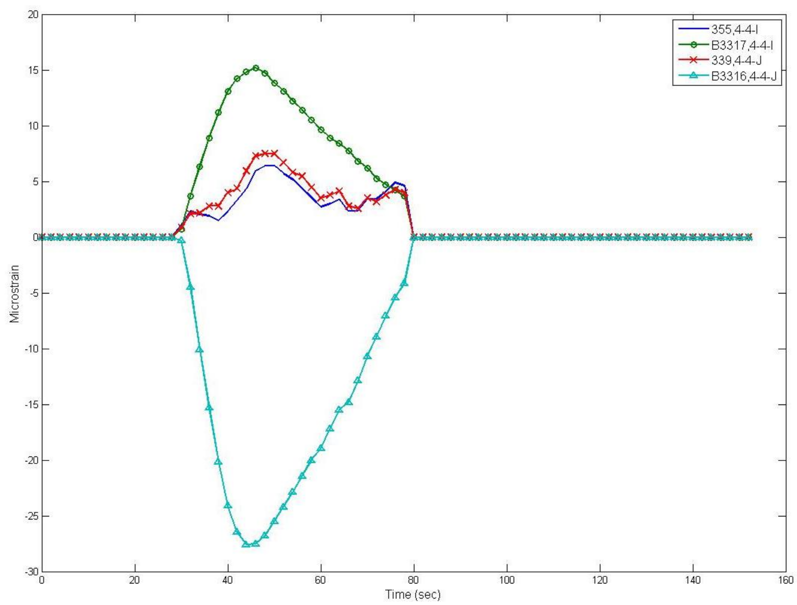

Figure B-60 SR 1 Over US 13 Day 2 Pass 2 Cross-frame 4-4, 3 of 3

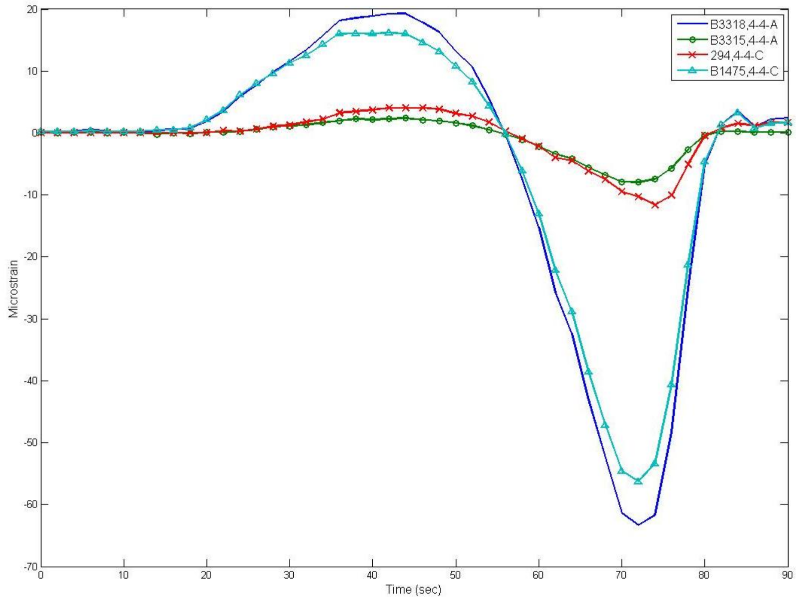

Figure B-61 SR 1 Over US 13 Day 2 Pass 3 Cross-frame 4-4, 1 of 3

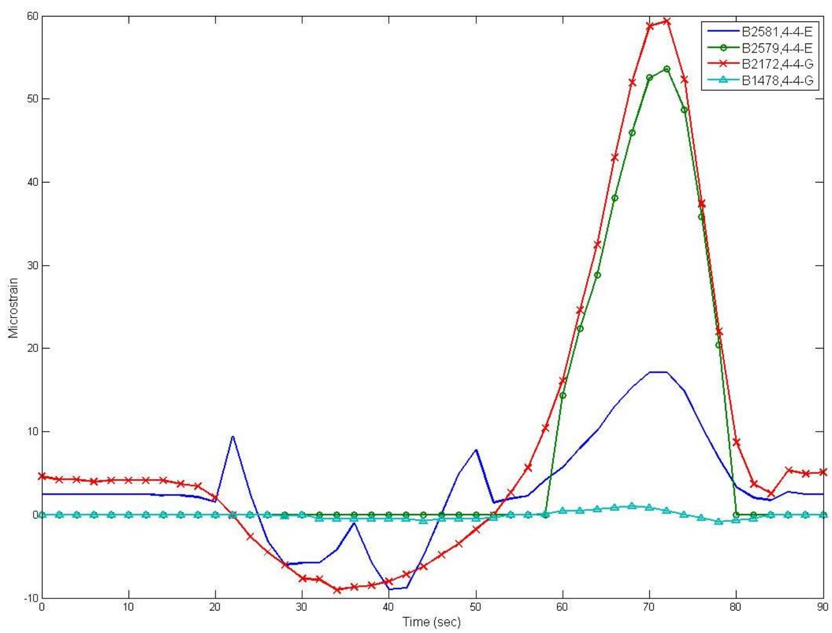

Figure B-62 SR 1 Over US 13 Day 2 Pass 3 Cross-frame 4-4, 2 of 3

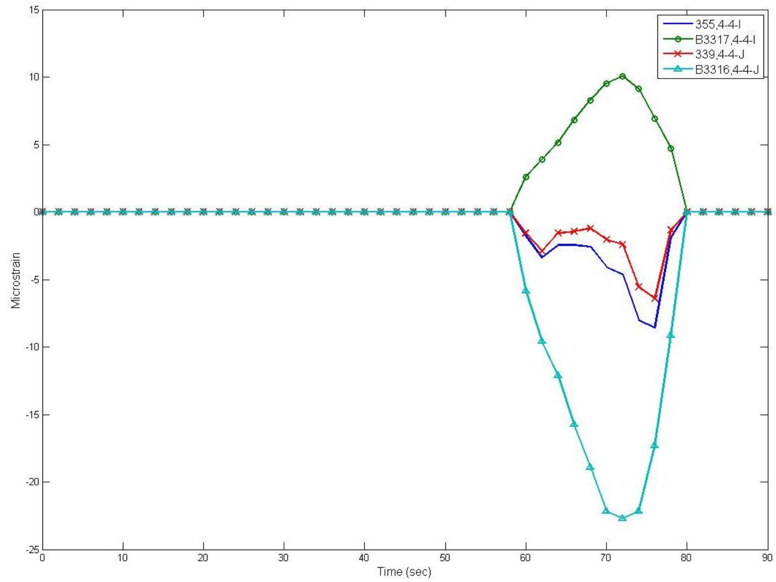

Figure B-63 SR 1 Over US 13 Day 2 Pass 3 Cross-frame 4-4, 3 of 3

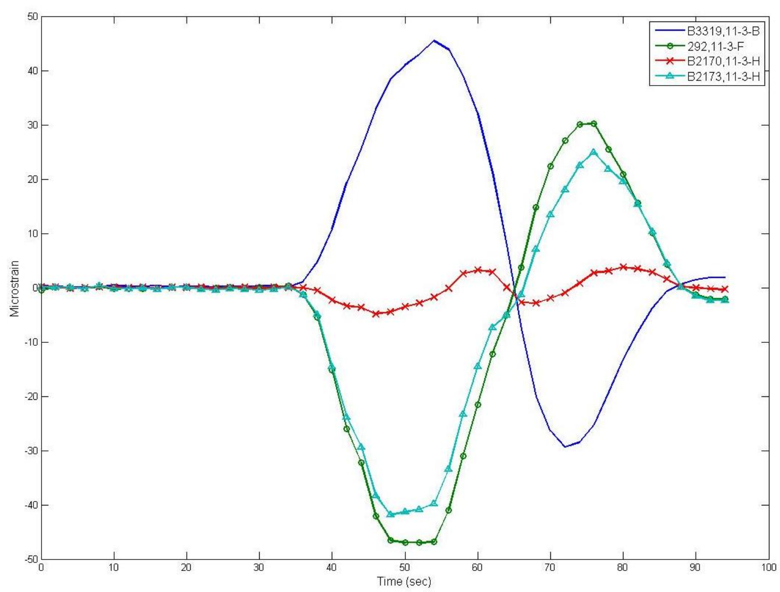

Figure B-64 SR 1 Over US 13 Day 2 Pass 1 Cross-frame 11-3, 1 of 2

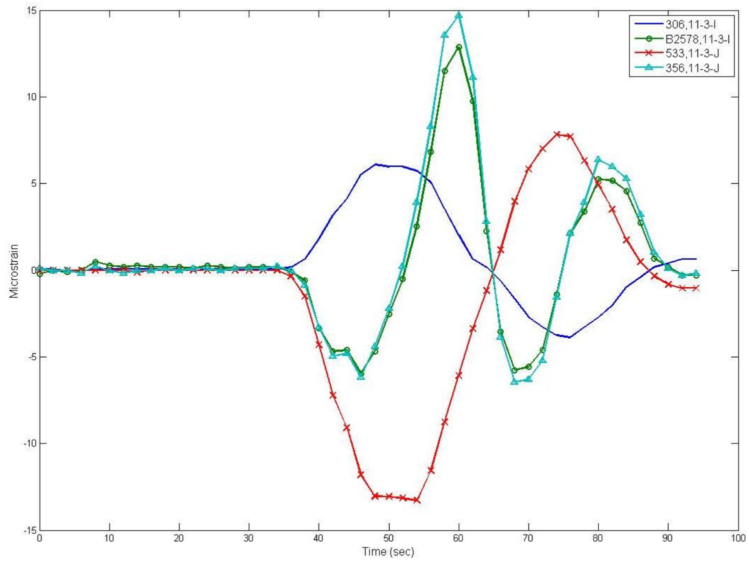

Figure B-65 SR 1 Over US 13 Day 2 Pass 1 Cross-frame 11-3, 2 of 2

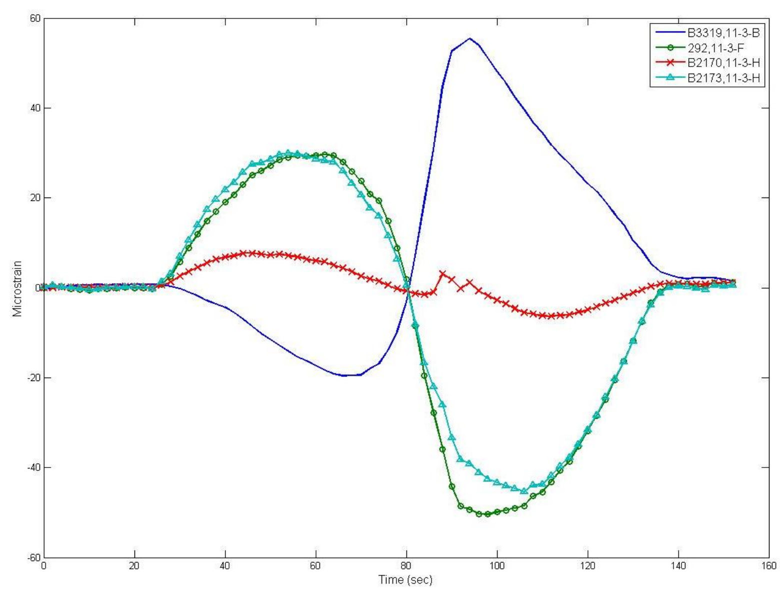

Figure B-66 SR 1 Over US 13 Day 2 Pass 2 Cross-frame 11-3, 1 of 2

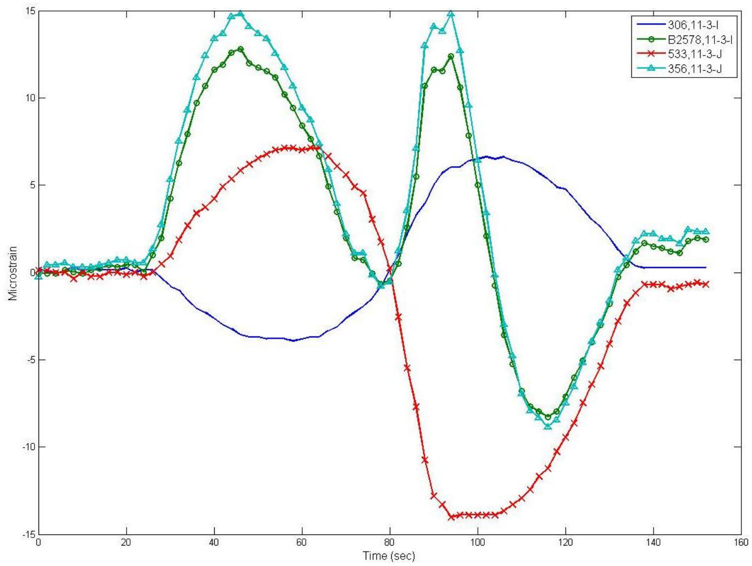

Figure B-67 SR 1 Over US 13 Day 2 Pass 2 Cross-frame 11-3, 2 of 2

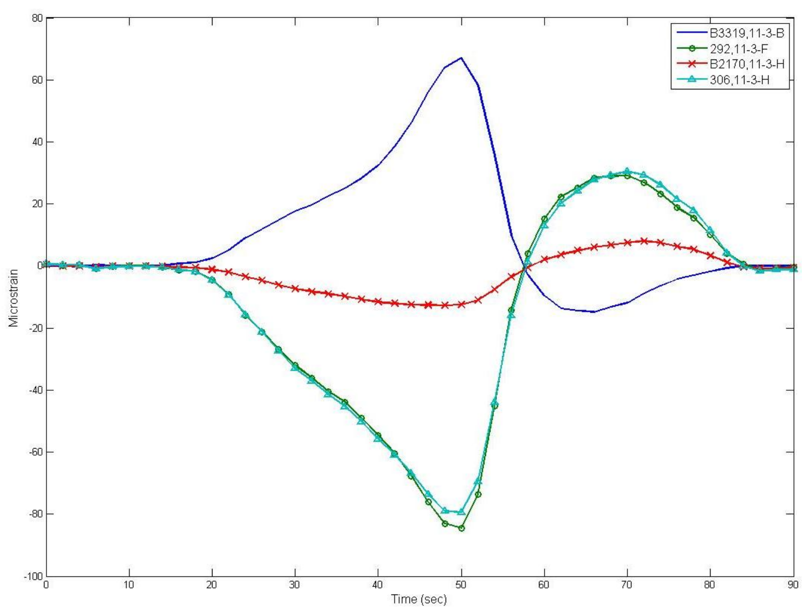

Figure B-68 SR 1 Over US 13 Day 2 Pass 3 Cross-frame 11-3, 1 of 2

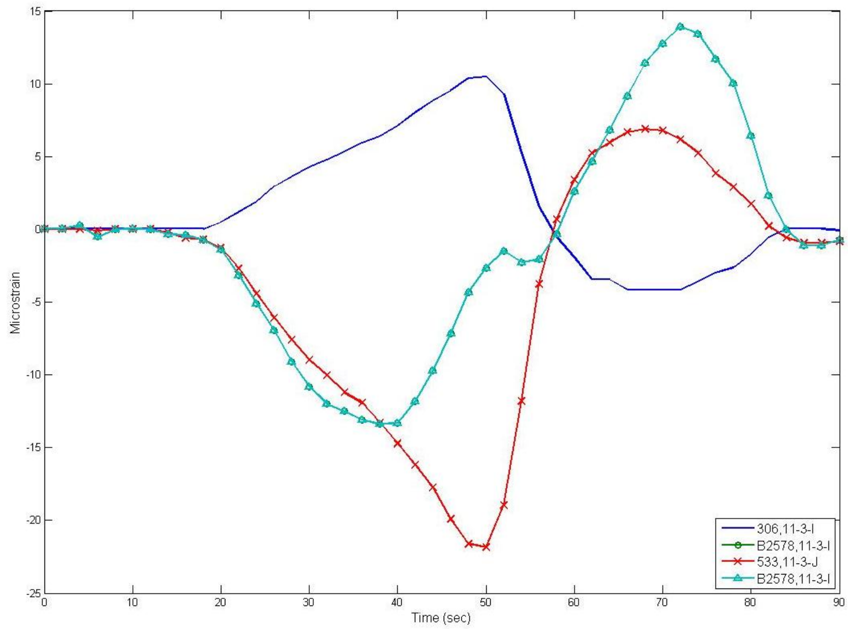

Figure B-69 SR 1 Over US 13 Day 2 Pass 3 Cross-frame 11-3, 2 of 2

Appendix C

HAND CALCULATIONS

As mentioned in Section 5.2, hand calculations using various methods of indeterminate analysis demonstrated the response of SR 299 over SR 1 according to theory. The hand calculations for the distribution factor according to the AASHTO LRFD Bridge Specifications are presented first. The two smaller cross-sections of the bridge were averaged and treated as one section using the averaged geometric properties when computing displacements in virtual work. When calculating properties, 5 ksi strength concrete was considered and short term composite section properties were used. Then, the method of consistent deformations was used to determine the reaction at the center support under live load. Virtual work was used to determine the deflection at the center support for use in the method of consistent deformations. With all of the reactions determined, the moment at Girder location 1 was determined due to the distributed live load. The moment was then divided by the section modulus at the G1 cross-section to determine the stress at Girder location 1 due to the factored live load. Calculations are included herein. A similar process was used, but automated in a spreadsheet, to determine the dead load stresses.

Distribution Factor Calculation

Concrete Deck on Steel Beams

$$0.06 + \left(\frac{S}{14}\right)^{0.4}\left(\frac{S}{L}\right)^{0.3}\left(\frac{K_g}{12.0 L t_s^3}\right)^{0.1}$$

$S = 9'\text{-}1'' = 9.083'$

$L = 134'$

$K_g = n(I + A e_g^2)$

$n = 7.0$ [5 ksi concrete]

$I \rightarrow$ based on average properties (non-composite)

$$I = \frac{29834 + 44353 + 85733}{3}$$

$= 53307 \text{ in.}^4$

$A \rightarrow$ based on average properties (non-composite)

$$A = \frac{63.375 \text{ in.}^2 + 78.375 \text{ in.}^2 + 129.38 \text{ in.}^2}{3}$$

$= 90.38 \text{ in.}^2$

$$e_g = \frac{38.87 + 33 + 33.75}{3} = 35.21 \text{ in.}$$

$K_g = 7(53307 + (90.38)(35.21)^2)$

$= 1.16 \times 10^6$

$t_s = 9 \text{ in.}$

$$0.06 + \left(\frac{9.083}{14}\right)^{0.4}\left(\frac{9.083}{134}\right)^{0.3}\left(\frac{1.16 \times 10^6}{12(134)(9)^3}\right)^{0.1}$$

$= 0.435$

$0.435(14550 \text{ lb}) = 6329 \text{ lb}$

$0.435(20533 \text{ lb}) = 8932 \text{ lb}$

$0.435(20300 \text{ lb}) = 8830 \text{ lb}$

Kelly Ambrose | | | 2/6

SR 299 Over US13 Hand Calcs.

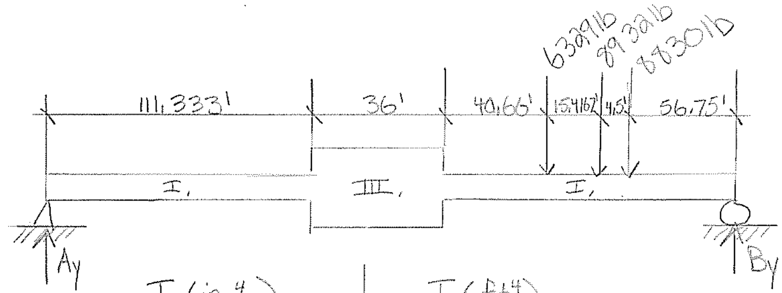

	I (in.⁴)	I (ft⁴)
I.	91833	4.43
III.	155981	7.52

$\circlearrowleft \Sigma M_A = 0 = B_y(262') - 8.83^k(207.91') - 8.932^k(203.41') - 6.329^k(187.993')$

$B_y = 18.4829^k$

$+\uparrow \Sigma F_y = 0 = A_y + 18.4829^k - 6.329^k - 8.932^k - 8.83^k$

$A_y = 5.6081^k$

$\boxed{1}$ $0 \le x \le 111.333'$

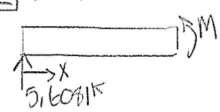

$\circlearrowleft \Sigma M_{cut} = 0 = M - 5.6081(x)$

$\boxed{M = 5.6081x}$

$\boxed{2}$ $111.333' \le x \le 147.333'$

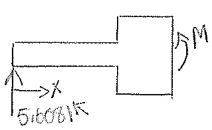

$\circlearrowleft \Sigma M_{cut} = 0 = M - 5.6081(x)$

$\boxed{M = 5.6081x}$

$\boxed{3}$ $147.333' \le x \le 187.993'$

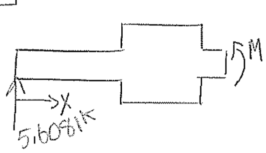

$\circlearrowleft \Sigma M_{cut} = 0 = M - 5.6081(x)$

$\boxed{M = 5.6081x}$

$\boxed{4}$ $187.993' \le x \le 203.41'$

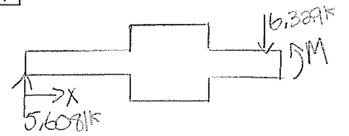

$\circlearrowleft \sum M_{cut} = 0 = M + 6.329(x - 187.993') - 5.6081(x)$

$\boxed{M = -0.7209x + 1189.81}$

$\boxed{5}$ $203.41' \le x \le 207.91'$

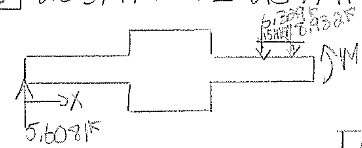

$\circlearrowleft \sum M_{cut} = 0 = M + 8.932(x - 203.41') + 6.329(x - 187.993') - 5.6081(x)$

$\boxed{M = -9.6529x + 3006.67}$

$\boxed{6}$ $207.91' \le x \le 265'$

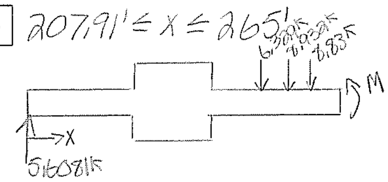

$\circlearrowleft \sum M_{cut} = 0 = M + 8.83(x - 207.91') + 8.932(x - 203.41') + 6.329(x - 187.993') - 5.6081(x)$

$\boxed{M = -18.4829x + 4842.51}$

Virtual Work

Apply a unit load at C

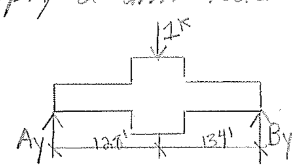

$\circlearrowleft \sum M_A = 0 = B_y(262') - 1^k(128')$

$B_y = 0.489^k$

$A_y = 0.511^k$

$\boxed{1}$ $0 \le x \le 111.333'$

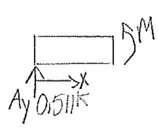

$\circlearrowleft \sum M_{cut} = 0 = M - 0.511(x)$

$\boxed{M = 0.511x}$

$\boxed{2}$ $111.333' \le x \le 129.333'$

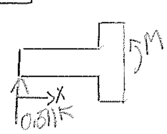

$\circlearrowleft \sum M_{cut} = 0 = M - 0.511(x)$

$\boxed{M = 0.511x}$

Kelly Ambrose | | | 4/6

$\boxed{2a}$ $129.333' \le x \le 147.33'$

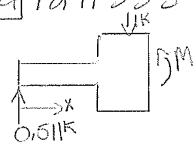

$\circlearrowleft \Sigma M_{cut} = 0 = M + 1(x - 129.333')$

$$\boxed{M = 129.333 - x}$$

$\boxed{3}$, $\boxed{4}$, $\boxed{5}$, $\boxed{6}$ $\boxed{M = 129.33 - x}$

Virtual Work; $1^k \cdot \Delta = \int_0^L \frac{mM}{EI} dx$

$$= \int_0^{111.333'} \frac{(5.6081x)(0.511x)}{E(4.43)} dx + \int_{111.33'}^{129.333'} \frac{(5.6081x)(0.511x)}{E(7.52)} dx$$

$$+ \int_{129.333'}^{147.333'} \frac{(5.6081x)(129.33-x)}{E(7.52)} dx + \int_{147.333'}^{187.993'} \frac{(5.6081x)(129.33-x)}{E(4.43)} dx$$

$$+ \int_{187.993'}^{203.41'} \frac{(-0.7209x + 1189.81)(129.33-x)}{E(4.43)} dx$$

$$+ \int_{203.41'}^{207.91'} \frac{(-9.6529 + 3006.67)(129.33-x)}{E(4.43)} dx$$

$$+ \int_{207.91'}^{262'} \frac{(-18.4829x + 4842.51)(129.33-x)}{E(4.43)} dx$$

$$\delta = -1.59^{ft} = 19.08'' = \Delta_B$$

$$0.064' = \Delta'_{BB}$$

Kelly Ambrose | | | 5/6

Δ_{BB}'

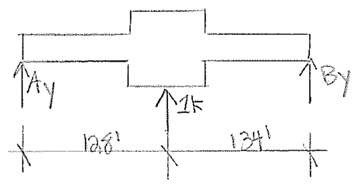

$\circlearrowleft \Sigma M_A = 0 = B_y(262') + 1^k(128')$

$B_y = -0.489^k$

$A_y = -0.511^k$

$\Delta_{BB}' = -0.064^{ft} = 0.768 \text{ in.}$

$\Delta_B + B_y f_{BB} = 0$

$-19.08 + B_y(0.768) = 0$

$\therefore B_y = 24.84^k$

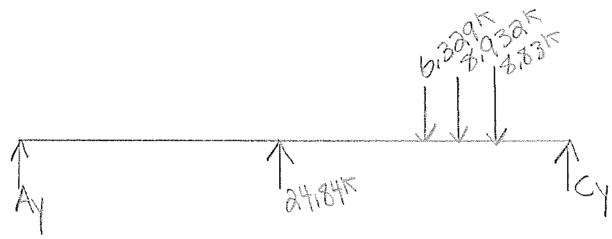

$\circlearrowleft \Sigma M_A = 0 = 24.84(128) - 6.329(187.993) - 8.932(203.41) - 8.83(207.91') + C_y(262)$

$C_y = 6.35^k$

$\uparrow \Sigma F_y = 0 = 24.84 + 6.35 + A_y - 6.329 - 8.932 - 8.83$

$A_y = -7.1^k$

Kelly Ambrose 6/6

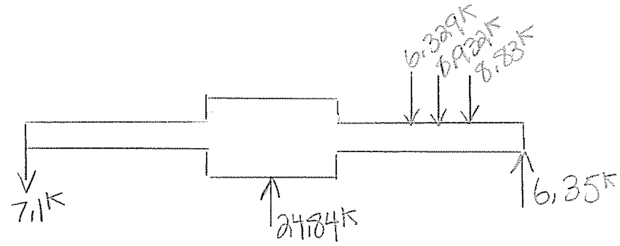

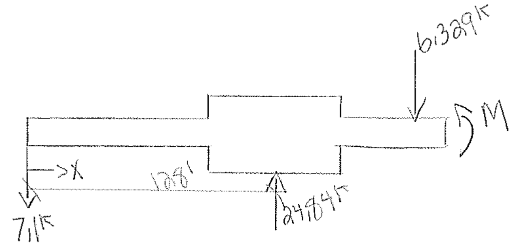

$$\circlearrowleft \sum M_{cut} = 0 = M + 6.329(x - 187.993) - 24.84(x - 128) + 7.1(x)$$

$$M = 11.411x - 1989.71$$

at $x = 203.41'$

$$M(x) = 11.411(203.41') - 1989.71 = 331.4 \text{ k·ft}$$

$$M = 331.4 \text{ k·ft} = 3976.82 \text{ k·in}$$

$$\text{stress} = \frac{M}{S_x} = \frac{3976.82 \text{ k·in}}{1913 \text{ in}^3}$$

$$= \boxed{2.08 \text{ ksi}}$$

Appendix D

SR 1 OVER US 13 CROSS-FRAME DATA

As mentioned in Section 5.4, the complete set of cross-frame data for SR 1 over US 13 is presented herein. This data includes the maximum stress at each gauge location converted from the maximum strain recorded during field testing by multiplying by the modulus of elasticity of steel, the top and bottom section points for both the fixed and pinned connection models, the two different cases for averaging the section points as discussed in Section 5.4, and the percent difference between each averaging case and the corresponding field test value. The cross-frame data from the first day of testing for all three passes is presented first followed by the cross-frame data from the second day for all three passes.

Table D-1 Cross-frame 12-3 Data for SR 1 Over US 13 Day 1 Pass 1

			Section Points FEA E1,C1,S5 Fixed						Section Points FEA E1 C1 S5 Pinned					
Gauge Location	σ_{MAX} (psi)	σ_{Avg} (psi)	Bottom (psi)	Top (psi)	Avg Case 1 (psi)	% Diff	Avg Case 2 (psi)	% Diff	Bottom (psi)	Top (psi)	Avg Case 1 (psi)	% Diff	Avg Case 2 (psi)	% Diff
12-3-B	1062	621	244	-240	2	100	-119	119	276	93	184	70	139	78
12-3-B	180													
12-3-D	458	504	244	-216	14	97	-101	120	264	20	142	72	81	84
12-3-D	549													
12-3-H	658	658	756	10	383	42	197	70	808	153	481	27	317	52
12-3-I	1391	746	1195	495	845	-13	670	10	1102	725	914	-22	819	-10
12-3-I	101													
12-3-J	1315	688	1360	-716	322	53	-197	129	1238	-242	498	28	128	81
12-3-J	61													

Table D-2 Cross-frame 12-4 Data for SR 1 Over US 13 Day 1 Pass 1

			Section Points FEA E1,C1,S5 Fixed						Section Points FEA E1 C1 S5 Pinned					
Gauge Location	σ_{MAX} (psi)	σ_{Avg} (psi)	Bottom (psi)	Top (psi)	Avg Case 1 (psi)	% Diff	Avg Case 2 (psi)	% Diff	Bottom (psi)	Top (psi)	Avg Case 1 (psi)	% Diff	Avg Case 2 (psi)	% Diff
12-4-A	-2467	-1489	-2710	-1091	-1901	-28	-1496	0	-2730	-2566	-2648	-78	-2607	-75
12-4-A	-510													
12-4-C	-2915	-1598	-2921	497	-1212	24	-358	78	-2946	-863	-1904	-19	-1383	13
12-4-C	-281													
12-4-G	2850	2850	2833	962	1897	33	1430	50	2828	1935	2381	16	2158	24
12-4-I	-167	121	100	-348	-124	202	-236	295	139	-508	-185	252	-347	386
12-4-I	410													
12-4-J	245	-357	-863	1779	458	228	1119	414	-721	1533	406	214	970	372
12-4-J	-958													

Table D-3 Cross-frame 14-3 Data for SR 1 Over US 13 Day 1 Pass 1

			Section Points FEA E1,C1,S5 Fixed						Section Points FEA E1 C1 S5 Pinned					
Gauge Location	σ_{MAX} (psi)	σ_{Avg} (psi)	Bottom (psi)	Top (psi)	Avg Case 1 (psi)	% Diff	Avg Case 2 (psi)	% Diff	Bottom (psi)	Top (psi)	Avg Case 1 (psi)	% Diff	Avg Case 2 (psi)	% Diff
14-3-B	1299	1299	-648	-193	-420	132	-307	124	-645	-110	-378	129	-244	119
14-3-F	918	972	1071	473	772	21	622	36	1215	548	881	9	714	27
14-3-F	1027													
14-3-H	1422	1123	1175	-595	290	74	-153	114	1321	-480	421	63	-29	103
14-3-H	823													
14-3-I	2453	1302	2050	-849	601	54	-124	110	2034	-361	836	36	238	82
14-3-I	151													
14-3-J	2491	1425	2108	-1162	473	67	-345	124	2113	-893	610	57	-142	110
14-3-J	360													

Table D-4 Cross-frame 12-3 Data for SR 1 Over US 13 Day 1 Pass 2

			Section Points FEA E1, C1, S5 Fixed						Section Points FEA E1, C1, S5 Pinned					
Gauge Location	σ_{MAX} (psi)	σ_{Avg} (psi)	Bottom (psi)	Top (psi)	Avg Case 1 (psi)	% Diff	Avg Case 2 (psi)	% Diff	Bottom (psi)	Top (psi)	Avg Case 1 (psi)	% Diff	Avg Case 2 (psi)	% Diff
12-3-B	2082	1199	2661	-515	1073	11	279	77	2728	281	1504	-25	892	26
12-3-B	316													
12-3-D	1226	1017	2363	2346	2355	-131	2351	-131	2464	2553	2509	-147	2531	-149
12-3-D	809													
12-3-H	-678	-678	-2080	703	-688	-1	8	101	-2080	219	-930	-37	-356	48
12-3-I	1191	718	684	116	400	44	258	64	637	24	330	54	177	75
12-3-I	245													
12-3-J	1121	347	668	-321	174	50	-74	121	556	219	387	-12	303	13
12-3-J	-426													

Table D-5 Cross-frame 12-4 Data for SR 1 Over US 13 Day 1 Pass 2

			Section Points FEA E1, C1, S5 Fixed						Section Points FEA E1, C1, S5 Pinned					
Gauge Location	σ_{MAX} (psi)	σ_{Avg} (psi)	Bottom (psi)	Top (psi)	Avg Case 1 (psi)	% Diff	Avg Case 2 (psi)	% Diff	Bottom (psi)	Top (psi)	Avg Case 1 (psi)	% Diff	Avg Case 2 (psi)	% Diff
12-4-A	-2705	-1628	-2273	-925	-1599	2	-1262	22	-2328	-2307	-2318	-42	-2312	-42
12-4-A	-552													
12-4-C	-2737	-1724	-2455	482	-986	43	-252	85	-2521	-718	-1620	6	-1169	32
12-4-C	-711													
12-4-G	1979	1979	1601	699	1150	42	924	53	1534	1251	1392	30	1322	33
12-4-I	-836	-200	-1303	-238	-771	-285	-504	-152	-1189	-1002	-1096	-447	-1049	-424
12-4-I	435													
12-4-J	-651	-830	-1866	3274	704	185	1989	340	-1789	2991	601	172	1796	316
12-4-J	-1008													

Table D-6   Cross-frame 14-3 Data for SR 1 Over US 13 Day 1 Pass 2

			Section Points FEA E1, C1, S5 Fixed						Section Points FEA E1, C1, S5 Pinned					
Gauge Location	σ_{MAX} (psi)	σ_{Avg} (psi)	Bottom (psi)	Top (psi)	Avg Case 1 (psi)	% Diff	Avg Case 2 (psi)	% Diff	Bottom (psi)	Top (psi)	Avg Case 1 (psi)	% Diff	Avg Case 2 (psi)	% Diff
14-3-B	3161	3161	2772	-647	1062	66	208	93	2960	-15	1472	53	728	77
14-3-F	-811	108	-645	-2040	-1343	1339	-1691	1661	-635	-1810	-1223	1229	-1517	1500
14-3-F	1027													
14-3-H	192	484	-861	-115	-488	201	-301	162	-800	-447	-623	229	-535	211
14-3-H	775													
14-3-I	2896	1629	2371	-1232	569	65	-331	120	2284	-988	648	60	-170	110
14-3-I	362													
14-3-J	3012	1453	2291	-989	651	55	-169	112	2179	-493	843	42	175	88
14-3-J	-106													

Table D-7 Cross-frame 12-3 Data for SR 1 Over US 13 Day 1 Pass 3

			Section Points FEA E1, C1, S5 Fixed						Section Points FEA E1, C1, S5 Pinned					
Gauge Location	σ_{MAX} (psi)	σ_{Avg} (psi)	Bottom (psi)	Top (psi)	Avg Case 1 (psi)	% Diff	Avg Case 2 (psi)	% Diff	Bottom (psi)	Top (psi)	Avg Case 1 (psi)	% Diff	Avg Case 2 (psi)	% Diff
12-3-B	2223	1283	2531	-434	1048	18	307	76	2606	290	1448	-13	869	32
12-3-B	342													
12-3-D	1504	1109	2245	2330	2288	-106	2309	-108	2352	2496	2424	-119	2460	-122
12-3-D	713													
12-3-H	-1246	-1246	-2155	718	-719	42	0	100	-2172	232	-970	22	-369	70
12-3-I	826	565	469	57	263	53	160	72	423	-97	163	71	33	94
12-3-I	303													
12-3-J	869	161	433	-242	95	41	-73	145	320	255	287	-78	271	-68
12-3-J	-546													

Table D-8 Cross-frame 12-4 Data for SR 1 Over US 13 Day 1 Pass 3

			Section Points FEA E1, C1, S5 Fixed						Section Points FEA E1, C1, S5 Pinned					
Gauge Location	σ_{MAX} (psi)	σ_{Avg} (psi)	Bottom (psi)	Top (psi)	Avg Case 1 (psi)	% Diff	Avg Case 2 (psi)	% Diff	Bottom (psi)	Top (psi)	Avg Case 1 (psi)	% Diff	Avg Case 2 (psi)	% Diff
12-4-A	-2591	-1579	-2159	-906	-1533	3	-1220	23	-2212	-2208	-2210	-40	-2209	-40
12-4-A	-566													
12-4-C	-2354	-1574	-2332	446	-943	40	-249	84	-2397	-682	-1540	2	-1111	29
12-4-C	-795													
12-4-G	1188	1188	1423	660	1041	12	850	28	1364	1157	1260	-6	1209	-2
12-4-I	-1136	-370	-1562	-176	-869	-135	-522	-41	-1456	-976	-1216	-229	-1096	-196
12-4-I	396													
12-4-J	-949	-953	-2171	3677	753	179	2215	332	-2103	3362	630	166	1996	309
12-4-J	-958													

Table D-9 Cross-frame 14-3 Data for SR 1 Over US 13 Day 1 Pass 3

			Section Points FEA E1, C1, S5 Fixed						Section Points FEA E1, C1, S5 Pinned					
Gauge Location	σ_{MAX} (psi)	σ_{Avg} (psi)	Bottom (psi)	Top (psi)	Avg Case 1 (psi)	% Diff	Avg Case 2 (psi)	% Diff	Bottom (psi)	Top (psi)	Avg Case 1 (psi)	% Diff	Avg Case 2 (psi)	% Diff
14-3-B	3645	3645	2720	-581	1070	71	244	93	2884	13	1449	60	731	80
14-3-F	-1622	-390	-667	-1973	-1320	-239	-1647	-322	-663	-1740	-1202	-208	-1471	-277
14-3-F	842													
14-3-H	-659	-9	-878	-72	-475	-5452	-273	-3095	-826	-384	-605	-6970	-494	-5680
14-3-H	642													
14-3-I	2713	1549	2168	-1124	522	66	-301	119	2073	-919	577	63	-171	111
14-3-I	385													
14-3-J	2868	1298	2090	-892	599	54	-147	111	1968	-422	773	40	176	86
14-3-J	-272													

Table D-10 Cross-frame 4-4 Data for SR 1 Over US 13 Day 2 Pass 1

			Section Points FEA E1, C1, S5 Fixed						Section Points FEA E1, C1, S5 Pinned					
Gauge Location	σ_{MAX} (psi)	σ_{Avg} (psi)	Bottom (psi)	Top (psi)	Avg Case 1 (psi)	% Diff	Avg Case 2 (psi)	% Diff	Bottom (psi)	Top (psi)	Avg Case 1 (psi)	% Diff	Avg Case 2 (psi)	% Diff
4-4-A	-2979	-1655	-2716	3374	329	120	1852	212	-2072	1725	-173	90	776	147
4-4-A	-332													
4-4-C	-3133	-1661	-2731	3437	353	121	1895	214	-2111	1993	-59	96	967	158
4-4-C	-190													
4-4-E	3300	2287	2451	-3037	-293	113	-1665	173	2187	-1569	309	86	-630	128
4-4-E	1275													
4-4-G	4218	1972	2456	-3004	-274	114	-1639	183	2173	-1292	441	78	-425	122
4-4-G	-274													
4-4-I	1162	938	508	-1302	-397	142	-850	191	-1250	1300	25	97	663	29
4-4-I	714													
4-4-J	1052	43	411	-792	-190	543	-491	1244	404	-790	-193	550	-492	1246
4-4-J	-966													

Table D-11 Cross-frame 11-3 Data for SR 1 Over US 13 Day 2 Pass 1

			Section Points FEA E1, C1, S5 Fixed						Section Points FEA E1, C1, S5 Pinned					
Gauge Location	σ_{MAX} (psi)	σ_{Avg} (psi)	Bottom (psi)	Top (psi)	Avg Case 1 (psi)	% Diff	Avg Case 2 (psi)	% Diff	Bottom (psi)	Top (psi)	Avg Case 1 (psi)	% Diff	Avg Case 2 (psi)	% Diff
11-3-B	1355	1355	1757	-1512	122	91	-695	151	1635	-1241	197	85	-522	139
11-3-F	-1540	-1540	-1376	-1424	-1400	9	-1412	8	-1388	-1473	-1431	7	-1452	6
11-3-H	-1384	-784	-1761	1742	-10	99	866	210	-1766	1525	-120	85	702	190
11-3-H	-184													
11-3-I	419	311	202	240	221	29	230	26	152	-110	21	93	-44	114
11-3-I	203													
11-3-J	478	19	234	-439	-102	643	-271	1537	179	-343	-82	536	-213	1229
11-3-J	-440													

Table D-12 Cross-frame 4-4 Data for SR 1 Over US 13 Day 2 Pass 2

			Section Points FEA E1, C1, S5 Fixed						Section Points FEA 5E1, C1, S5 Pinned					
Gauge Location	σ_{MAX} (psi)	σ_{Avg} (psi)	Bottom (psi)	Top (psi)	Avg Case 1 (psi)	% Diff	Avg Case 2 (psi)	% Diff	Bottom (psi)	Top (psi)	Avg Case 1 (psi)	% Diff	Avg Case 2 (psi)	% Diff
4-4-A	-2571	-1437	-1386	1601	107	107	854	159	-1437	1078	-179	88	449	131
4-4-A	-303													
4-4-C	-2395	-1381	-1402	1696	147	111	922	167	-1472	1336	-68	95	634	146
4-4-C	-368													
4-4-E	2223	1487	1552	-1602	-25	102	-814	155	1883	-1335	274	82	-530	136
4-4-E	751													
4-4-G	2571	1217	1549	-1531	9	99	-761	163	1870	-1096	387	68	-354	129
4-4-G	-137													
4-4-I	236	339	462	-688	-113	133	-400	218	329	-349	-10	103	-179	153
4-4-I	441													
4-4-J	263	-284	-1056	1857	401	241	1129	498	-1013	1628	308	208	968	441
4-4-J	-830													

Table D-13 Cross-frame 11-3 Data for SR 1 Over US 13 Day 2 Pass 2

			Section Points FEA E1, C1, S5 Fixed						Section Points FEA 5E1, C1, S5 Pinned					
Gauge Location	σ_{MAX} (psi)	σ_{Avg} (psi)	Bottom (psi)	Top (psi)	Avg Case 1 (psi)	% Diff	Avg Case 2 (psi)	% Diff	Bottom (psi)	Top (psi)	Avg Case 1 (psi)	% Diff	Avg Case 2 (psi)	% Diff
11-3-B	1710	1710	2383	-1944	219	87	-863	150	2336	-1652	342	80	-655	138
11-3-F	-1408	-1408	-1971	-2064	-2017	-43	-2040	-45	-2123	-2247	-2185	-55	-2216	-57
11-3-H	-1325	-539	-2532	2548	8	101	1278	337	-2709	2428	-141	74	1144	312
11-3-H	247													
11-3-I	368	268	642	-827	-93	135	-460	272	603	-620	-9	103	-314	217
11-3-I	168													
11-3-J	475	9	699	-1182	-242	2789	-712	8021	671	-1083	-206	2388	-644	7266
11-3-J	-457													

Table D-14 Cross-frame 4-4 Data for SR 1 Over US 13 Day 2 Pass 3

			Section Points FEA E1, C1, S5 Fixed						Section Points FEA E1, C1, S5 Pinned					
Gauge Location	σ_{MAX} (psi)	σ_{Avg} (psi)	Bottom (psi)	Top (psi)	Avg Case 1 (psi)	% Diff	Avg Case 2 (psi)	% Diff	Bottom (psi)	Top (psi)	Avg Case 1 (psi)	% Diff	Avg Case 2 (psi)	% Diff
4-4-A	-2078	-1175	-1271	1461	95	108	778	166	-1404	1063	-171	85	446	138
4-4-A	-271													
4-4-C	-1829	-1106	-1285	1556	135	112	846	176	-1437	1309	-64	94	623	156
4-4-C	-383													
4-4-E	1713	1126	1417	-1413	2	100	-706	163	1804	-1276	264	77	-506	145
4-4-E	538													
4-4-G	1747	894	1414	-1341	36	96	-652	173	1791	-1048	371	58	-338	138
4-4-G	41													
4-4-I	-355	-18	-1102	1601	249	1498	925	5286	-914	983	34	293	509	2953
4-4-I	319													
4-4-J	-263	-509	-1177	2136	479	194	1308	357	-1219	2063	422	183	1243	344
4-4-J	-755													

Table D-15 Cross-frame 11-3 Data for SR 1 Over US 13 Day 2 Pass 3

			Section Points FEA E1, C1, S5 Fixed						Section Points FEA E1, C1, S5 Pinned					
Gauge Location	σ_{MAX} (psi)	σ_{Avg} (psi)	Bottom (psi)	Top (psi)	Avg Case 1 (psi)	% Diff	Avg Case 2 (psi)	% Diff	Bottom (psi)	Top (psi)	Avg Case 1 (psi)	% Diff	Avg Case 2 (psi)	% Diff
11-3-B	1947	1947	2236	-1760	238	88	-761	139	2155	-1467	344	82	-562	129
11-3-F	-2479	-2479	-2019	-1924	-1972	20	-1948	21	-2173	-2101	-2137	14	-2119	15
11-3-H	-2342	-1368	-2580	2663	42	103	1353	199	-2762	2563	-100	93	1232	190
11-3-H	-394													
11-3-I	469	395	692	-896	-102	126	-499	226	657	-685	-14	104	-349	189
11-3-I	320													
11-3-J	469	-87	-1587	2609	511	687	1560	1893	-1529	2408	439	605	1423	1736
11-3-J	-643													